

**Engineering of a Type III Rubisco from a Hyperthermophilic Archaeon  
Aimed to Enhance Catalytic Performance at Ambient Temperatures**

**Shosuke YOSHIDA**

**2008**



## **PREFACE**

This is a thesis submitted by the author to Kyoto University for the degree of Doctor of Engineering. The study presented in this thesis has been performed under the supervision of Professor Tadayuki Imanaka in the Laboratory of Biochemical Engineering, Department of Synthetic Chemistry and Biological Chemistry, Graduate School of Engineering, Kyoto University during 2004-2008.

The author wishes to express his sincere gratitude to Professor Tadayuki Imanaka for his continual guidance, criticism, and encouragement. The author is deeply grateful to Associate Professor Haruyuki Atomi for his fruitful discussion, heartwarming support, and encouragement throughout the course of this study. He would like to acknowledge Assistant Professor Tamotsu Kanai for his guidance and helpful suggestions.

It should be emphasized that the study in CHAPTER 1 of this study was made possible through a fruitful collaboration. Grateful acknowledgement is dedicated to Dr. Hideaki Yukawa, Dr. Masayuki Inui, and Dr. Ken-ichi Tomizawa, Research Institute of Innovative Technology for the Earth (RITE).

The contribution of Dr. Tadayoshi Kanao, who participated in some of the work presented in CHAPTER 1, is greatly appreciated.

The author would also like to acknowledge Professor Kunio Miki and Assistant Professor Masahiro Fujihashi of the Department of Chemistry, Graduate School of

Science, Kyoto University, with whom the author is now collaborating in structural studies on Rubisco mutant proteins.

The author would like to acknowledge all members, past and present, of Professor Imanaka's Laboratory for their kind support, encouragement, and friendship.

The author acknowledges the Japan Society for the Promotion of Science for financial support (21st Century Center of Excellence Program).

Finally, the author would like to express his deep appreciation to his parents, Shotaro and Yukiko for their unfailing affection and heartwarming encouragement throughout the period.

**Shosuke YOSHIDA**

Laboratory of Biochemical Engineering

Department of Synthetic Chemistry and Biological Chemistry,

Graduate School of Engineering

Kyoto University

March 2008

Kyoto

## TABLE OF CONTENTS

	<b>Pages</b>
<b>GENERAL INTRODUCTION</b>	<b>1</b>
<b>SYNOPSIS</b>	<b>21</b>
<b>CHAPTER 1</b> <b>Phototrophic growth of a Rubisco-deficient mesophilic purple nonsulfur bacterium harboring a Type III Rubisco from a hyperthermophilic archaeon</b>	<b>25</b>
<b>CHAPTER 2</b> <b>Engineering of a Type III Rubisco from a hyperthermophilic archaeon aimed to enhance catalytic performance in mesophilic host cells</b>	<b>55</b>
<b>CHAPTER 3</b> <b>Optimizing the <math>\alpha</math>-helix6 region of <i>Tk</i>-Rubisco to enhance catalytic performance of the enzyme at ambient temperatures</b>	<b>87</b>
<b>GENERAL CONCLUSIONS</b>	<b>102</b>
<b>LIST OF PUBLICATIONS</b>	<b>104</b>



## GENERAL INTRODUCTION

### 1. Biological carbon dioxide fixation.

The living organisms on our planet display diverse mechanisms in terms of how they obtain energy for cellular functions and what they utilize as a carbon source. In a heterotrophic mode of growth, organic substrates are utilized to synthesize cell material, and in many cases, energy is obtained through the oxidation of these compounds. In some cases, energy is obtained from inorganic chemical reactions or light. In an autotrophic mode of growth, carbon dioxide is utilized as the sole carbon source, and all cell components are synthesized via the reduction of carbon dioxide. Autotrophic organisms obtain their energy and reducing equivalents from various chemical reactions or light. The obligate heterotrophs/autotrophs are dependent on a single mode of growth, whereas the facultative heterotrophs/autotrophs can switch between the two modes of carbon assimilation depending on their environments.

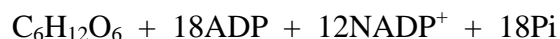
To date, four different carbon dioxide fixation mechanisms have been identified, the Calvin-Benson-Bassham cycle (CBB pathway, reductive pentose phosphate cycle), the reductive citric acid cycle, the reductive acetyl-CoA pathway, and the 3-hydroxypropionate cycle (15, 29, 35, 36) (Table 1). All four pathways are found in prokaryotes, while only the CBB pathway is also found in eukaryotes such as plants and algae. Among the four carbon dioxide fixation mechanisms, the CBB pathway is considered by far the most predominant. It can thus be supposed that the production of organic compounds on the surface of our planet largely depends on the CBB pathway.

**Table 1. Biological carbon dioxide fixation pathways.**

Pathway	CO <sub>2</sub> -fixing enzymes	Distribution
Calvin-Benson-Bassham cycle	Ribulose-1, 5-bisphosphate carboxylase/oxygenase	Plants Algae Cyanobacteria Many bacteria
Reductive citric acid cycle	2-Oxoglutarate synthase Isocitrate dehydrogenase Phosphoenolpyruvate carboxylase Pyruvate synthase	Green sulfur bacteria Some archaea
Reductive acetyl-CoA pathway	Acetyl-CoA synthase /CO dehydrogenase Formate dehydrogenase Pyruvate synthase	Methanogens Acetogens
3-Hydroxypropionate cycle	Acetyl-CoA carboxylase Propionyl-CoA carboxylase	Green nonsulfur bacteria Some archaea

## 2. Calvin-Benson-Bassham cycle (CBB pathway).

Thirteen enzymes contribute to the CBB pathway (Fig. 1), and the overall stoichiometry is as follows:



Ribulose-1, 5-bisphosphate carboxylase/oxygenase (Rubisco; EC 4.1.1.39), phosphoribulokinase (PRK), and sedoheptulose-1, 7-bisphosphatase (SBPase) are unique to the CBB pathway and are considered as the key enzymes. The CBB pathway is composed of three distinct phases, irreversible carboxylation, reduction of carboxyl groups to the aldehyde level, and regeneration of ribulose 1, 5-bisphosphate (RuBP). In



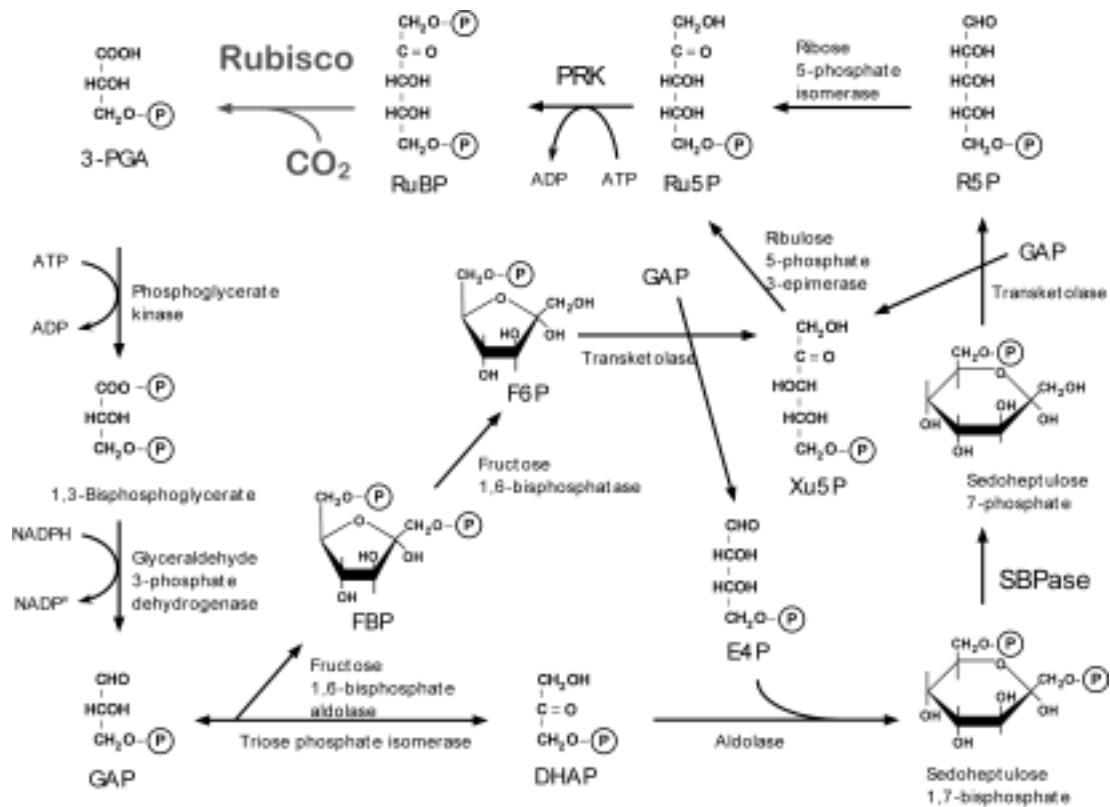


**Fig. 1. The Calvin-Benson-Bassham cycle.**

Enzyme abbreviations; Rubisco: Ribulose-1, 5-bisphosphate carboxylase/oxygenase, PRK: phosphoribulokinase, SBPase: sedoheptulose-1, 7-bisphosphatase.

Substrate abbreviations; RuBP: ribulose 1, 5- bisphosphate, 3-PGA: 3-phosphoglycerate, GAP: glyceraldehyde 3-phosphate, Xu5P: xylulose 5-phosphate, E4P: erythrose 4-phosphate, DHAP: dihydroxyacetone phosphate, R5P: ribose 5-phosphate, Ru5P: ribulose 5-phosphate, FBP: fructose 1, 6-bisphosphate, F6P: fructose 6-phosphate.

the irreversible carboxylation phase, Rubisco catalyzes the covalent addition of CO<sub>2</sub> and H<sub>2</sub>O to RuBP, producing two molecules of 3-phosphoglycerate (3-PGA). The resulting 3-PGA is converted into glyceraldehyde 3-phosphate (GAP) by 3-phosphoglycerate kinase and glyceraldehyde-3-phosphate dehydrogenase at the expense of ATP and NAD(P)H. The regeneration of RuBP is carried out by two similar metabolic units, made up of an aldolase, a phosphatase, and a transketolase (APT). The first APT unit generates xylulose 5-phosphate (Xu5P) and erythrose 4-phosphate (E4P) from two molecules of GAP and one molecule of dihydroxyacetone phosphate (DHAP). The

second APT unit converts DHAP, GAP and E4P into Xu5P and ribose 5-phosphate (R5P). In this second unit, SBPase is utilized for the dephosphorylation of sedoheptulose 1, 7-bisphosphate. Xu5P and R5P are then converted into ribulose 5-phosphate (Ru5P) by ribulose-5-phosphate-3-epimerase and ribose-5-phosphate isomerase, respectively. Finally, PRK concludes the regeneration of RuBP by phosphorylating Ru5P in an ATP-dependent manner (35).

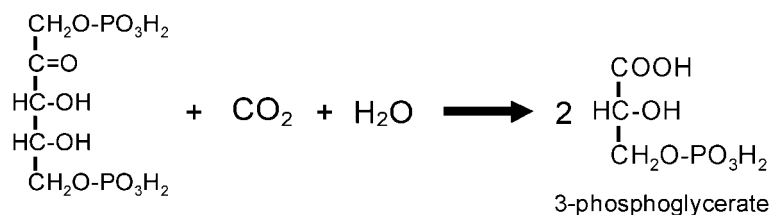
### **3. Ribulose-1, 5-bisphosphate carboxylase/oxygenase (Rubisco).**

As mentioned above, Rubisco is the key enzyme of the CBB pathway, and is found in autotrophic organisms such as plants, algae, cyanobacteria, and some photoautotrophic and chemoautotrophic bacteria, and is probably the most abundant enzyme on earth (6). The enzyme catalyzes two competing reactions. Besides the carboxylase reaction that produces two molecules of 3-PGA from RuBP, CO<sub>2</sub> and H<sub>2</sub>O, the enzyme also catalyzes the addition of O<sub>2</sub> to RuBP, producing one molecule of 3-PGA and 2-phosphoglycolate (Fig. 2). This oxygenation reaction reduces the efficiency of photosynthesis. Moreover, Rubisco is a very inefficient enzyme in terms of turnover. It is presumed that the photosynthetic organisms produce this enzyme in large quantities to compensate for this low activity (3, 13).

Rubiscos had long been classified into the Type I and Type II enzymes. Type I Rubiscos are heterohexamers composed of eight large subunits and eight small subunits (L<sub>8</sub>S<sub>8</sub>), with the catalytic centers residing in the large subunit. Type I Rubiscos are the predominant Rubisco found in most autotrophic organisms that are dependent on the CBB pathway. In contrast, Type II Rubiscos, composed solely of two large subunits (L<sub>2</sub>), are only found in some photoautotrophic and chemoautotrophic bacteria. In the

eukaryotic plants and green algae, the large subunit of the Type I Rubisco is encoded by the chloroplast *rbcL* gene, whereas the small subunit is encoded by the nuclear *rbcS* gene (11, 43).

### Carboxylase reaction



### Oxygenase reaction

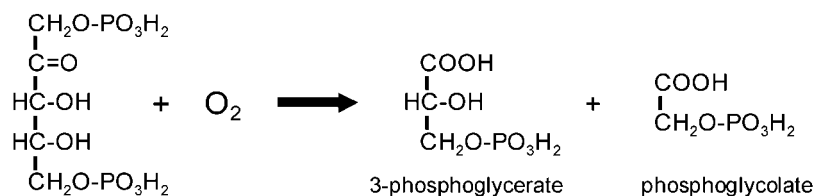


**Fig. 2. The carboxylase and oxygenase reactions catalyzed by Rubisco.**

As the large subunit of Rubisco is responsible for catalytic activity (14), the overall protein fold of the large subunit is almost identical among Type I and Type II enzymes, and the conformation of the active site is well conserved (34). The large subunit is composed of two domains, the N-terminal domain and the C-terminal domain (14). The N-terminal domain is built from a five-stranded  $\beta$ -sheet and two  $\alpha$ -helices. The C-terminal domain is composed of an eight-stranded  $\beta/\alpha$ -barrel structure. A homodimer of the large subunit is the smallest catalytic unit because the active site is formed at the interface of the N-terminal and C-terminal domains of adjacent subunits. The role of the small subunit of Type I Rubisco remains poorly understood, but some reports have indicated that the small subunit affects the catalytic performance of the

large subunit (2, 31, 38).

Studies on the reaction mechanism of Rubiscos have revealed that the enzyme is activated with a carbon dioxide and a magnesium ion (14). The  $\epsilon$ -amino group of a lysine residue at the active site is carbamated, and the activation process concludes with the insertion of a magnesium ion that stabilizes the carbamate. RuBP is bound to the activated enzyme, and deprotonated at the C3 position of RuBP, resulting in the generation of a labile intermediate, 2, 3-enediol. The enediol accepts a  $\text{CO}_2$  or  $\text{O}_2$  molecule, resulting in the carboxylase reaction or oxygenase reaction, respectively. The ratio between the catalytic performances of the carboxylase reaction and oxygenase reaction is designated as the  $\tau$  value and can be defined with the following equation (16).

$$\tau = V_{\text{CO}_2} K_{\text{O}_2} / V_{\text{O}_2} K_{\text{CO}_2}$$

$V_{\text{CO}_2}$  and  $V_{\text{O}_2}$  represent the maximum velocities ( $V_{\text{max}}$ ) of the carboxylase reaction and oxygenase reaction, and  $K_{\text{CO}_2}$  and  $K_{\text{O}_2}$  represent the  $K_m$  values of the carboxylase and oxygenase reactions, respectively. In general, the  $\tau$  values of Type I Rubisco (30~240) are higher than those of Type II Rubisco (10~15), indicating that in our atmosphere, the former group can be considered superior to the latter group as a carboxylase (41).

#### **4. Strategies to elevate the efficiency of the CBB pathway.**

As described above, the catalytic performance of the Rubisco protein is low, and thus the Rubisco reaction is regarded as the rate-limiting step for  $\text{CO}_2$  fixation in the CBB pathway. Therefore an improvement in the Rubisco (carboxylase) activity can be expected to have great impact on agricultural productivity and net  $\text{CO}_2$  fixation. A number of studies are pursuing the possibilities of raising the  $\text{CO}_2$  concentration in the

chloroplast matrix, leading to an increase in the velocity of the carboxylase reaction of Rubisco. One example has attempted to introduce an oxaloacetate/malate shuttle (C4 pathway) in C3 plants (23), and another is considering the introduction of cyanobacterial components into the plant cell. These include bicarbonate transporters and factors constituting the carboxysome, all involved in elevating intracellular CO<sub>2</sub> levels in cyanobacteria (28). However, most studies have focused on the catalytic improvement of the Rubisco protein itself. The two main targets of Rubisco engineering are clear; one is an increase in catalytic turnover and the other is an increase in carboxylase specificity.

Attempts to enhance the function of Rubisco have been carried out since long ago on Rubisco proteins from various organisms. However, protein engineering of the eukaryotic Type I enzymes has been hampered by the fact that functional expression of these enzymes in conventional host cells such as *Escherichia coli* is not possible (10, 42). We are therefore not able to introduce specific mutations and examine their effects with recombinant proteins. Bacterial Type I and Type II Rubiscos can be functionally expressed in *E. coli*, and extensive studies have been carried out in order to understand the structural elements that control the specificity and activity levels of these enzymes. Mutagenesis experiments have also been carried out with the aim to improve the catalytic efficiency of bacterial Rubiscos. From these studies, a wealth of information has accumulated on the relationships between specific mutated residues and the enzymatic performance of the resulting mutant proteins (14, 26, 39). Site-directed mutagenesis studies have confirmed that loop6 and  $\alpha$ -helix6 regions play a role in defining the catalytic performance of Rubisco, however, the number of mutant proteins with enhanced properties in terms of carboxylase specificity or turnover is surprisingly

low. The very few mutations that displayed a positive effect involved residues residing in the  $\alpha$ -helix6 regions (Table 2). However, many of the mutations that led to even the slightest improvement in carboxylase specificity resulted in a decrease in turnover rate (12, 20, 27). The only successful example was that of an A340N mutant of a cyanobacterial Type I Rubisco which led to an improvement in both carboxylase specificity (9%) and turnover rate (19%) compared with the wild-type protein (20).

**Table 2. Mutations incorporated into the loop6 and  $\alpha$ -helix6 regions of cyanobacterial Rubisco, and their effects on the carboxylase specificity ( $\tau$ ) and carboxylase activity ( $V_{\max}$ ) of the enzyme.**

<i>loop6 region</i>				<i><math>\alpha</math>-helix6 region</i>			
Mutation	Change (%)		Reference	Mutation	Change (%)		Reference
	$\tau$	$V_{\max}$			$\tau$	$V_{\max}$	
V331G	-64	-99	(12)	D338E	4	-6	(27)
V331A	-46	-95	(12)	K339P	-3	-85	(32)
V331A	-3	-92	(27)	A340L	-8	-34	(32)
V331L	-13	-95	(12)	A340E	-18	-12	(27)
V331M	-71	-99	(12)	A340H	<b>13</b>	-33	(20)
K334R	-99	-99	(12)	A340N	<b>9</b>	<b>19</b>	(20)
K334P	-10	-83	(30)	A340D	<b>5</b>	-33	(20)
KA334-335PL	-6	-69	(30)	A340G	-6	-31	(20)
KAS334-336PLM	-8	-86	(24, 30)	A340R	<b>3</b>	-4	(20)
KAST334-337PLMV	-7	-92	(30)	A340Y	<b>12</b>	-25	(20)
KASTL334-338PLMVK	-10	-80	(30)	S341I	-1	-9	(27)
KASTL334-338PLMVK, V341Y	N.T.	N. D.	(30)	S341M	8	-1	(32)
KASTL334-338PLMVK, VD341-342YN	N.T.	N. D.	(30)	T342I	-18	-45	(32)
KASTL334-338PLMVK, VDL341-343YNT	N.T.	N. D.	(30)	T342I	-7	-70	(12)
L335M	-54	-65	(19)	T342L	-7	-60	(12)
L335I	-67	-86	(19)	T342M	-11	-4	(12)
L335V	-60	-61	(19)	T342V	-23	-48	(32)
L335T	-35	-46	(19)	DKAS338-341EREI	7	-8	(27)
L335A	-55	-70	(19)	DKAS338-341ERDI	3	-40	(12)
				DKAS338-341ERDI	5	N.T.	(17)
				F345V	-31	-7	(37)

N.D. : not detected, N.T. : not tested.

## 5. The hyperthermophilic archaeon, *Thermococcus kodakaraensis* KOD1.

Through progress in genetic technology, it is now possible to examine organisms in a phylogenetic manner based on protein/nucleotide sequences. The phylogenetic tree based on 16S and 18S ribosomal RNA genes, which are present in all living organisms, reveal that all known organisms can be divided into three domains, *Bacteria*, *Eucarya* and *Archaea* (45).

Hyperthermophiles are referred to as microorganisms that can grow optimally at temperatures above 80°C (40). The majority of hyperthermophilic organisms are members of the domain *Archaea*, whereas a limited number of genera, such as *Aquifex*, *Thermotoga* and *Geothermobacterium*, belong to the *Bacteria*. As is shown in Fig. 3, all hyperthermophiles are positioned near the root of the phylogenetic tree, suggesting that these organisms are relatively closely related to the last common ancestors of the bacterial and archaeal domains.

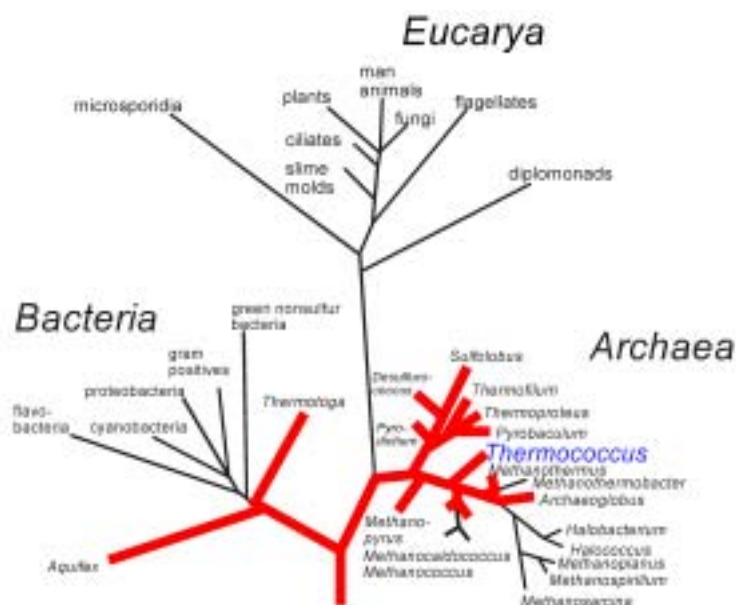


**Fig. 3.** A phylogenetic tree based on sequences of 16S and 18S ribosomal RNA genes. Hyperthermophiles are indicated in red.

The hyperthermophilic archaeon, *Thermococcus kodakaraensis* KOD1, was isolated from a solfatara at a wharf of Kodakara Island, Kagoshima, Japan. The strain is an obligate heterotroph and anaerobe. The cells are irregular cocci with a diameter of 1 to 2  $\mu\text{m}$  and have several polar flagella. The growth temperature of the strain ranges from 60°C to 100°C with an optimum temperature of 85°C. The optimum pH and NaCl concentration for growth are 6.5 and 3%, respectively (5, 25). A number of physiologically important proteins have been characterized from *T. kodakaraensis*, and many of the proteins show distinct structures and characteristics compared with their counterparts from eukaryotes and bacteria. The complete genome sequence of *T. kodakaraensis* KOD1 has recently been determined and annotated (Fig. 4). The genome consists of 2,088,737 bp and is predicted to harbor 2,306 open reading frames (9).

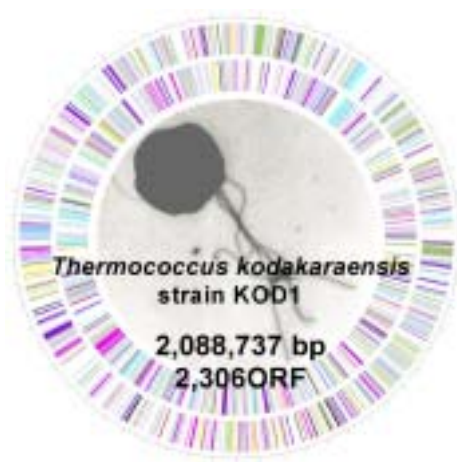


**Fig. 4. Complete genome map of *T. kodakaraensis* KOD1.**

#### **6. A novel Type III Rubisco from *T. kodakaraensis*.**

Although archaea do not seem to harbor a functional CBB pathway, it has recently become clear that Rubiscos are present in the *Archaea*. Archaeal Rubiscos were



first discovered in *T. kodakaraensis* (7). The enzyme exhibits Rubisco activity and the protein has been detected in the native cells. Catalytically active Rubisco proteins have also been identified from the hyperthermophilic *Methanococcus* (now *Methanocaldococcus*) *jannaschii* (44), and *Archaeoglobus fulgidus* (8), and the mesophilic *Methanosarcina acetivorans* (8). Genome sequences indicate they are also present in *Pyrococcus* species, other methanogens, and *Natronomonas pharaonis*, and are now structurally classified as Type III enzymes (1, 4) (Fig. 5).

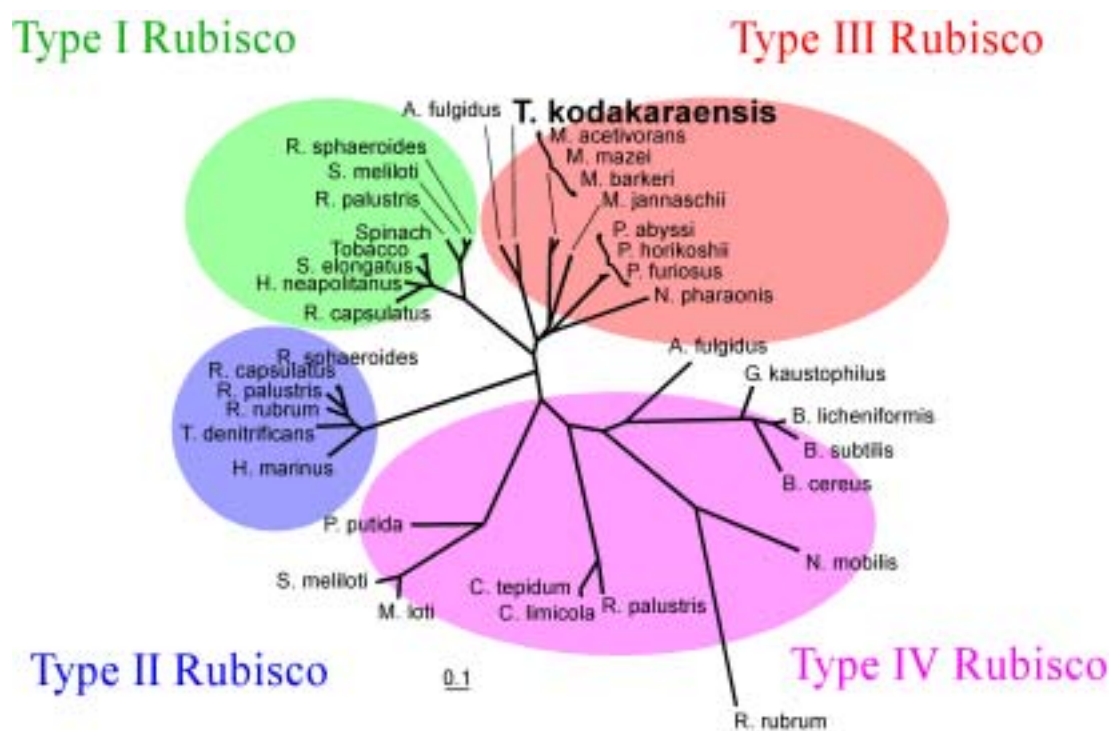


**Fig. 5. A phylogenetic tree constructed with the primary structures of Rubiscos and their homologs.**

The enzyme from *T. kodakaraensis* (*Tk*-Rubisco) displayed extreme thermostability, and a high carboxylase activity was observed at high temperature ranges (Fig. 6). *Tk*-Rubisco was crystallized, and the three-dimensional structure has been determined (18, 22). The enzyme is composed only of large subunits, as in the case

of the Type II Rubiscos. The overall fold of the monomer highly resembles those of Type I and Type II enzymes (Fig. 7). However, *Tk*-Rubisco exhibits a novel quaternary structure, and was found to be a toroid-shaped pentagonal decamer comprised of five  $L_2$  dimers, clearly distinct to the quaternary structures of Type I and Type II Rubiscos (Fig. 8). This unique quaternary structure was shown to support the high thermostability of the enzyme. Although the dimeric unit of *Tk*-Rubisco itself is much more stable than those of mesophilic enzymes (denaturation at  $95^\circ\text{C}$ ), the decameric structure maintained its structure at temperatures up to  $113^\circ\text{C}$  (21). In terms of physiological function, it has recently been shown that archaeal Type III Rubiscos are components of a novel metabolic pathway involved in the degradation of AMP, distinct to the roles of the Type I and Type II enzymes that function in the CBB pathway (33).

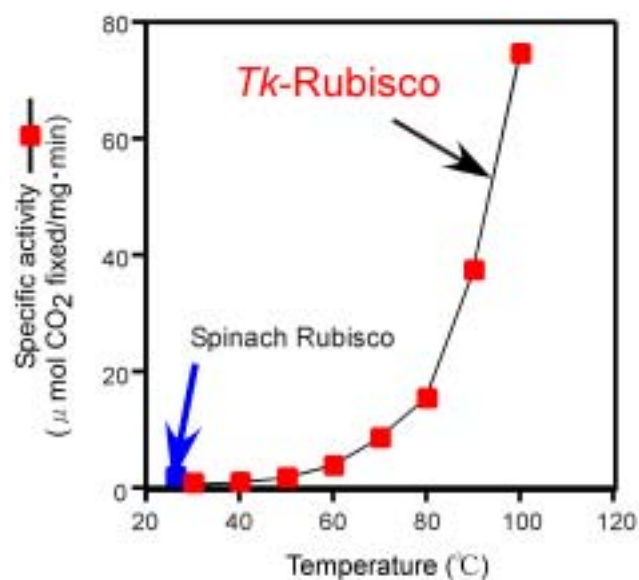


**Fig. 6. Carboxylase activity of *Tk*-Rubisco at various temperatures.**

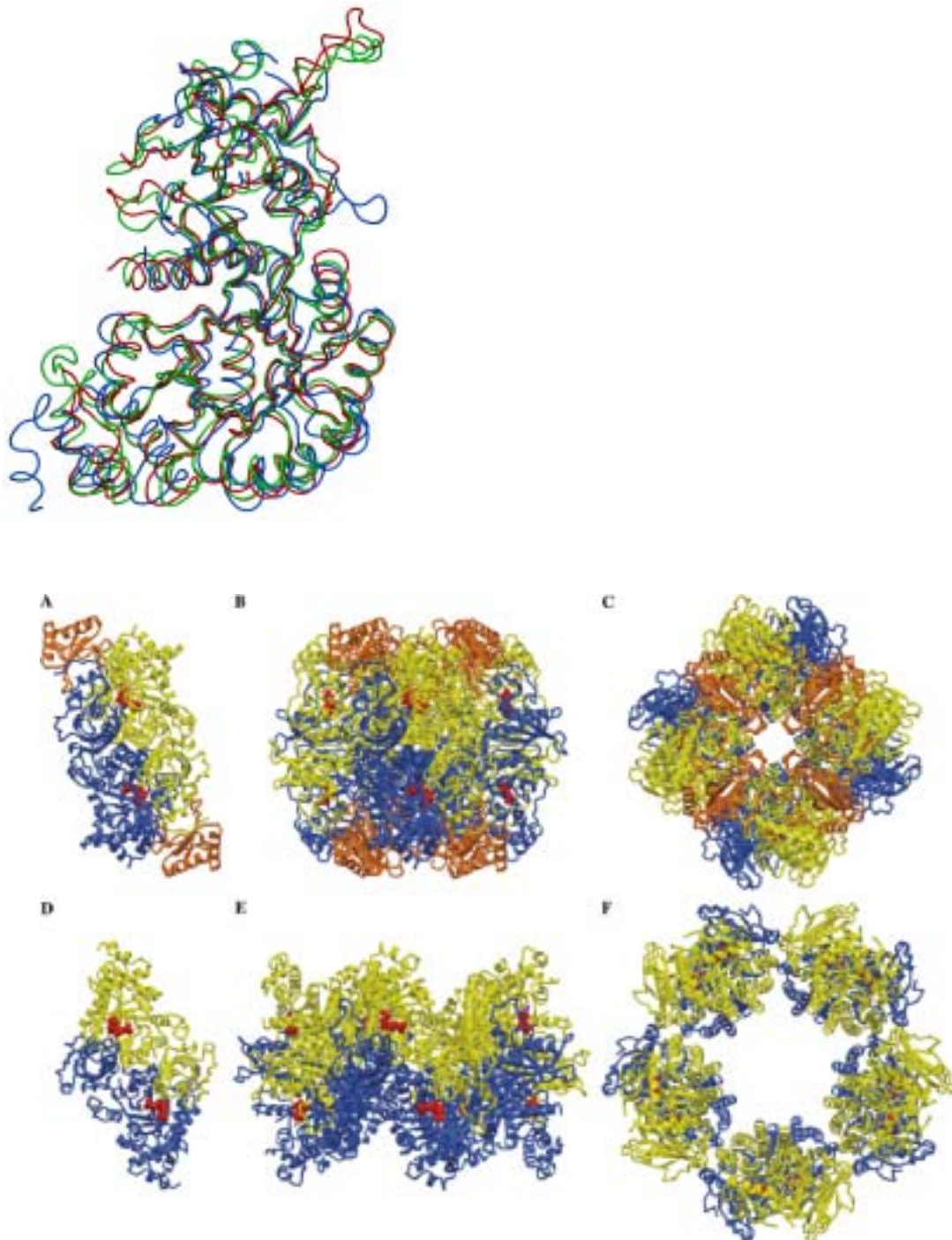


**Fig. 8. The quaternary structures of Type I, Type II and Type III Rubiscos.** Large subunits are represented in yellow and blue. Small subunits are colored in orange. (A)  $L_2S_2$  unit of Type I Rubisco from spinach. The  $L_8S_8$  hexadecamer viewed from the side (B) and top (C). (D) Dimeric ( $L_2$ ) Type II Rubisco from *Rhodospirillum rubrum*. Decameric ( $L_{10}$ ) Type III Rubisco from *T. kodakaraensis* viewed from the side (E) and top (F). Diagrams are taken from Andersson and Taylor (1).

At ambient temperature, the carboxylase activity of *Tk*-Rubisco is lower than that of spinach Rubisco. The author assumed that this is most likely due to the rigidity of the protein at lower temperatures, brought about by structural elements necessary to maintain the structure of the protein at higher temperatures. However, an important feature of *Tk*-Rubisco was the fact that the protein was readily expressed at high levels in an active form in *E. coli*. Another factor is the high (thermo)stability of the enzyme, suggesting that the enzyme provides a stable protein scaffold that should be able to tolerate higher degrees of mutations at ambient temperatures compared to mesophilic Rubiscos. These properties, along with the novel three-dimensional structure of the protein, make *Tk*-Rubisco an attractive target for structure-function studies and protein engineering of Rubiscos.

In this study, the author examined whether a Type III Rubisco from a hyperthermophilic archaeon (*Tk*-Rubisco) could support the growth of a mesophilic, photosynthetic organism. A Rubisco-deficient mutant strain of the purple nonsulfur bacterium *Rhodospseudomonas palustris* No. 7 was used as the host strain. In order to improve the enzymatic performance of *Tk*-Rubisco, an extensive amount of site-directed mutageneses was performed. The catalytic properties of purified recombinant proteins were examined *in vitro*, and the *R. palustris* Rubisco-deficient strain was utilized as a host strain for evaluating the performance of these mutant proteins *in vivo*. A further attempt to enhance Rubisco performance was carried out by constructing an artificial fusion protein of *Tk*-Rubisco with carbonic anhydrase from the mesophilic algae *Dunaliella salina*. The performances of the recombinant purified fusion proteins were investigated *in vitro*.

## REFERENCES

1. **Andersson, I., and T. C. Taylor.** 2003. Structural framework for catalysis and regulation in ribulose-1,5-bisphosphate carboxylase/oxygenase. *Arch. Biochem. Biophys.* **414**:130-140.
2. **Andrews, T. J., and B. Ballment.** 1983. The function of the small subunits of ribulose bisphosphate carboxylase-oxygenase. *J. Biol. Chem.* **258**:7514-7518.
3. **Andrews, T. J., and G. H. Lorimer.** 1987. Rubisco: Structure, mechanisms, and prospects for improvement., p. 131-218. *In* M. D. Hatch and N. K. Boardman (ed.), *The Biochemistry of Plants*. Academic Press, San Diego.
4. **Atomi, H.** 2002. Microbial enzymes involved in carbon dioxide fixation. *J. Biosci. Bioeng.* **94**:497-505.
5. **Atomi, H., T. Fukui, T. Kanai, M. Morikawa, and T. Imanaka.** 2004. Description of *Thermococcus kodakaraensis* sp. nov., a well studied hyperthermophilic archaeon previously reported as *Pyrococcus* sp. KOD1. *Archaea* **1**:263-267.
6. **Ellis, R. J.** 1979. Most abundant protein in the world. *Trends Biochem. Sci.* **4**:241-244.
7. **Ezaki, S., N. Maeda, T. Kishimoto, H. Atomi, and T. Imanaka.** 1999. Presence of a structurally novel type ribulose-bisphosphate carboxylase/oxygenase in the hyperthermophilic archaeon, *Pyrococcus kodakaraensis* KOD1. *J. Biol. Chem.* **274**:5078-5082.
8. **Finn, M. W., and F. R. Tabita.** 2003. Synthesis of catalytically active form III ribulose 1,5-bisphosphate carboxylase/oxygenase in archaea. *J. Bacteriol.* **185**:3049-3059.

9. **Fukui, T., H. Atomi, T. Kanai, R. Matsumi, S. Fujiwara, and T. Imanaka.** 2005. Complete genome sequence of the hyperthermophilic archaeon *Thermococcus kodakaraensis* KOD1 and comparison with *Pyrococcus* genomes. *Genome Res* **15**:352-363.
10. **Gatenby, A. A.** 1988. Synthesis and assembly of bacterial and higher plant Rubisco subunits in *Escherichia coli*. *Photosynth. Res.* **17**:145-157.
11. **Gatenby, A. A., and R. J. Ellis.** 1990. Chaperone function: the assembly of ribulose biphosphate carboxylase-oxygenase. *Annu. Rev. Cell Biol.* **6**:125-149.
12. **Gutteridge, S., D. F. Rhoades, and C. Herrmann.** 1993. Site-specific mutations in a loop region of the C-terminal domain of the large subunit of ribulose biphosphate carboxylase/oxygenase that influence substrate partitioning. *J. Biol. Chem.* **268**:7818-7824.
13. **Harpel, M. R., E. H. Serpersu, and F. C. Hartman.** 1995. Utilization of partial reactions, side reactions, and chemical rescue to analyse site-directed mutants of ribulose 1,5-biphosphate (RuBP) carboxylase/oxygenase (Rubisco), p. 357-364. *In* J. W. Crabb (ed.), *Techniques in Protein Chemistry*. Academic Press, San Diego.
14. **Hartman, F. C., and M. R. Harpel.** 1994. Structure, function, regulation, and assembly of D-ribulose-1,5-biphosphate carboxylase/oxygenase. *Annu. Rev. Biochem.* **63**:197-234.
15. **Herter, S., J. Farfsing, N. Gad'On, C. Rieder, W. Eisenreich, A. Bacher, and G. Fuchs.** 2001. Autotrophic CO<sub>2</sub> fixation by *Chloroflexus aurantiacus*: study of glyoxylate formation and assimilation via the 3-hydroxypropionate cycle. *J. Bacteriol.* **183**:4305-4316.

16. **Jordan, D. B., and W. L. Ogren.** 1981. Species variation in the specificity of ribulose biphosphate carboxylase-oxygenase. *Nature* **291**:513-515.
17. **Kane, H. J., J. Viil, B. Entsch, K. Paul, M. K. Morell, and T. J. Andrews.** 1994. An improved method for measuring the CO<sub>2</sub>/O<sub>2</sub> specificity of ribulosebisphosphate carboxylase-oxygenase. *Aust. J. Plant Physiol.* **21**:449-461.
18. **Kitano, K., N. Maeda, T. Fukui, H. Atomi, T. Imanaka, and K. Miki.** 2001. Crystal structure of a novel-type archaeal Rubisco with pentagonal symmetry. *Structure* **9**:473-481.
19. **Lee, G. J., K. A. McDonald, and B. A. McFadden.** 1993. Leucine 332 influences the CO<sub>2</sub>/O<sub>2</sub> specificity factor of ribulose-1,5-bisphosphate carboxylase/oxygenase from *Anacystis nidulans*. *Protein Sci.* **2**:1147-1154.
20. **Madgwick, P. J., S. Parmar, and M. A. Parry.** 1998. Effect of mutations of residue 340 in the large subunit polypeptide of Rubisco from *Anacystis nidulans*. *Eur. J. Biochem.* **253**:476-479.
21. **Maeda, N., T. Kanai, H. Atomi, and T. Imanaka.** 2002. The unique pentagonal structure of an archaeal Rubisco is essential for its high thermostability. *J. Biol. Chem.* **277**:31656-31662.
22. **Maeda, N., K. Kitano, T. Fukui, S. Ezaki, H. Atomi, K. Miki, and T. Imanaka.** 1999. Ribulose bisphosphate carboxylase/oxygenase from the hyperthermophilic archaeon *Pyrococcus kodakaraensis* KOD1 is composed solely of large subunits and forms a pentagonal structure. *J. Mol. Biol.* **293**:57-66.
23. **Matsuoka, M., R. T. Furbank, H. Fukayama, and M. Miyao.** 2001.

- Molecular engineering of C<sub>4</sub> photosynthesis. *Annu. Rev. Plant Physiol. Plant Mol. Biol.* **52**:297-314.
24. **Miziorko, H. M., and G. H. Lorimer.** 1983. Ribulose-1,5-bisphosphate carboxylase-oxygenase. *Annu. Rev. Biochem.* **52**:507-535.
  25. **Morikawa, M., Y. Izawa, N. Rashid, T. Hoaki, and T. Imanaka.** 1994. Purification and characterization of a thermostable thiol protease from a newly isolated hyperthermophilic *Pyrococcus* sp. *Appl. Environ. Microbiol.* **60**:4559-4566.
  26. **Parry, M. A. J., P. J. Andralojc, R. A. Mitchell, P. J. Madgwick, and A. J. Keys.** 2003. Manipulation of Rubisco: the amount, activity, function and regulation. *J. Exp. Bot.* **54**:1321-1333.
  27. **Parry, M. A. J., P. Madgwick, S. Parmar, M. J. Cornelius, and A. J. Keys.** 1992. Mutations in loop six of the large subunit of ribulose-1,5-bisphosphate carboxylase affect substrate-specificity. *Planta* **187**:109-112.
  28. **Price, G. D., M. R. Badger, F. J. Woodger, and B. M. Long.** 2007. Advances in understanding the cyanobacterial CO<sub>2</sub>-concentrating-mechanism (CCM): functional components, Ci transporters, diversity, genetic regulation and prospects for engineering into plants. *J. Exp. Bot.* **Published On-line.**
  29. **Ragsdale, S. W.** 1991. Enzymology of the acetyl-CoA pathway of CO<sub>2</sub> fixation. *Crit. Rev. Biochem. Mol. Biol.* **26**:261-300.
  30. **Ramage, R. T., B. A. Read, and F. R. Tabita.** 1998. Alteration of the  $\alpha$  helix region of cyanobacterial ribulose 1,5-bisphosphate carboxylase/oxygenase to reflect sequences found in high substrate specificity enzymes. *Arch. Biochem. Biophys.* **349**:81-88.



31. **Read, B. A., and F. R. Tabita.** 1992. Amino acid substitutions in the small subunit of ribulose-1,5-bisphosphate carboxylase/oxygenase that influence catalytic activity of the holoenzyme. *Biochemistry* **31**:519-525.
32. **Read, B. A., and F. R. Tabita.** 1994. High substrate specificity factor ribulose bisphosphate carboxylase/oxygenase from eukaryotic marine algae and properties of recombinant cyanobacterial Rubisco containing "algal" residue modifications. *Arch. Biochem. Biophys.* **312**:210-218.
33. **Sato, T., H. Atomi, and T. Imanaka.** 2007. Archaeal type III RuBisCOs function in a pathway for AMP metabolism. *Science* **315**:1003-1006.
34. **Schneider, G., S. Knight, I. Andersson, C. I. Brändén, Y. Lindqvist, and T. Lundqvist.** 1990. Comparison of the crystal structures of L<sub>2</sub> and L<sub>8</sub>S<sub>8</sub> Rubisco suggests a functional role for the small subunit. *EMBO J.* **9**:2045-2050.
35. **Shively, J. M., G. van Keulen, and W. G. Meijer.** 1998. Something from almost nothing: carbon dioxide fixation in chemoautotrophs. *Annu. Rev. Microbiol.* **52**:191-230.
36. **Sirevåg, R.** 1995. Carbon metabolism in green bacteria., p. 871-883. *In* R. E. Blankenship, Madigan, M. T., and Bauer, C. E. (ed.), *Anoxygenic Photosynthetic bacteria*. Kluwer Academic Publishers, Dordrecht, The Netherlands.
37. **Smith, S. A., and F. R. Tabita.** 2003. Positive and negative selection of mutant forms of prokaryotic (cyanobacterial) ribulose-1,5-bisphosphate carboxylase/oxygenase. *J. Mol. Biol.* **331**:557-569.
38. **Spreitzer, R. J.** 2003. Role of the small subunit in ribulose-1,5-bisphosphate carboxylase/oxygenase. *Arch. Biochem. Biophys.* **414**:141-149.

39. **Spreitzer, R. J., and M. E. Salvucci.** 2002. Rubisco: structure, regulatory interactions, and possibilities for a better enzyme. *Annu. Rev. Plant. Biol.* **53**:449-475.
40. **Stetter, K. O.** 1996. Hyperthermophilic procaryotes. *FEMS Microbiol. Rev.* **18**:149-158.
41. **Tabita, F. R.** 1995. The biochemistry and metabolic regulation of carbon metabolism and CO<sub>2</sub> fixation in purple bacteria., p. 885-914. *In* R. E. Blankenship, Madigan, M. T., and Bauer, C. E. (ed.), *Anoxygenic Photosynthetic bacteria*. Kluwer Academic Publishers, Dordrecht, The Netherlands.
42. **van der Vies, S. M., D. Bradley, and A. A. Gatenby.** 1986. Assembly of cyanobacterial and higher plant ribulose biphosphate carboxylase subunits into functional homologous and heterologous enzyme molecules in *Escherichia coli*. *EMBO J.* **5**:2439-2444.
43. **Watson, G. M., and F. R. Tabita.** 1997. Microbial ribulose 1,5-bisphosphate carboxylase/oxygenase: a molecule for phylogenetic and enzymological investigation. *FEMS Microbiol. Lett.* **146**:13-22.
44. **Watson, G. M., J. P. Yu, and F. R. Tabita.** 1999. Unusual ribulose 1,5-bisphosphate carboxylase/oxygenase of anoxic *archaea*. *J. Bacteriol.* **181**:1569-1575.
45. **Woese, C. R., O. Kandler, and M. L. Wheelis.** 1990. Towards a natural system of organisms: proposal for the domains Archaea, Bacteria, and Eucarya. *Proc. Natl. Acad. Sci. USA* **87**:4576-4579.

## SYNOPSIS

In this study, the author examined the possibilities of utilizing a Type III Rubisco from a hyperthermophilic archaeon as a CO<sub>2</sub>-fixing enzyme in the Calvin-Benson-Bassham (CBB) cycle of a mesophilic photoautotrophic organism. The study was expected to display a novel alternative in Rubisco engineering, which has been hampered by the difficulties in manipulating eukaryotic Type I Rubiscos. The author also aimed to gain insight on the structure-function relationships of the Type III Rubiscos, which have only recently been identified and characterized. The Type III Rubisco from *Thermococcus kodakaraensis* (*Tk*-Rubisco) was chosen as the enzyme for examination based on the following properties. *Tk*-Rubisco (i) was biochemically proven to exhibit Rubisco activity, (ii) is comprised only from large subunits, (iii) is readily expressed in an active form in *Escherichia coli*, (iv) is not inactivated or affected by the presence of oxygen, and (v) harbors a (thermo)stable protein scaffold that can be expected to tolerate a high extent of mutations. *Rhodospseudomonas palustris* was chosen as the mesophilic host cell as the organism displays both heterotrophic and autotrophic modes of growth. This allows one to isolate strains whose endogenous Rubisco gene(s) are disrupted under heterotrophic conditions, as the function of Rubisco is not essential. Furthermore, heterogenous Rubisco genes can be introduced to these strains under heterotrophic conditions. Rubisco function can then be examined with these cells when they are grown under photoautotrophic or photoheterotrophic conditions.

In CHAPTER 1, the author first prepared a mutant strain of *R. palustris* No. 7 whose endogenous Rubisco genes were disrupted. Three Rubisco genes (Type I *rbc<sub>Rp</sub>I-1*,

Type II *rbc<sub>Rp</sub>*II and Type I *rbc<sub>Rp</sub>*I-2) were disrupted, resulting in the isolation of *R. palustris*  $\Delta 3$ . This strain, although displaying normal growth under heterotrophic conditions, was not capable of growing under photoheterotrophic or photoautotrophic conditions, and was thereby utilized as the host strain. The author introduced the *rbc<sub>Tk</sub>* gene into the  $\Delta 3$  strain either on a plasmid, or by integrating a single copy of the gene onto the chromosome. The two transformant strains harboring *rbc<sub>Tk</sub>* displayed growth under photoautotrophic and photoheterotrophic conditions, both dependent on CO<sub>2</sub> fixation. Specific growth rates and Rubisco activity levels were compared under photoheterotrophic conditions among the two transformants and the wild-type strain. An important observation was that the levels of Rubisco activity in the respective cell-free extracts correlated well with the specific growth rates. Immunoprecipitation experiments revealed that Rubisco activity detected in the transformants was derived solely from *Tk*-Rubisco. The results of CHAPTER 1 demonstrated that the Type III *Tk*-Rubisco from a hyperthermophile could support CO<sub>2</sub> fixation in a mesophilic organism, and that the specific growth rate of the transformant can be used as a convenient parameter for selection of engineered proteins with improved Rubisco activity.

In CHAPTER 2, the author utilized the system described above to evaluate the performance of various mutant proteins of *Tk*-Rubisco. Two sets of mutant proteins were designed and constructed, aiming to enhance the catalytic performance of *Tk*-Rubisco in the mesophilic *R. palustris* host cells. The first set was designed to confer greater flexibility to the protein at ambient temperatures. Various residues indicated to form ionic interactions were disrupted by site-directed mutagenesis. A second set was based on sequence differences in the loop6 and  $\alpha$ -helix6 regions among *Tk*-Rubisco and

the enzymes from spinach, *Galdieria partita*, and *Rhodospirillum rubrum*. Structural studies on Type I and Type II enzymes have revealed that loop6 covers the  $\alpha/\beta$  barrel of Rubisco and acts as a lid during Rubisco catalysis. Biochemical studies have confirmed that this region plays a significant role in governing the catalytic properties of Type I and Type II Rubiscos. The author thus replaced various residues or regions of the loop6 region and the adjacent  $\alpha$ -helix6 region of *Tk*-Rubisco with corresponding residues found in the enzymes from spinach, *G. partita*, and *R. rubrum*. Among the two sets of mutant proteins, the latter set had greater effects on the enzymatic performance of *Tk*-Rubisco. Replacing the *Tk*-Rubisco loop6 with the loop6 regions from the three enzymes led to dramatic decreases in activity. Six mutant enzymes, mostly with mutations in the  $\alpha$ -helix6 of *Tk*-Rubisco, were selected and their genes were introduced into *R. palustris*  $\Delta 3$ . Cells harboring mutant protein SP6 displayed a 31% increase in specific growth rate under photoheterotrophic conditions compared to cells harboring the wild-type enzyme. SP6 corresponds to a complete substitution of the original  $\alpha$ -helix6 of *Tk*-Rubisco with that of the spinach enzyme. Compared to the wild-type *Tk*-Rubisco, the purified SP6 mutant protein exhibited a 32% increase in turnover number ( $k_{cat}$ ) of the carboxylase activity and a 17% increase in  $k_{cat}/K_m$  value. The results confirmed that the *R. palustris* system utilized in this chapter can be used to evaluate Rubisco function and indicated that the  $\alpha$ -helix6 region is a promising target for future engineering of *Tk*-Rubisco.

CHAPTER 3 describes a detailed site-directed mutagenesis analysis on the  $\alpha$ -helix6 region of *Tk*-Rubisco. This region was focused upon based on the results of the previous chapter that the mutant protein SP6, which harbors the entire  $\alpha$ -helix6 region of spinach Rubisco, displayed improved catalytic properties at ambient temperatures

compared to the wild-type protein. Single residue replacements were introduced in the SP4 and SP5 proteins, which harbor the N- and C-terminal portions of the spinach  $\alpha$ -helix6 region, respectively. Individual genes were introduced into *R. palustris*  $\Delta 3$ , and specific growth rates were compared under photoheterotrophic conditions. In the N-terminal half of  $\alpha$ -helix6, a Val to Thr replacement at position 330 based on SP4 was found to be the most effective, whereas an Asn to Phe exchange at position 333 based on SP5 was most favorable. It should be noted that the effects of T330 were relevant only when the SP5 portion of the  $\alpha$ -helix6 region was occupied with residues from spinach Rubisco. The activity of the V330T (SP3) and V330T/N333F mutant protein did not reach the levels exhibited by SP5-V330T, indicating the presence of a complex structural relationship among the residues present in the  $\alpha$ -helix6 region.

Among the mutant proteins examined in this and the previous chapter, SP5V-330T displayed the most efficient  $k_{\text{cat}(\text{CO}_2)}/K_{\text{CO}_2}$  value, and supported the highest growth rates under photoheterotrophic conditions when introduced into *R. palustris*  $\Delta 3$ . *R. palustris* cells harboring SP5-V330T displayed a 55% increase in specific growth rate compared to the strain expressing wild-type *Tk*-Rubisco, which corresponds to 80% of that observed in the wild-type *R. palustris* utilizing its three endogeneous Rubiscos.

## CHAPTER 1

### **Phototrophic growth of a Rubisco-deficient mesophilic purple nonsulfur bacterium harboring a Type III Rubisco from a hyperthermophilic archaeon**

#### **INTRODUCTION**

Ribulose-1, 5-bisphosphate carboxylase/oxygenase (Rubisco; EC 4.1.1.39) is the sole CO<sub>2</sub>-fixing enzyme of the Calvin-Benson-Bassham (CBB) pathway. Rubisco and the CBB pathway support the autotrophic growth of all plants, algae, and cyanobacteria, as well as many photoautotrophic and chemoautotrophic bacteria. The Rubisco carboxylase reaction produces two molecules of 3-phosphoglycerate (3-PGA) from ribulose 1, 5-bisphosphate (RuBP), CO<sub>2</sub> and H<sub>2</sub>O. However, the enzyme also catalyzes the addition of O<sub>2</sub> to RuBP, producing one molecule of 3-PGA and 2-phosphoglycolate. This oxygenation reaction, along with the extremely low turnover number of Rubisco proteins, has been considered to be one of the major factors that limit the efficiency of photosynthesis.

Rubiscos involved in the CBB pathway are classified into the Type I and Type II enzymes. Type I Rubiscos are heterohexamers composed of eight large subunits and eight small subunits (L<sub>8</sub>S<sub>8</sub>). They are found in all eukaryotic CBB pathways and are also present in all cyanobacteria and many other autotrophic bacteria. Type II enzymes are composed solely of two large subunits (L<sub>2</sub>), and their distribution is limited to photoautotrophic and chemoautotrophic bacteria. In the case of the Type I Rubiscos in eukaryotic plants and green algae, the large subunit is encoded by the *rbcL* gene residing in the chloroplast, whereas the small subunit is encoded by the nuclear *rbcS* gene (12, 30).

As described in the GENERAL INTRODUCTION, the enhancement of Rubisco activity has been an attractive target of research in the fields of protein and (plant) cell engineering. It has been presumed that increasing the CO<sub>2</sub>-fixing capacity of Rubiscos should lead to direct improvement of agricultural productivity. However, structure-function studies of the eukaryotic Type I enzymes have not seen progress due to the fact that functional expression of these enzymes in conventional host cells such as *Escherichia coli* is not possible (11). This may be related to the complex folding process that takes place in the chloroplast between the nuclear genome-encoded small subunit and the large subunit protein that is produced in the chloroplast. Technology to genetically transform chloroplasts has been developed and utilized in recent years, enabling gene insertion and/or manipulation of genes on the chloroplast genome (plastome) (3). At present, the number of studies with Rubisco is still limited, and further exploration will be needed to produce a functionally active Type I enzyme in the chloroplast. When a large subunit gene from a foreign source is introduced in the plastome, compatibility between the foreign large subunit and the native small subunit seems to be low (18). Incorporating both large and small subunit genes into the plastome leads to the accumulation of unassembled Rubisco proteins (32). One recent breakthrough has been the report on the active production of the Type II Rubisco from *Rhodospirillum rubrum* in tobacco chloroplasts, sufficient to support autotrophic growth (33). This indicates that the chloroplast environment at least allows the proper folding and assembly of highly divergent Rubisco large subunits.

Although archaea do not utilize a CBB pathway, many archaea harbor active Rubisco proteins. The archaeal Rubiscos can be distinguished from the Type I and Type II enzymes in terms of primary structure, and are now classified as Type III enzymes (2,



4). The enzyme from *Thermococcus kodakaraensis* (*Tk*-Rubisco) is composed only of large subunits and forms a novel decameric structure (GENERAL INTRODUCTION, Fig. 8). *Tk*-Rubisco displayed high carboxylase activity at high temperatures, but activity was lower than that of spinach Rubisco at ambient temperature. However, an attractive feature of *Tk*-Rubisco was the fact that the protein was readily produced in an active form in *E. coli*. The thermostable enzyme should also provide a stable protein scaffold that can tolerate high degrees of mutations at ambient temperatures. These properties, along with the unique quaternary structure of the protein, make *Tk*-Rubisco an attractive target for structure-function studies and protein engineering of Rubiscos, and may provide an alternative to the conventional Type I and Type II enzymes.

In this chapter, the author has performed an initial examination as to whether a Type III Rubisco from a hyperthermophilic archaeon could support the growth of a mesophilic, photosynthetic organism. A Rubisco-deficient mutant strain of the purple nonsulfur bacterium *Rhodospseudomonas palustris* No. 7 was constructed and used as the host strain for the expression of the *Tk*-Rubisco gene (*rbc<sub>Tk</sub>*). Recombinant cells with *rbc<sub>Tk</sub>* on a multicopy plasmid, or integrated onto the chromosome as a single copy, were examined for their ability to grow photoautotrophically or photoheterotrophically. Activity and protein levels of *Tk*-Rubisco were investigated and confirmed that the enzyme could support the growth of a mesophilic host organism dependent on CO<sub>2</sub> fixation.

## **MATERIALS AND METHODS**

### **Strains, media, and growth conditions.**

The *rbc<sub>Tk</sub>* gene is derived from *T. kodakaraensis* KOD1, a hyperthermophilic

archaeon isolated from Kodakara Island, Kagoshima, Japan (5, 22). Gene manipulation and plasmid construction was performed with *E. coli* DH5 $\alpha$ , grown aerobically at 37°C in Luria-Bertani (LB) medium (per liter: 10 g Tryptone, 5 g Yeast Extract, 10 g NaCl) with ampicillin (100  $\mu$ g/ml). *E. coli* DH5 $\alpha$  was transformed by the CaCl<sub>2</sub> method. For heterotrophic growth, *R. palustris* No. 7 and its mutants were cultivated aerobically in the dark at 30°C in LB medium. Photoautotrophic growth was carried out under anaerobic conditions with light at 25°C in synthetic minimal medium without Yeast Extract (BS medium) (Table 2) (10) containing 50 mM NaHCO<sub>3</sub> and 50 mM Na<sub>2</sub>S<sub>2</sub>O<sub>3</sub>. The gas phase was exchanged with anaerobic gas (N<sub>2</sub>:CO<sub>2</sub>:H<sub>2</sub>=92:5:3) in an anaerobic chamber for 20 h. Photoheterotrophic growth was carried out with light at 25°C in BS medium containing NaHCO<sub>3</sub> and 50 mM ethanol. In this case, the gas phase was atmospheric air. For both photoautotrophic and photoheterotrophic growth, cells were grown in a sealed glass vial with a rubber serum stopper. When appropriate, media were supplemented with antibiotics.

### **DNA manipulation.**

DNA manipulation was carried out with standard methods as described by Sambrook and Russell (26). Plasmid DNA was isolated with QIAGEN Plasmid Mini Kit (QIAGEN, Hilden, Germany). Restriction enzymes were purchased from Toyobo (Osaka, Japan) or Takara (Kyoto, Japan). DNA ligation was performed with a DNA ligation kit (Toyobo). KOD Plus (Toyobo) was used as a polymerase for PCR, and a GFX PCR DNA and gel band purification kit (GE Healthcare Bio-Sciences, Piscataway, NJ) was used to recover DNA fragments from agarose gels after electrophoresis. DNA sequencing was performed with a BigDye Terminator Cycle sequencing kit (versions

3.0-3.1) and a model 3100 capillary DNA sequencer (Applied Biosystems, Foster City, CA). DNA labeling was carried out with the DIG DNA Labeling and Detection Kit (Roche Diagnostics, Basal, Switzerland).

**Table 1. Bacterial strains and plasmids used in this study.**

Strain or plasmid	Relevant characteristics	Reference or source
<i>E. coli</i>		
DH5 $\alpha$	<i>supE44</i> $\Delta$ <i>lacU169</i> ( $\phi$ 80 <i>lacZ</i> DM15) <i>hsdR17 recA1 endA1 gyrA96 thi-1 relA1</i>	Stratagene
SM10 $\lambda$ pir	<i>thi-1 thr leu tonA lacY supE recA::RP4-2Tc::Mu</i> , Km <sup>r</sup> $\lambda$ pir	(21)
<i>R. palustris</i>		
No.7	Wild-type	(10)
$\Delta$ 3	<i>rbc<sub>RpI-1</sub>::Tc<sup>r</sup> rbc<sub>RpI-2</sub>::Gm<sup>r</sup> rbc<sub>RpII</sub>::Km<sup>r</sup></i>	This study
$\Delta$ 3pRbc <sub>Tk</sub>	$\Delta$ 3 harboring pM3EZRbc	This study
$\Delta$ 3cRbc <sub>Tk</sub>	$\Delta$ 3 with pSZMRbc integrated into the <i>rbc<sub>RpII</sub>::Km<sup>r</sup></i> locus	This study
Plasmids		
pUC118	Ap <sup>r</sup> , $\alpha$ -lac/MCS cloning vector	Takara
pEM7/Zeo	Ap <sup>r</sup> , EM7 promoter-Zeo <sup>r</sup> , pUC <i>ori</i>	Invitrogen
pET-21a(+)/ <i>rbc<sub>Tk</sub></i>	source of <i>rbc<sub>Tk</sub></i> gene	(7)
pBR2119	source of Rubisco gene of <i>Rhodospirillum rubrum</i>	(28)
pBR322	source of Tc <sup>r</sup> gene	Takara
pUC4K	source of Km <sup>r</sup> gene	GE Healthcare Bio-Sciences
pGP704	Ap <sup>r</sup> , <i>ori</i> R6K, <i>mob</i> RP4	(21) (29)
pMG300	pGP704, Gm <sup>r</sup> , source of Gm <sup>r</sup> gene	(15)
pMG301	pGP704, <i>lacZ</i>	This study
pMG802	pMG300, <i>rbc<sub>RpI-1</sub>::Tc<sup>r</sup></i>	This study
pMG412	pMG300, <i>rbc<sub>RpII</sub>::Km<sup>r</sup></i>	This study
pMG822	pMG301, <i>rbc<sub>RpI-2</sub>::Gm<sup>r</sup></i>	This study
pMG103	Km <sup>r</sup> , $\alpha$ -lac/MCS, pHSG298, <i>E. coli</i> - <i>R. palustris</i> shuttle vector	(16)
pM3EZRbc	<i>rbc<sub>Tk</sub></i> expression vector	This study
pSZMRbc	<i>rbc<sub>Tk</sub></i> integration vector	This study

Tc<sup>r</sup>; tetracycline resistant gene, Km<sup>r</sup>; kanamycin resistant gene, Gm<sup>r</sup>; gentamycin resistant gene, Zeo<sup>r</sup>; zeocin resistant gene, Ap<sup>r</sup>; ampicillin resistant gene.

**Table 2. The composition of BS medium.**

NH <sub>4</sub> Cl	1.0 g
KH <sub>2</sub> PO <sub>4</sub>	1.0 g
NaCl	0.1 g
CaCl <sub>2</sub> 2H <sub>2</sub> O	50 mg
MgSO <sub>4</sub> 7H <sub>2</sub> O	0.4 g
Metal solution	0.5 ml
Vitamin solution <sup>a</sup>	1.0 ml
Distilled water <sup>b</sup>	1000 ml

<sup>a</sup> Metal solution

ZnSO <sub>4</sub> 7H <sub>2</sub> O	1000 mg
FeSO <sub>4</sub> 7H <sub>2</sub> O	700 mg
MnSO <sub>4</sub> 4H <sub>2</sub> O	150 mg
CuSO <sub>4</sub> 5H <sub>2</sub> O	50 mg
CoCl <sub>2</sub> 6H <sub>2</sub> O	20 mg
Na <sub>2</sub> MoO <sub>4</sub>	75 mg
EDTA 2Na	250 mg
Distilled water	100 ml

<sup>b</sup> Vitamin solution

D-Biotin	1.0 mg
Nicotinic acid	100 mg
Thiamine HCl	20 mg
<i>p</i> -Aminobenzoic sodium salt	100 mg
Distilled water	100 ml

**Isolation and disruption of Rubisco genes (Type I *rbc<sub>Rp</sub>I-1* and Type II *rbc<sub>Rp</sub>II*) from *R. palustris* No. 7.**

A genomic DNA library of *R. palustris* No. 7 was screened by colony hybridization with a DNA probe encoding the Rubisco gene of *Rhodospirillum rubrum* (2.4-kb BamHI-BamHI DNA fragment from plasmid pRR2119) (28). Plasmids were designed to disrupt each Rubisco gene via double crossover homologous recombination. pMG300 (15), which harbors a gentamycin resistant marker gene on pGP704 (21) for counterselection of single crossover transformants, was applied. A DNA fragment containing the tetracycline resistant marker gene (Tc<sup>r</sup>) was amplified from plasmid pBR322 (Takara). The fragment was inserted within the Type I-1 coding region at a BglIII site, inactivating the gene. This fragment was then inserted into pMG300 at the XbaI site, resulting in pMG802. Likewise, a DNA fragment containing the kanamycin

resistant marker gene ( $Km^r$ ) was isolated from plasmid pUC4K (GE Healthcare Bio-Sciences) and inserted within the Type II coding region at the XhoI site. This fragment was then inserted into pMG300 at the XbaI site, resulting in pMG412. *R. palustris* was transformed by conjugation as described elsewhere (15), leading to the isolation of strain  $\Delta I-1\Delta II$ .

### **Purification of a third Rubisco (Type I-2 *rbc<sub>RP</sub>I-2*) from *R. palustris*.**

The *R. palustris*  $\Delta I-1\Delta II$  strain was cultured photoheterotrophically in 30 L of BS medium containing 50 mM ethanol and 20 mM  $NaHCO_3$ . All procedures indicated below were performed at 4°C. After cultivation, harvested cells were suspended in 600 ml of 50 mM Tris-HCl (pH 8.5) containing 1 mM dithiothreitol (DTT) and 1 mM phenylmethylsulfonyl fluoride (PMSF). Cells were disrupted by sonication, and cell-free extracts were prepared. Ammonium sulfate was added to a final concentration of 2.5 M, and incubated for 2 h. After centrifugation, ammonium sulfate was added to the supernatant to a final concentration of 6 M, and incubated for 12 h. The pellet after centrifugation was dissolved in 50 mM Tris-HCl (pH 8.5) containing 1 mM DTT, and dialyzed with the same solution. The sample was then applied to an anion-exchange column, Super-Q Toyopearl (Tosoh, Tokyo, Japan). After washing with 50 mM Tris-HCl containing 1 mM DTT, proteins were eluted with a 0-0.6 M NaCl gradient. To the fraction with carboxylase activity, ammonium sulfate was added to a final concentration of 2.5 M, and applied to a hydrophobic column, Butyl-Toyopearl (Tosoh). After washing with 2.5 M ammonium sulfate, 1 mM DTT in 50 mM Tris-HCl (pH 8.5), proteins were eluted with a 2.5-0 M ammonium sulfate gradient. To the fraction with carboxylase activity, ammonium sulfate was added to a final concentration of 6 M, and

incubated for 12 h. The precipitate was dissolved in 50 mM Tris-HCl (pH 8.5) containing 1 mM DTT, and applied to a gel-filtration column, Cellulofine GCL-2000 (Seikagaku Kogyo, Tokyo, Japan) equilibrated with the same buffer. Fractions with activity were collected and analyzed by sodium dodecylsulfate polyacrylamide gel electrophoresis (SDS-PAGE) as described elsewhere (19).

#### **Determination of N-terminal amino acid sequences.**

In order to determine N-terminal amino acid sequences, proteins were electroblotted onto a polyvinylidene difluoride membrane after SDS-PAGE. The membrane was stained with an amido black solution (1.5% amido black, 30% methanol, 10% acetic acid) for 2 min and destained with 30% methanol/10% acetic acid. N-terminal amino acid sequences were determined with a protein sequencer (491 cLC; Applied Biosystems).

#### **Isolation and disruption of the Type I-2 Rubisco gene (*rbc<sub>Rp</sub>I-2*) from *R. palustris*.**

Degenerate PCR was performed to amplify the *rbc<sub>Rp</sub>I-2* gene from genomic DNA of *R. palustris* No. 7, using two primers, Nu-2 and RBC0. Nu-2 (5'-MGIGGIAARGAYMGITAYMG-3') was designed from the N-terminal amino acid sequence, and RBC0 (5'-IARICCIARYTTIGGYTT-3') from a conserved region in various Rubiscos (M, A/C; I, inosine; R, A/G; Y, C/T). A 364 bp fragment from 43 bp to 406 bp in the *rbc<sub>Rp</sub>I-2* sequence was used as a DNA probe for colony hybridization. The *rbc<sub>Rp</sub>I-2* disruption vector pMG822 was constructed for disruption of *rbc<sub>Rp</sub>I-2* by double crossover homologous recombination. A DNA fragment containing the gentamycin resistant marker gene ( $Gm^r$ ) was isolated from plasmid pMG300 and inserted within the

Type I-2 coding region at an SfiI site. This fragment was then inserted into the SmaI site of pMG301, which harbors a *lacZ* gene on pGP704 for counterselection of single-crossover transformants. *R. palustris* ( $\Delta$ I-1 $\Delta$ II) was transformed by conjugation, leading to the isolation of *R. palustris*  $\Delta$ 3.

### **Construction of expression and integration vectors.**

pM3EZRbc was constructed for expression of *rbc<sub>Tk</sub>* in *R. palustris*  $\Delta$ 3. First, the author prepared a *R. palustris* No. 7 phosphoenolpyruvate carboxykinase (PEPCK) promoter (15) cassette. A DNA fragment including the PEPCK promoter region and a small portion of the PEPCK coding region (-165 to +26 relative to the initiation codon) was amplified from the genomic DNA of *R. palustris* No. 7 using the primers pckpF (5'-GGCGGTAAACGAATTCATGCCGGCCGGGTTGGC-3', the introduced EcoRI site is underlined) and pckpR (5'-CCGTTATGGTTCGACCGTCTCTTGCATATG TGGATCCTCCTCG -3', the introduced Sall, NdeI, BamHI sites are underlined). The fragment was digested with EcoRI and Sall, and ligated with pUC118 (Takara) digested with the same enzymes. The plasmid was then digested with BamHI and NdeI, and a BamHI-NdeI fragment including the entire *rbc<sub>Tk</sub>* gene digested from pET-21a (+)/*rbc<sub>Tk</sub>* (7) was inserted into the plasmid. The PEPCK promoter (-149 to -6) - *rbc<sub>Tk</sub>* fusion gene was introduced into the *E. coli-R. palustris* shuttle vector pMG103 (16) at the EcoRI and Sall sites, giving pM3Rbc. Finally, an EM7 promoter-Zeo<sup>r</sup> cassette was amplified from pEM7/Zeo (Invitrogen, Carlsbad, CA) by the use of primers ZeoF (5'-GCAAGGTCGACACGTGTTGACAATTAATC-3', the introduced Sall site is underlined), and ZeoR (5'-AAGGGTCTGACTCAGTCCTGCTCCTCGGCCACG-3' the introduced Sall site is underlined), and inserted downstream of *rbc<sub>Tk</sub>* on pM3Rbc.

pSMZRbc was constructed for single-copy insertion of *rbc<sub>TK</sub>* into the *R. palustris*  $\Delta 3$  genome by homologous single-crossover recombination. First, the author introduced the PEPCK promoter (-149 to -6) - *rbc<sub>TK</sub>* fusion gene into the pEM7/Zeo vector at EcoRI and SalI sites, giving pEM7/Zeo/*rbc<sub>TK</sub>*. The *rbc<sub>RpII</sub>::Km<sup>r</sup>* region (1772 bp) for homologous recombination was amplified from the genomic DNA of *R. palustris*  $\Delta 3$  with primers *rbcRpIIF* (5'-GAAGATCTGGCGATGACCGGCGTGTTCCGCAAGGTCG-3', the introduced BglII site is underlined) and *kanaR* (5'-AAGGAAAAAGCGGCCGCAAATCACCATGAGTGACGACTGAATCCGGTG-3', the introduced NotI site is underlined). This fragment was ligated with pEM7/Zeo/*rbc<sub>TK</sub>* digested with BglII and NotI, giving pSZMRbc. *R. palustris*  $\Delta 3$  was transformed by electroporation (6). Transformants were selected on LB medium containing zeocin and appropriate antibiotics.

### **Southern blot analysis.**

The probe corresponding to *rbc<sub>RpII</sub>* was constructed for the confirmation of single-crossover insertion of pSZMRbc into the *R. palustris*  $\Delta 3$  chromosome, using the primers *rbcM-F* (5'-CCTCAACCTCAAAGAGAGCGAGCTGATCGC-3') and *rbcM7-R* (5'-CCGCGCGCCAGCATCTCGTAGTG-3'). Hybond-N<sup>+</sup> membranes (GE Healthcare Bio-Sciences) were used for blotting. Total DNA (4  $\mu$ g) was digested with KpnI for 24 h at 37°C, and applied to agarose gel electrophoresis.

### **Growth measurements.**

Cells were first cultivated in LB medium supplemented with the appropriate antibiotics for 2 d. Cells were collected and the pellet was washed and resuspended in



BS medium containing 50 mM NaHCO<sub>3</sub>, and 50 mM Na<sub>2</sub>S<sub>2</sub>O<sub>3</sub> or 50 mM ethanol. Cells were inoculated at an initial OD<sub>660</sub> of 0.1 into the same medium. After 10-20 d, cells in the log phase were harvested, washed, and inoculated into BS medium containing 0, 2, 10, or 50 mM NaHCO<sub>3</sub>, with 50 mM Na<sub>2</sub>S<sub>2</sub>O<sub>3</sub> or 50 mM ethanol at an initial OD<sub>660</sub> of 0.05. The phototrophic cultures were performed with a light intensity of 2,400-2,500 lux. These cultures were used to measure specific growth rates. Growth levels were measured by sampling 100 µl aliquots of the culture. All cultures were performed in duplicate.

#### **Activity measurements.**

For preparing cell-free extracts, cells in the log phase of photoheterotrophic culture were harvested by centrifugation (10 min, 5,000 x g, 4°C) and washed with 100 mM Bicine-NaOH (pH 8.3), 10 mM MgCl<sub>2</sub> (buffer A). The pellet was resuspended in the same buffer and disrupted by sonication on ice for thirty 10 sec periods, each interrupted by 20 sec cooling intervals. Cell debris was removed by centrifugation (5 min, 5,000 x g, 4°C) and ultra centrifugation (20 min, 110,000 x g, 4°C). The protein concentration was determined with a protein assay kit (Bio-Rad, Hercules, CA), according to the instructions from the manufacturer using bovine serum albumin as a standard. The supernatant was diluted to 1 mg/ml with buffer A and used as the cell-free extract for enzyme assays. Carboxylase activity was measured as described elsewhere (27) with slight modifications. (i) 40 µl of 2 mM NADH in buffer A, (ii) 40 µl of 100 mM RuBP in buffer A, (iii) 200 µl of 10 mM ATP, 20 mM MgCl<sub>2</sub>, and 10 mM reduced glutathione in 200 mM Bicine-NaOH (pH 8.3), (iv) 40 µl of coupling enzyme solution, and (v) 40 µl of cell-free extract were thoroughly mixed. The coupling enzyme solution

contained 563 units/ml 3-phosphoglycerate phosphokinase, 125 units/ml glyceraldehyde-3-phosphate dehydrogenase, 260 units/ml triose-phosphate isomerase, and 22.5 units/ml glycerophosphate dehydrogenase with 5 mM reduced glutathione, 0.1 mM EDTA, 20% glycerol in 50 mM Bicine-NaOH (pH 8.0). Separately, 40  $\mu$ l of 1 M NaHCO<sub>3</sub> was prepared. Both solutions were incubated at 25°C for 3 min in order to equilibrate the solution temperature. After confirming a steady value of OD<sub>340</sub> in the former solution, assays were initiated by adding the NaHCO<sub>3</sub>. The linear decrease in absorbance at 340 nm was measured. All assays were performed in at least duplicate.

#### **Western blot analysis and immunoprecipitation.**

SDS-PAGE was performed with 12.5% gels. Proteins were blotted from the polyacrylamide gel to polyvinylidene difluoride membranes (Millipore, Bedford, MA). Antisera, containing polyclonal rabbit antibodies against purified, recombinant *Tk*-Rubisco, were diluted 1,000-fold and used to detect recombinant *Tk*-Rubisco in *R. palustris* strains. Immunoprecipitation experiments have been described elsewhere (20). Resin with or without antibodies were mixed with the cell-free extracts at 4°C for 2 h. Supernatants after the resin was removed were used for activity measurements.

## **RESULTS**

#### **Construction of a Rubisco deletion mutant of *Rhodospseudomonas palustris*.**

*Rhodospseudomonas palustris* is a purple nonsulfur photosynthetic bacterium belonging to the  $\alpha$ -proteobacteria, and is widely distributed in nature. These organisms are metabolically versatile and capable of growth in four metabolic modes: photosynthetic, photoheterotrophic, chemoheterotrophic, and chemoautotrophic (14). As

a host cell that can grow both autotrophically and heterotrophically is essential for constructing Rubisco-deficient cells in order to examine the functional capacity of *Tk*-Rubisco *in vivo*, the author selected *R. palustris* No. 7 as the host strain in this study.

In order to accurately examine the *in vivo* function of *Tk*-Rubisco in *R. palustris*, the removal of endogenous Rubisco proteins was necessary. Using the Rubisco gene from *Rhodospirillum rubrum* as a probe, two Rubisco genes from *R. palustris* No. 7 (Type I *rbc<sub>Rp</sub>I-1* and Type II *rbc<sub>Rp</sub>II*) were identified and isolated. The *rbc<sub>Rp</sub>I-1* gene was disrupted with a tetracycline resistant marker gene ( $Tc^r$ ) and the *rbc<sub>Rp</sub>II* gene with a kanamycin resistant marker gene ( $Km^r$ ) (Fig. 1A). After isolating the double gene disruption mutant ( $\Delta I-1\Delta II$ ) and confirming the genotype, the cells were grown under photoheterotrophic conditions. Surprisingly, photoheterotrophic growth of the  $\Delta I-1\Delta II$  strain was observed, suggesting the presence of further Rubisco gene(s). Rubisco activity was detected in these cells, and the activity was strictly inhibited in the presence of 25  $\mu$ M 2-carboxyarabinitol 1, 5-bisphosphate (CABP), a well known Rubisco inhibitor. By purifying the protein and determining its N-terminal amino acid sequence, a third Rubisco gene (Type I *rbc<sub>Rp</sub>I-2*) was identified. This gene was disrupted from the  $\Delta I-1\Delta II$  strain with a gentamycin resistant marker gene ( $Gm^r$ ), leading to the isolation of the triple gene disruptant mutant  $\Delta I-1\Delta I-2\Delta II$  (*R. palustris*  $\Delta 3$ , Table 1). The genotype of this strain was confirmed by PCR (Fig. 1B) and DNA sequencing (data not shown). Although the  $\Delta 3$  strain displays similar growth levels to strain No. 7 under heterotrophic conditions, its ability to grow photoautotrophically or photoheterotrophically is completely abolished (see below).

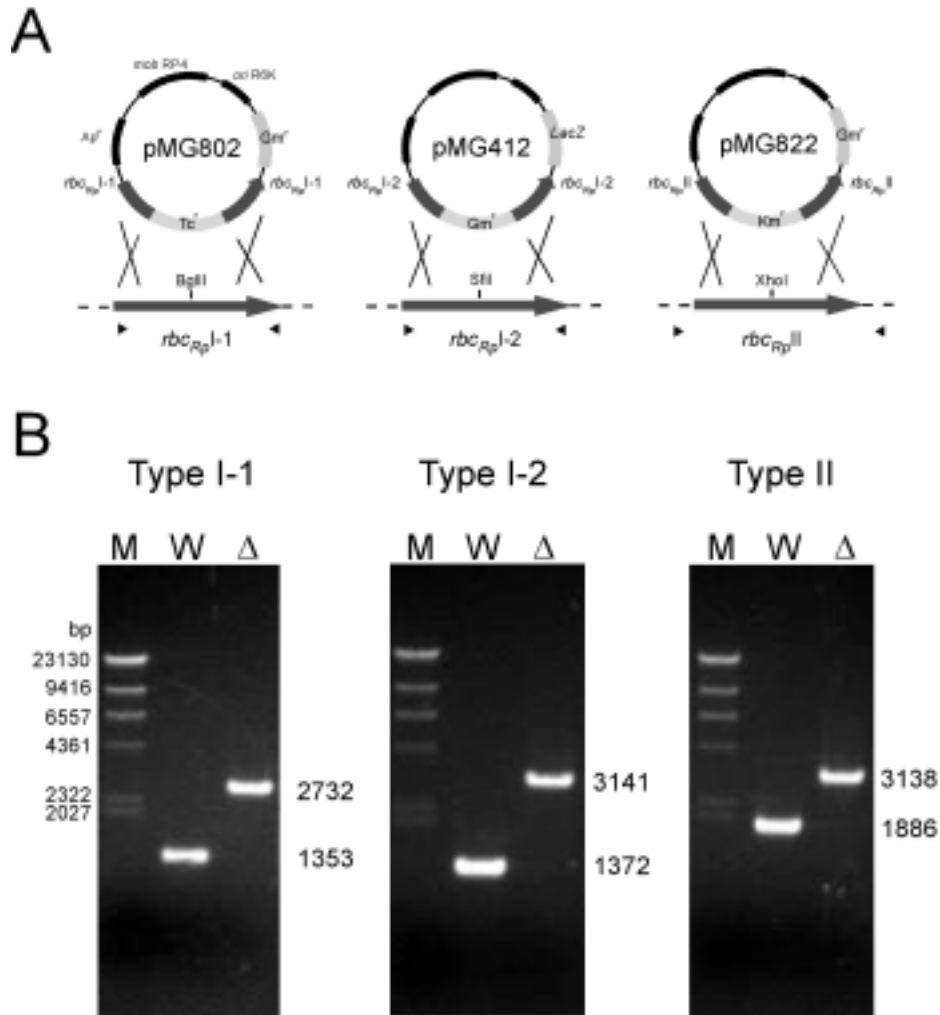


**Fig. 1. Disruption of *rbc<sub>Rp</sub>* genes.** (A) Strategy and plasmid constructs used for disruption of the *rbc<sub>Rp</sub>I-1*, *rbc<sub>Rp</sub>I-2*, and *rbc<sub>Rp</sub>II* genes of *R. palustris* via double-crossover recombination. Marker genes were inserted into the restriction sites indicated in the central region of each gene. (B) Confirmation of *rbc<sub>Rp</sub>* gene disruption by PCR analysis. The positions of the primers are indicated with arrowheads in (A). Each locus was amplified from the *R. palustris* No. 7 (W) and the *R. palustris* Δ3 (Δ) genomic DNA. The increase in size of PCR fragments confirms the insertion of the marker genes into the chromosome. The expected number of base pairs in each DNA fragment is indicated at the right side of each panel.

### **Introduction of the *rbc<sub>Tk</sub>* gene into *R. palustris* $\Delta 3$ .**

The author designed two plasmids to introduce the *rbc<sub>Tk</sub>* gene into the mesophilic *R. palustris*  $\Delta 3$ . The plasmid pM3EZRbc, deriving from an *E. coli*-*R. palustris* shuttle vector pMG103 (16), was constructed so that the *rbc<sub>Tk</sub>* gene would be present on an autonomously replicating plasmid. A zeocin resistant marker gene (*Zeo<sup>r</sup>*) was inserted into the plasmid, and the *rbc<sub>Tk</sub>* gene was placed downstream of the phosphoenolpyruvate carboxykinase (PEPCK) promoter (15) from *R. palustris* No. 7 (Fig. 2A). Alternatively, in order to limit the copy number of the *rbc<sub>Tk</sub>* gene, the author constructed the plasmid pSMZRbc, designed for single-crossover insertion into the *R. palustris*  $\Delta 3$  chromosome (Fig. 2B). The locus for insertion was that of the Type II Rubisco of *R. palustris*, disrupted with the kanamycin resistant gene described above.

pM3EZRbc was introduced into the *R. palustris*  $\Delta 3$  strain, and transformants able to grow on LB plate medium containing 200  $\mu\text{g/ml}$  zeocin were selected. Stable maintenance of the plasmid was observed when zeocin was present in the medium at 150  $\mu\text{g/ml}$ . A selected transformant was designated as strain  $\Delta 3\text{pRbc}_{\text{Tk}}$ . The plasmid pSMZRbc was also introduced into *R. palustris*  $\Delta 3$ , and zeocin-resistant transformants were selected on LB medium containing 400  $\mu\text{g/ml}$  zeocin. PCR analyses and Southern blot analyses were performed to confirm the genotype of a selected transformant (strain  $\Delta 3\text{cRbc}_{\text{Tk}}$ ) (Fig. 2C). The increase in length of the signal observed with the genomic DNA of  $\Delta 3\text{cRbc}_{\text{Tk}}$  compared to that of  $\Delta 3$  confirmed that strain  $\Delta 3\text{cRbc}_{\text{Tk}}$  harbored only one copy of the *rbc<sub>Tk</sub>* gene integrated into the chromosome.

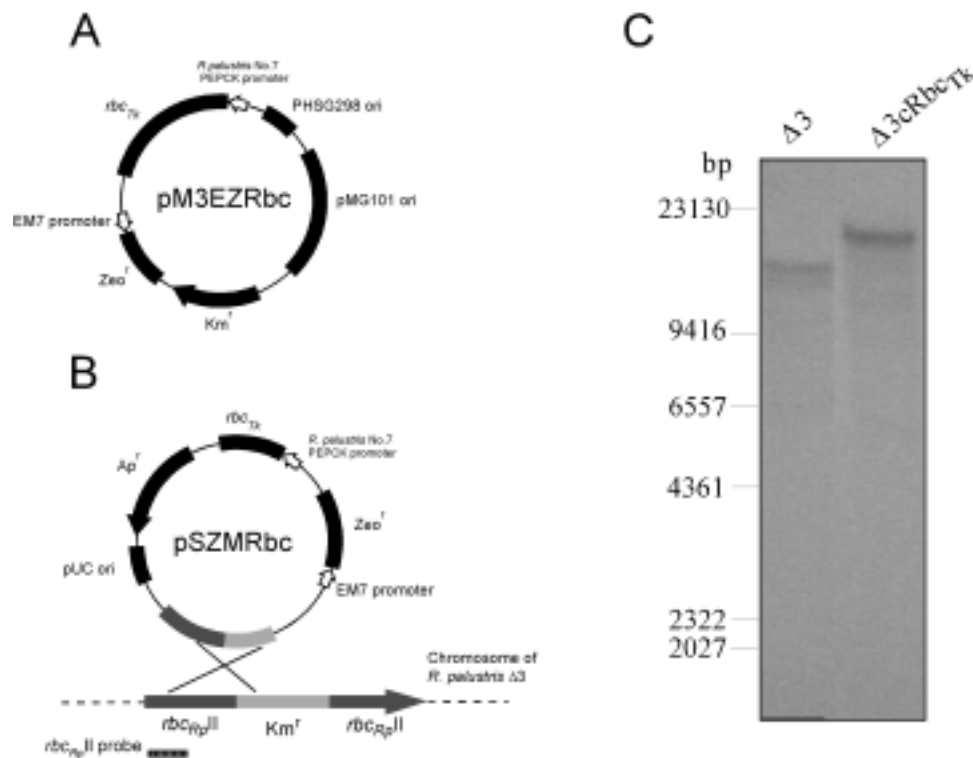


**Fig. 2. Schematic drawings of the plasmids pM3EZRbc (A) and pSZMRbc (B) used to introduce the *rbc<sub>Tk</sub>* gene into *R. palustris* Δ3. (C) Southern blot analysis using the *rbc<sub>RpII</sub>* probe. Genomic DNA of *R. palustris* Δ3 and Δ3cRbc<sub>Tk</sub> were digested with KpnI and hybridized with the *rbc<sub>RpII</sub>* probe.**

### **Photoautotrophic growth of the recombinant strains Δ3pRbc<sub>Tk</sub> and Δ3cRbc<sub>Tk</sub>.**

Δ3pRbc<sub>Tk</sub> and Δ3cRbc<sub>Tk</sub> were cultivated aerobically in LB medium for 2 d, and the cells were washed and transferred to BS medium containing NaHCO<sub>3</sub> as the sole carbon source and Na<sub>2</sub>S<sub>2</sub>O<sub>3</sub> as an electron donor. The gas phase was exchanged with N<sub>2</sub>:CO<sub>2</sub>:H<sub>2</sub> = 92:5:3, in order to remove oxygen. After 5 d, cell growth of Δ3pRbc<sub>Tk</sub> was clearly observed (Fig. 3), along with the wild-type No. 7 strain. After 12 d, the author also observed growth of Δ3cRbc<sub>Tk</sub>. The specific growth rates of the three strains were

0.030 (No. 7), 0.023 ( $\Delta 3pRbc_{Tk}$ ), and 0.016 ( $\Delta 3cRbc_{Tk}$ )  $h^{-1}$ . The results indicated that the  $rbc_{Tk}$  gene was expressed in *R. palustris*  $\Delta 3$ , leading to an active *Tk*-Rubisco protein that could support photoautotrophic growth in *R. palustris*. When atmospheric air was present in the gas phase of the cultures, the author did not observe photoautotrophic growth. This was the case in both recombinant strains, as well as in the wild-type No. 7 strain.

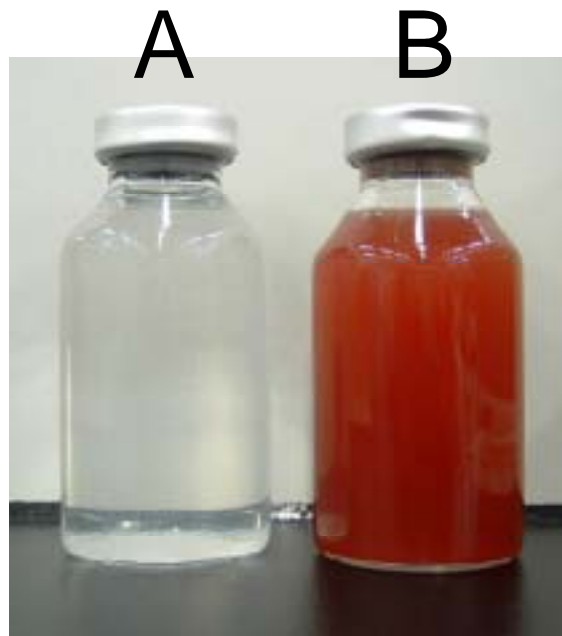


**Fig. 3. Cultures of the (A)  $\Delta 3$  strain and (B)  $\Delta 3pRbc_{Tk}$  strain after 14 days under photoautotrophic conditions are shown.**

#### **Comparison of growth rates among *R. palustris* No. 7, $\Delta 3pRbc_{Tk}$ , and $\Delta 3cRbc_{Tk}$ .**

The author next grew the recombinant cells under photoheterotrophic conditions by replacing  $Na_2S_2O_3$  with the addition of 50 mM ethanol. Under these

conditions, cell yield is enhanced, but growth is still dependent on a functional CBB pathway. No growth was observed when cells were grown in sealed vials depleted of CO<sub>2</sub> by purging with argon gas. The author determined the specific growth rates of the wild-type *R. palustris* No. 7 and the recombinant strains  $\Delta 3pRbc_{Tk}$  and  $\Delta 3cRbc_{Tk}$  under photoheterotrophic conditions. The gas phase in these experiments was atmospheric air. NaHCO<sub>3</sub> was added at a concentration of 50 mM and the vials were incubated at 25°C with 2,500 lux illumination. Representative growth curves are shown in Fig. 4A. No growth was observed for *R. palustris*  $\Delta 3$ , confirming that an active Rubisco was necessary for growth under these conditions. However, in the mutant strains harboring *Tk*-Rubisco, photoheterotrophic growth was clearly observed. Both mutants exhibited lower growth rates than that of the wild-type strain, with  $\Delta 3cRbc_{Tk}$ , harboring only a single copy of *rbc<sub>Tk</sub>*, displaying slowest growth. The specific growth rates of each strain calculated from multiple experiments were 0.040 (No. 7), 0.026 ( $\Delta 3pRbc_{Tk}$ ), and 0.019 ( $\Delta 3cRbc_{Tk}$ ) h<sup>-1</sup>.

The author next examined the effects of the NaHCO<sub>3</sub> concentration in the medium on the growth of the three strains (Fig. 4B). NaHCO<sub>3</sub> was added at concentrations of 0, 2, 10, and 50 mM. All strains displayed equivalent growth rates at concentrations between 2 and 50 mM NaHCO<sub>3</sub>, with only the cell yield affected. The author also observed growth in media where no NaHCO<sub>3</sub> was added, indicating that the cells could grow on the low levels of CO<sub>2</sub> dissolved in the media deriving from atmospheric air.



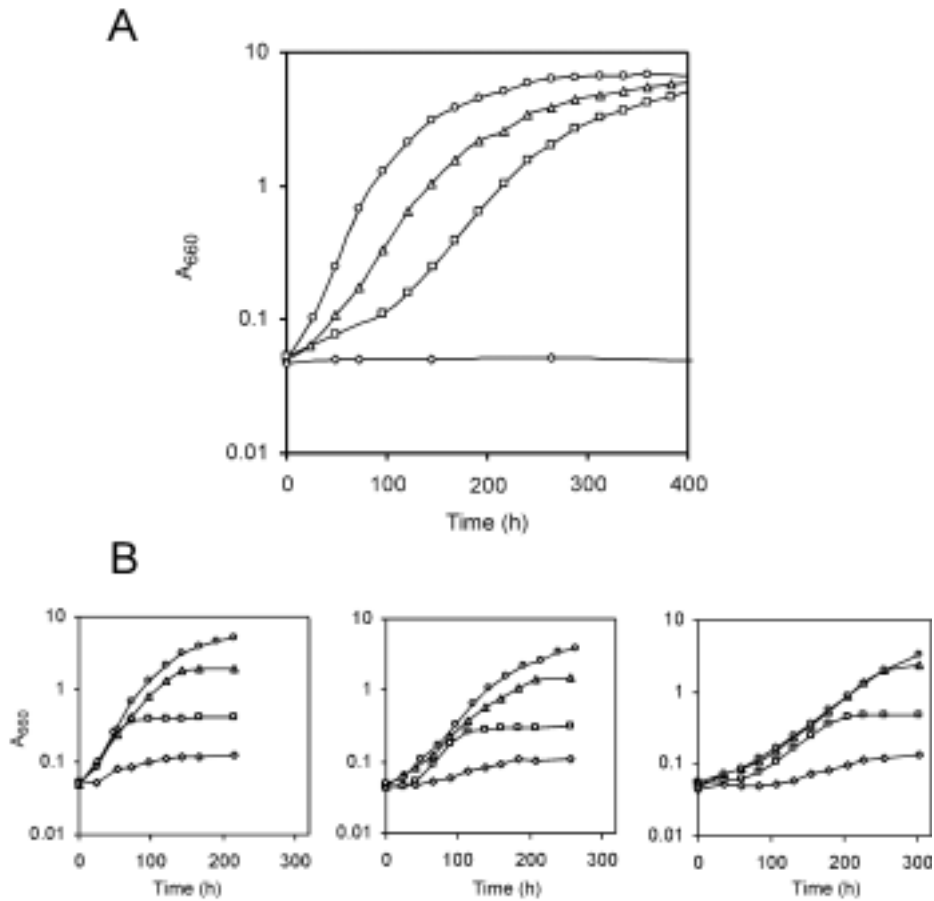


**Fig. 4. Growth curves of *R. palustris* under photoheterotrophic conditions.**

Exponentially growing cells from a photoheterotrophic medium were inoculated into fresh medium except for  $\Delta 3$ . Strain  $\Delta 3$  was cultivated in LB medium, and inoculated into photoheterotrophic medium. (A) The growth curves of *R. palustris* No. 7 (circles),  $\Delta 3pRbc_{TK}$  (triangles),  $\Delta 3cRbc_{TK}$  (squares) and  $\Delta 3$  (diamonds) with the addition of 50 mM  $NaHCO_3$ . (B) Growth curves of *R. palustris* No. 7 (left panel),  $\Delta 3pRbc_{TK}$  (middle panel), and  $\Delta 3cRbc_{TK}$  (right panel) with the addition of 0 mM (diamonds), 2 mM (squares), 10 mM (triangles), and 50 mM (circles) of  $NaHCO_3$ .

### Expression levels of *Tk*-Rubisco in *R. palustris*.

As the growth experiments indicated that *Tk*-Rubisco could support CO<sub>2</sub> fixation in *R. palustris*, the intracellular levels of *Tk*-Rubisco protein were examined.  $\Delta 3pRbc_{Tk}$ ,  $\Delta 3cRbc_{Tk}$  and the wild-type *R. palustris* No. 7 strains were grown photoheterotrophically, and Western blot analysis was performed using polyclonal rabbit antibodies raised against purified recombinant *Tk*-Rubisco (Fig. 5). The antibodies did not cross-react with any of the Rubiscos from the wild-type *R. palustris* No. 7 (lane 1). A specific band with a molecular mass identical with the purified *Tk*-Rubisco protein was observed in the cell extracts of  $\Delta 3pRbc_{Tk}$  and  $\Delta 3cRbc_{Tk}$ . The amount of *Tk*-Rubisco was higher in  $\Delta 3pRbc_{Tk}$  than in  $\Delta 3cRbc_{Tk}$ . The protein was also found to be thermostable, as it did not precipitate with heat treatment at 85°C for 15 min (Fig. 5, lanes 3 and 5). This clearly indicates that *Tk*-Rubisco was produced and present in the recombinant *R. palustris* cells.

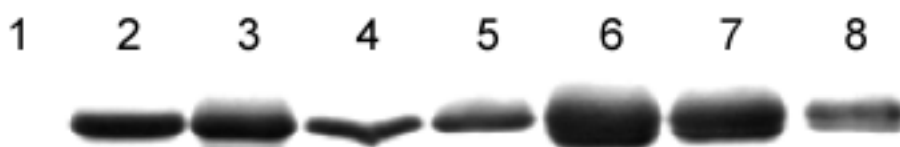


**Fig. 5. Western blot analysis of cell-free extracts from exponentially growing *R. palustris* cells using polyclonal antibodies against *Tk*-Rubisco.** Lane 1; *R. palustris* No. 7 (10 μg), lane 2;  $\Delta 3pRbc_{Tk}$  (10 μg), lane 3; supernatant after heat-treatment (85°C, 15 min) of  $\Delta 3pRbc_{Tk}$  (cell free extracts), lane 4;  $\Delta 3cRbc_{Tk}$  (10 μg), lane 5 (cell free extracts); supernatant after heat-treatment (85°C, 15 min) of  $\Delta 3cRbc_{Tk}$ , lanes 6, 7, 8; purified recombinant *Tk*-Rubisco (1.3 μg, 0.65 μg, and 0.13 μg, respectively).

### Carboxylase activities in the wild-type, $\Delta 3pRbc_{Tk}$ , and $\Delta 3cRbc_{Tk}$ strains.

The author further measured the carboxylase activities in the cell-free extracts from the three strains at ambient temperature (25°C). Along with the wild-type strain, the author observed significant levels of carboxylase activity in the recombinant strains. The specific activities detected in the recombinant strains were lower than that of the wild-type strain, and as expected from the results of Western blot analysis, Rubisco activity in  $\Delta 3cRbc_{Tk}$  was lower than that in  $\Delta 3pRbc_{Tk}$  (Table 3). Taken together with the observed growth rates (Fig. 4), the specific activities and the amount of *Tk*-Rubisco protein seem to correlate well with the specific growth rates of these three strains.

**Table 3. Rubisco activities of cell-free extracts from exponentially growing cells and their specific growth rates.**

	Specific activity ( $\mu\text{mol}/\text{min}/\text{mg}$ )	Total activity ( $\mu\text{mol}/\text{min}$ ) <sup>a</sup>		Specific growth rate ( $\text{h}^{-1}$ )
		(a)	(b)	
<i>R. palustris</i> No. 7	0.028	0.028	0.001	0.037
$\Delta 3pRbc_{Tk}$	0.018	0.018	0.018	0.026
$\Delta 3cRbc_{Tk}$	0.008	0.008	0.008	0.019

<sup>a</sup> (a) Total activity of cell-free extracts before heat treatment. (b) Total activity of cell-free extracts after heat treatment (85°C, 15 min).

In order to determine whether the carboxylase activity in  $\Delta 3pRbc_{Tk}$  derived solely from *Tk*-Rubisco, the author carried out immunoprecipitation experiments with the polyclonal antibodies against recombinant *Tk*-Rubisco (Fig. 6). In the wild-type No. 7 strain, addition of antibodies to the resin did not lead to a major decrease in Rubisco activity after precipitation. In contrast, almost all the Rubisco activity observed in the

cell-free extracts of  $\Delta 3pRbc_{Tk}$  was removed after immunoprecipitation. The residual activity found in  $\Delta 3pRbc_{Tk}$  was completely excluded with a second experiment. These results demonstrate that *Tk*-Rubisco, a Type III Rubisco from a hyperthermophilic archaeon, can function as the CO<sub>2</sub>-fixing enzyme of the CBB cycle in the mesophilic *R. palustris*  $\Delta 3$ .

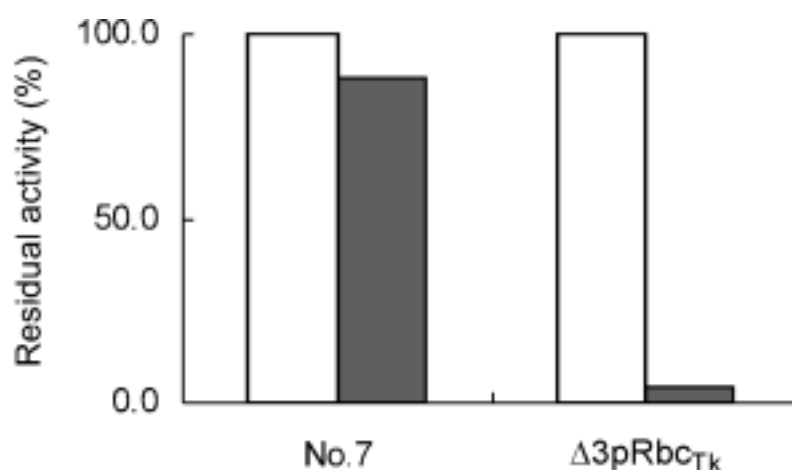


**Fig. 6. Residual Rubisco activities in the supernatant after immunoprecipitation.** Immunoprecipitation experiments were performed against the cell-free extracts of strains No. 7 and  $\Delta 3pRbc_{Tk}$ . Closed bars indicate the residual Rubisco activity using resin coated with anti- *Tk*-Rubisco antibodies. Residual activity after precipitation using resin without antibodies was defined as 100% (open bars).

## DISCUSSION

The results of this chapter have revealed that *R. palustris* No. 7 harbors three Rubisco enzymes, two Type I enzymes (Type I-1 and Type I-2) and a single Type II Rubisco. As the disruption of these three genes led to a strain that could not grow under photoautotrophic or photoheterotrophic conditions, it can be presumed that the three enzymes are the only functional Rubiscos in *R. palustris* No. 7. It is also known that

*Acidithiobacillus ferrooxidans* (13) and *Hydrogenovibrio marinus* (23, 34) have three sets of Rubisco genes, composed of two Type I and one Type II enzymes. Previous studies have implied that the expression levels of these multiple Rubisco genes are regulated in response to the CO<sub>2</sub> concentration in the cell environment (35).

In order to obtain a suitable host cell to evaluate the CO<sub>2</sub>-fixing capacities of *Tk*-Rubisco and its mutant proteins in future research, the author constructed a Rubisco deficient mutant strain *R. palustris* Δ3. Similar approaches have been reported in order to express exogenous Rubisco genes, and for the *in vivo* selection of Rubisco mutant proteins (1, 8, 24).

Finn et al. have previously demonstrated that the Type III Rubisco gene (*rbcL*) from a mesophilic heterotrophic methanogen *Methanosarcina acetivorans* complemented Rubisco deletion mutants of the photosynthetic bacteria *Rhodobacter capsulatus* and *Rhodobacter sphaeroides* under photoautotrophic and photoheterotrophic growth conditions at ambient temperature (9). This clearly indicated that mesophilic, archaeal Type III Rubiscos are able to replace the function of bacterial Rubiscos that support autotrophic growth. On the other hand, the Type III Rubisco from the hyperthermophilic archaeon *Methanococcus jannaschii* was expressed and found to assemble in a catalytically active state in the photosynthetic bacteria, but could not support the photoautotrophic or photoheterotrophic growth of these strains. This may be due to the large difference between the temperature at which the *M. jannaschii* Rubisco functions and the growth temperature of the host strain. Although much lower than the activity levels observed at high temperatures, *Tk*-Rubisco does exhibit carboxylase activity at ambient temperatures (7), and this activity can be presumed to be supporting the growth of the transformants observed in this study. In addition, it was found that

anaerobic conditions were necessary for *R. capsulatus* and *R. sphaeroides* Rubisco deletion mutants harboring *M. acetivorans* Rubisco to grow photoautotrophically and photoheterotrophically. This may be due to the high sensitivity to molecular oxygen observed for these enzymes (9, 31). *Tk*-Rubisco, although deriving from an anaerobic host, has been previously found to be unaffected by exposure to oxygen (7). This may be one of the reasons that enable the *R. palustris*  $\Delta 3$  strains harboring *Tk*-Rubisco to grow photoheterotrophically without an exchange to a strictly anaerobic atmosphere.

One interesting observation in this study was that the activity of *Tk*-Rubisco at ambient temperature after heat treatment at 85°C for 15 min was equivalent to the activity observed before heat treatment. In many cases, when hyperthermophilic proteins are produced in mesophilic host cells such as *E. coli*, the recombinant proteins are trapped in a semi-optimal conformation with lower specific activities. Incubation of these proteins at high temperatures leads to slight conformational changes, resulting in a significant increase in specific activity even after they are returned to ambient temperatures (17, 25). As shown in Fig. 5 and Table 3, no change in the amount of *Tk*-Rubisco protein and the total activity in the cell-free extracts was observed after heat treatment. This indicates that *Tk*-Rubisco obtains its optimal conformation in *R. palustris*  $\Delta 3$  even at ambient temperatures.

Another point, that will be important for screening procedures of mutant proteins of *Tk*-Rubisco, is that the specific growth rates of *R. palustris*  $\Delta 3$  harboring *Tk*-Rubisco correlated well with the levels of *Tk*-Rubisco carboxylase activity in the cell-free extracts. This should allow us to efficiently determine whether engineered *Tk*-Rubisco proteins exhibit improved enzymatic properties *in vivo*. This will also allow us to perform enrichment cultures with cells harboring a random mutant library of

*Tk*-Rubisco proteins. With the three-dimensional structure of the protein available, these approaches can be expected to provide valuable information on the structural elements that govern the enzymatic properties of *Tk*-Rubisco, along with the Type I and Type II Rubiscos.

## SUMMARY

In this chapter, the author examined whether a Type III Rubisco from the hyperthermophilic archaeon, *Thermococcus kodakaraensis* KOD1 (*Tk*-Rubisco) could support growth of a mesophilic organism dependent on CO<sub>2</sub> fixation. Three Rubisco genes present on the chromosome of the photosynthetic mesophile *Rhodospseudomonas palustris* No. 7 were deleted via double crossover homologous recombination. The mutant strain ( $\Delta$ 3) could neither grow under photoautotrophic nor photoheterotrophic conditions. The author introduced the *rbc<sub>Tk</sub>* gene into the strain  $\Delta$ 3 either on a plasmid, or by integrating the gene onto the chromosome. The two transformant strains harboring *rbc<sub>Tk</sub>* displayed growth under photoautotrophic and photoheterotrophic conditions, both dependent on CO<sub>2</sub> fixation. Specific growth rates and Rubisco activity levels were compared under photoheterotrophic conditions among the two transformants and the wild-type strain. The author observed that the levels of Rubisco activity in the respective cell-free extracts correlated well with the specific growth rates. Immunoprecipitation experiments revealed that Rubisco activity detected in the transformants was derived solely from *Tk*-Rubisco. These results demonstrated that the Type III *Tk*-Rubisco from a hyperthermophile could support CO<sub>2</sub> fixation in a mesophilic organism, and that the specific growth rate of the transformant can be used as a convenient parameter for selection of engineered proteins with improved function.

## REFERENCES

1. **Amichay, D., R. Levitz, and M. Gurevitz.** 1993. Construction of a *Synechocystis* PCC6803 mutant suitable for the study of variant hexadecameric ribulose biphosphate carboxylase/oxygenase enzymes. *Plant. Mol. Biol.* **23**:465-476.
2. **Andersson, I., and T. C. Taylor.** 2003. Structural framework for catalysis and regulation in ribulose-1,5-bisphosphate carboxylase/oxygenase. *Arch. Biochem. Biophys.* **414**:130-140.
3. **Andrews, T. J., and S. M. Whitney.** 2003. Manipulating ribulose bisphosphate carboxylase/oxygenase in the chloroplasts of higher plants. *Arch. Biochem. Biophys.* **414**:159-169.
4. **Atomi, H.** 2002. Microbial enzymes involved in carbon dioxide fixation. *J. Biosci. Bioeng.* **94**:497-505.
5. **Atomi, H., T. Fukui, T. Kanai, M. Morikawa, and T. Imanaka.** 2004. Description of *Thermococcus kodakaraensis* sp. nov., a well studied hyperthermophilic archaeon previously reported as *Pyrococcus* sp. KOD1. *Archaea* **1**:263-267.
6. **Donohue, T. J., and S. Kaplan.** 1991. Genetic techniques in *rhodospirillaceae*. *Methods Enzymol.* **204**:459-485.
7. **Ezaki, S., N. Maeda, T. Kishimoto, H. Atomi, and T. Imanaka.** 1999. Presence of a structurally novel type ribulose-bisphosphate carboxylase/oxygenase in the hyperthermophilic archaeon, *Pyrococcus kodakaraensis* KOD1. *J. Biol. Chem.* **274**:5078-5082.
8. **Falcone, D. L., and F. R. Tabita.** 1991. Expression of endogenous and foreign



- ribulose 1,5-bisphosphate carboxylase-oxygenase (RubisCO) genes in a RubisCO deletion mutant of *Rhodobacter sphaeroides*. J. Bacteriol. **173**:2099-2108.
9. **Finn, M. W., and F. R. Tabita.** 2003. Synthesis of catalytically active form III ribulose 1,5-bisphosphate carboxylase/oxygenase in archaea. J. Bacteriol. **185**:3049-3059.
  10. **Fujii, T., A. Nakazawa, N. Sumi, H. Tani, A. Ando, and M. Yabuki.** 1983. Utilization of alcohols by *Rhodopseudomonas* sp. No. 7 isolated from *n*-propanol-enrichment cultures. Agr. Biol. Chem. **47**:2747-2753.
  11. **Gatenby, A. A.** 1988. Synthesis and assembly of bacterial and higher-plant Rubisco subunits in *Escherichia coli*. Photosynth. Res. **17**:145-157.
  12. **Gatenby, A. A., and R. J. Ellis.** 1990. Chaperone function: the assembly of ribulose bisphosphate carboxylase-oxygenase. Annu. Rev. Cell. Biol. **6**:125-149.
  13. **Heinhorst, S., S. H. Baker, D. R. Johnson, P. S. Davies, G. C. Cannon, and J. M. Shively.** 2002. Two copies of form I RuBisCO genes in *Acidithiobacillus ferrooxidans* ATCC 23270. Curr. Microbiol. **45**:115-117.
  14. **Imhoff, J. F.** 1995. Taxonomy and physiology of phototrophic purple bacteria and green sulfur bacteria, p. 1-15, Advances in photosynthesis, vol. 2. Kluwer Academic Publishers, Amsterdam, The Netherlands.
  15. **Inui, M., K. Nakata, J. H. Roh, K. Zahn, and H. Yukawa.** 1999. Molecular and functional characterization of the *Rhodopseudomonas palustris* No. 7 phosphoenolpyruvate carboxykinase gene. J. Bacteriol. **181**:2689-2696.
  16. **Inui, M., J. H. Roh, K. Zahn, and H. Yukawa.** 2000. Sequence analysis of the cryptic plasmid pMG101 from *Rhodopseudomonas palustris* and construction of

- stable cloning vectors. *Appl. Environ. Microbiol.* **66**:54-63.
17. **Izumikawa, N., K. Shiraki, S. Nishikori, S. Fujiwara, T. Imanaka, and M. Takagi.** 2004. Biophysical analysis of heat-induced structural maturation of glutamate dehydrogenase from a hyperthermophilic archaeon. *J. Biosci. Bioeng.* **97**:305-309.
  18. **Kanevski, I., P. Maliga, D. F. Rhoades, and S. Gutteridge.** 1999. Plastome engineering of ribulose-1,5-bisphosphate carboxylase/oxygenase in tobacco to form a sunflower large subunit and tobacco small subunit hybrid. *Plant Physiol.* **119**:133-142.
  19. **Laemmli, U. K.** 1970. Cleavage of structural proteins during the assembly of the head of bacteriophage T4. *Nature* **227**:680-685.
  20. **Maeda, N., K. Kitano, T. Fukui, S. Ezaki, H. Atomi, K. Miki, and T. Imanaka.** 1999. Ribulose bisphosphate carboxylase/oxygenase from the hyperthermophilic archaeon *Pyrococcus kodakaraensis* KOD1 is composed solely of large subunits and forms a pentagonal structure. *J. Mol. Biol.* **293**:57-66.
  21. **Miller, V. L., and J. J. Mekalanos.** 1988. A novel suicide vector and its use in construction of insertion mutations - osmoregulation of outer-membrane proteins and virulence determinants in *Vibrio cholerae* requires *toxR*. *J. Bacteriol.* **170**:2575-2583.
  22. **Morikawa, M., Y. Izawa, N. Rashid, T. Hoaki, and T. Imanaka.** 1994. Purification and characterization of a thermostable thiol protease from a newly isolated hyperthermophilic *Pyrococcus* sp. *Appl. Environ. Microbiol.* **60**:4559-4566.

23. **Nishihara, H., T. Yaguchi, S. Y. Chung, K. Suzuki, M. Yanagi, K. Yamasato, T. Kodama, and Y. Igarashi.** 1998. Phylogenetic position of an obligately chemoautotrophic, marine hydrogen-oxidizing bacterium, *Hydrogenovibrio marinus*, on the basis of 16S rRNA gene sequences and two form I RuBisCO gene sequences. Arch. Microbiol. **169**:364-368.
24. **Pierce, J., T. J. Carlson, and J. G. Williams.** 1989. A cyanobacterial mutant requiring the expression of ribulose biphosphate carboxylase from a photosynthetic anaerobe. Proc. Natl. Acad. Sci. USA **86**:5753-5757.
25. **Rahman, R. N. Z. A., S. Fujiwara, M. Takagi, S. Kanaya, and T. Imanaka.** 1997. Effect of heat treatment on proper oligomeric structure formation of thermostable glutamate dehydrogenase from a hyperthermophilic archaeon. Biochem. Biophys. Res. Commun. **241**:646-652.
26. **Sambrook, J., and D. W. Russell.** 2001. Molecular cloning: a laboratory manual, 3rd ed. Cold Spring Harbor Laboratory Press, Cold Spring Harbor, New York.
27. **Schloss, J. V., E. F. Phares, M. V. Long, I. L. Norton, C. D. Stringer, and F. C. Hartman.** 1982. Ribulosebiphosphate carboxylase/oxygenase from *Rhodospirillum rubrum*. Methods Enzymol. **90**:522-528.
28. **Somerville, C. R., and S. C. Somerville.** 1984. Cloning and expression of the *Rhodospirillum rubrum* ribulosebiphosphate carboxylase gene in *Escherichia coli*. Mol. Gen. Genet. **193**:214-219.
29. **van der Vies, S. M., D. Bradley, and A. A. Gatenby.** 1986. Assembly of cyanobacterial and higher plant ribulose biphosphate carboxylase subunits into functional homologous and heterologous enzyme molecules in *Escherichia coli*.

- EMBO J. **5**:2439-2444.
30. **Watson, G. M., and F. R. Tabita.** 1997. Microbial ribulose 1,5-bisphosphate carboxylase/oxygenase: a molecule for phylogenetic and enzymological investigation. FEMS Microbiol. Lett. **146**:13-22.
  31. **Watson, G. M., J. P. Yu, and F. R. Tabita.** 1999. Unusual ribulose 1,5-bisphosphate carboxylase/oxygenase of anoxic *archaea*. J. Bacteriol. **181**:1569-1575.
  32. **Whitney, S. M., and T. J. Andrews.** 2001. Plastome-encoded bacterial ribulose-1,5-bisphosphate carboxylase/oxygenase (RubisCO) supports photosynthesis and growth in tobacco. Proc. Natl. Acad. Sci. USA **98**:14738-14743.
  33. **Whitney, S. M., P. Baldett, G. S. Hudson, and T. J. Andrews.** 2001. Form I Rubiscos from non-green algae are expressed abundantly but not assembled in tobacco chloroplasts. Plant J. **26**:535-547.
  34. **Yaguchi, T., S. Y. Chung, Y. Igarashi, and T. Kodama.** 1994. Cloning and sequence of the L<sub>2</sub> form of RubisCO from a marine obligately autotrophic hydrogen-oxidizing bacterium, *Hydrogenovibrio marinus* strain MH-110. Biosci. Biotechnol. Biochem. **58**:1733-1737.
  35. **Yoshizawa, Y., K. Toyoda, H. Arai, M. Ishii, and Y. Igarashi.** 2004. CO<sub>2</sub>-responsive expression and gene organization of three ribulose-1,5-bisphosphate carboxylase/oxygenase enzymes and carboxysomes in *Hydrogenovibrio marinus* strain MH-110. J. Bacteriol. **186**:5685-5691.

## CHAPTER 2

### **Engineering of a Type III Rubisco from a hyperthermophilic archaeon aimed to enhance catalytic performance in mesophilic host cells**

#### **INTRODUCTION**

The Calvin-Benson-Bassham (CBB) pathway is responsible for the CO<sub>2</sub> fixation in all plants, algae, cyanobacteria, and many other autotrophic bacteria. Ribulose-1, 5-bisphosphate carboxylase/oxygenase (Rubisco) is the key enzyme of this pathway and can thus be considered the main gateway for organic carbon production from CO<sub>2</sub> on our planet.

The oxygenase activity that competes with the carboxylase activity of Rubisco and the low turnover rate of the enzyme are the two main factors considered to place limitations on the overall efficiency of photosynthesis (1, 7). Improvements in Rubisco function are thus expected to have a large impact in various fields of agriculture. However, structure-function studies on the eukaryotic Type I enzymes, which exhibit the most favorable properties among the characterized Rubisco proteins, have been hampered by the fact that functional expression of these proteins in conventional host cells such as *Escherichia coli* is not possible (3, 26). On the other hand, bacterial Type I enzymes from cyanobacteria and Type II Rubiscos can be functionally expressed in *E. coli* (4, 6, 21), and extensive studies have been carried out in order to understand the structural elements that control the specificity and activity levels of these enzymes (18).

Rubisco from *T. kodakaraensis* (*Tk*-Rubisco), classified as a Type III Rubisco, is composed only of large subunits and displays extreme thermostability with high carboxylase activity at high temperatures (2, 15). Although the carboxylase activity of

*Tk*-Rubisco was expected to be lower than those of mesophilic Rubiscos at ambient temperature, the studies described in CHAPTER 1 have revealed that *Tk*-Rubisco is capable of supporting both photoautotrophic and photoheterotrophic growth of a Rubisco-deficient mutant strain (strain  $\Delta 3$ ) of the mesophilic, purple nonsulfur bacterium *Rhodospseudomonas palustris*. This encouraged the author to examine the enzymatic properties of *Tk*-Rubisco at mesophilic temperatures and the possibilities of improving the catalytic performance of the enzyme at these temperatures via protein engineering. This would provide an entirely different approach in obtaining a Rubisco protein with improved or desired enzymatic properties. *Tk*-Rubisco has the advantage that it can be readily expressed at high levels in an active form in *E. coli*, and as the protein is comprised only of large subunits (15), it may also be easier to express the protein in a functional form in other host environments such as the eukaryotic chloroplast. The high (thermo)stability of the enzyme (14) suggests that the enzyme provides a stable protein scaffold that should be able to tolerate higher degrees of mutations at ambient temperatures than the mesophilic Rubiscos. These properties, along with the elucidated three-dimensional structure of the protein (10), should allow the author to introduce robust mutations to *Tk*-Rubisco, and possibly improve its performance at mesophilic temperatures.

In this chapter, the author aimed to improve the function of *Tk*-Rubisco and gain insight on the structure-function relationship of the enzyme at ambient temperature. The author has performed site-directed mutagenesis on *Tk*-Rubisco, based on a comparison between sequences of *Tk*-Rubisco and Type I/II Rubiscos. The catalytic properties of purified proteins were examined *in vitro*, and *R. palustris*  $\Delta 3$  was utilized as a host strain for evaluating the performance of these mutant proteins *in vivo*.

## **MATERIALS AND METHODS**

### **Strains, media, and growth conditions.**

*R. palustris*  $\Delta 3$  is a derivative of *R. palustris* No. 7, disrupted of its three Rubisco genes, *rbc* I-1, *rbc* I-2 and *rbc* II (described in CHAPTER 1). Gene manipulation and plasmid construction was performed with *E. coli* DH5 $\alpha$ , and *E. coli* BL21(DE3)CodonPlus RIL (Stratagene, La Jolla, CA) was used for gene expression. *E. coli* cells were grown aerobically at 37°C in LB medium with ampicillin (100  $\mu$ g/ml). *R. palustris* cells were first cultivated aerobically in the dark at 30°C in LB medium containing 0.3% NaCl and zeocin (400  $\mu$ g/ml) (heterotrophic growth) for 2 d. Cells were collected and the pellet was washed and resuspended in BS medium containing 5 mM NaHCO<sub>3</sub> and 50 mM ethanol. Cells were inoculated at an initial OD<sub>660</sub> of 0.05 into BS medium containing 5 mM NaHCO<sub>3</sub> and 50 mM ethanol, and photoheterotrophic growth was carried out with a light intensity of 3,200 lux at 25°C. Under photoheterotrophic conditions, cells were grown in a sealed glass vial filled with medium so that the head space was minimal. Specific growth rates were determined in the exponential growth phase.

### **Mutagenesis and plasmid construction.**

For construction of expression plasmids, inverse-PCR was performed with pET-21a(+)/*rbc*<sub>TK</sub> (2) or plasmids harboring *rbc*<sub>TK</sub> mutant genes (SP2 and GP1) as template DNA. Primers for inverse-PCR were constructed so that the regions to be exchanged were removed. 5'-Phosphorylated oligonucleotides harboring the mutant sequences were annealed and ligated with the DNA fragments amplified by inverse-PCR. Point mutagenesis was carried out using a QuikChange XL site-directed

kit (Stratagene), using pET21a(+)/*rbc<sub>TK</sub>* as the template plasmid. The DNA manipulation strategy and primers are described in Fig. 1 and Tables 1-1 to 1-4.

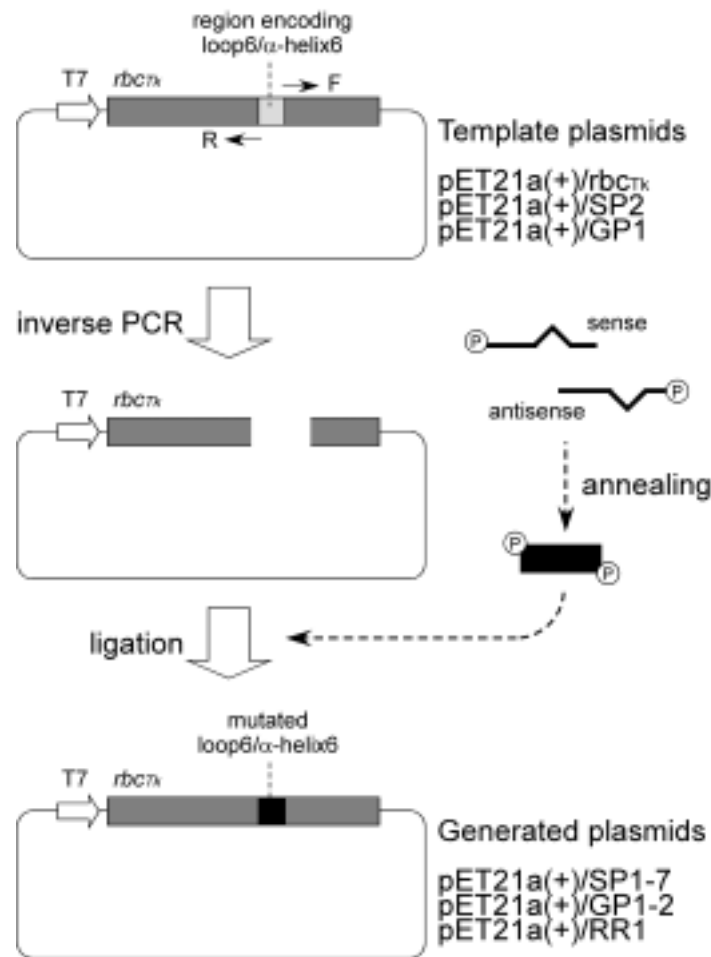


**Fig. 1. Construction of expression vectors harboring mutant *rbc<sub>TK</sub>* genes.**

Inverse-PCR was first performed with pET-21a(+)/*rbc<sub>TK</sub>* or plasmids harboring *rbc<sub>TK</sub>* mutants (SP2 and GP1) as template DNA. Primers for inverse-PCR were constructed so that the regions to be exchanged were removed (Table 1-1). Next, 5'-phosphorylated oligonucleotides (sense and antisense) harboring the mutant sequences (Table 1-2) were annealed to produce phosphorylated double stranded DNA fragments, which were ligated with the inverse PCR products (A to E in Table 1-1). Arrows indicate forward (F) and reverse (R) primers.



**Table 1-1. Forward (F) and Reverse (R) primers used for inverse PCR.**

PCR product	Template plasmid	Forward /Reverse	Primer	Sequence
A	pET21a(+)/ <i>rbc<sub>Tk</sub></i>	Forward	Tkr-991f	5' -GTGGAGCTGGTCAATGCCTATGAGCC-3'
		Reverse	Tkr-942r	5' -ATTCAGAACGCCAGGATTCTCAGGGAGAGCCAC-3'
B	pET21a(+)/ <i>rbc<sub>Tk</sub></i>	Forward	Tkr-1015f	5' -GCCCTCAAGCTTGCCAGCTCCAGCGGTC-3'
		Reverse	Tkr-975r	5' -GAGAGCCACTACAAGCCCAGTAAAAACG-3'
C	pET21a(+)/SP2	Forward	SP2-1009f	5' -GAGAGCCACTACAAGCCCAGTAAAAACG-3'
		Reverse	SP2-969r	5' -GCCCTCAAGCTTGCCAAACAACGGTGCCAG-3'
D	pET21a(+)/GP1	Forward	GP1-961f	5' -GTGGAGCTGGTCAATGCCTATGAGCC-3'
		Reverse	GP1-942r	5' -GGCAAGCTTGAGGGCGACTTCATAATAACCAGGGG-3'
E	pET21a(+)/ <i>rbc<sub>Tk</sub></i>	Forward	Tkr-961f	5' -GTGGAGCTGGTCAATGCCTATGAGCC-3'
		Reverse	Tkr-942r	5' -GGCAAGCTTGAGGGCGCAAGTGGGACGTCATTC-3'

**Table 1-2. Sense and antisense oligonucleotides used to incorporate mutations.**

Mutant	Inverse PCR product	Sense/ Antisense	Sequence
SP1	A	Sense	5' -GTTGGAACCGTT---GTTGGCAAGCTTGAGGGCGGCAAGTGGGACGTC-3'
		Antisense	5' -GACGTCCCACCTTGCCGCCCTCAAGCTTGCCAAC---AACGGTTCACAC-3'
SP2	A	Sense	5' - <u>TCT</u> GGaACCGTT---GTTGGCAAGCTTGAGGGCGGCAAGTGGGACGTC-3'
		Antisense	5' -GACGTCCCACCTTGCCGCCCTCAAGCTTGCCAAC---AACGGTtCC <u>AGA</u> -3'
SP3	A	Sense	5' -GTTGGAACCGCTGGAGCTGGCAAGCTTGAGGGCGGCAAGTGGGAC <u>ACC</u> -3'
		Antisense	5' - <u>GGT</u> GTCCCACCTTGCCGCCCTCAAGCTTGCCAGCTCCAGCGGTTCCACAC-3'
SP4	A	Sense	5' -GTTGGAACCGCTGGAGCTGGCAAGCTTGAGGGCG <u>GAGCGGACATAACC</u> -3'
		Antisense	5' - <u>GGTTATGTGCGGCTC</u> GCCCTCAAGCTTGCCAGCTCCAGCGGTTCCACAC-3'
SP5	B	Sense	5' -GGCAAGTGGGACGTC <u>CTCGGCTTCGTTGACCTC</u> CTCAGG-3'
		Antisense	5' -CCTGAGG <u>GAGGTCAACGAAGCCGAG</u> GACGTCCCACCTTGCC-3'
SP6	B	Sense	5' - <u>GAGCGGACATAACCCTCGGCTTCGTTGACCTC</u> CTCAGG-3'
		Antisense	5' -CCTGAGG <u>GAGGTCAACGAAGCCGAGGGTTATGTGCGGCTC</u> -3'
SP7	C	Sense	5' - <u>GAGCGGACATAACCCTCGGCTTCGTTGACCTC</u> CTCAGG-3'
		Antisense	5' -CCTGAGG <u>GAGGTCAACGAAGCCGAGGGTTATGTGCGGCTC</u> -3'
GP1	B	Sense	5' - <u>GACTTCATAATAACCAGGGGCTTCTACAAGACC</u> CTCCTC-3'
		Antisense	5' - <u>GAGGAGGGTCTTGTAGAAGCCCTGGTTATTATGAAGTC</u> -3'
GP2	D	Sense	5' - <u>GCCGGCACC</u> GTT---GTT-3'
		Antisense	5' - <u>AAC</u> --- <u>AAC</u> GGTGCCGGC-3'
RR1	E	Sense	5' - <u>ACC</u> GGAACC <u>ATGGCTTC</u> -3'
		Antisense	5' - <u>GAAGCCCAT</u> GGTTCCGGT-3'

The three consecutive hyphens represent the positions where nucleotides have been removed. The underlined nucleotides correspond to the codons that have been changed.

**Table 1-3. Primers used for single residue deletion.**

Mutant	Sense/ Antisense	Sequence
ΔT317	Sense	5' -GACCAGCTCCACGTTGGA---GCTGGAGCTGGCAAGCTTG-3'
	Antisense	5' -CAAGCTTGCCAGCTCCAGC---TCCAACGTGGAGCTGGTC-3'
ΔA318	Sense	5' -GCTCCACGTTGGAACC---GGAGCTGGCAAGCTTG-3'
	Antisense	5' -CAAGCTTGCCAGCTCC---GGTTCCAACGTGGAGC-3'

The three consecutive hyphens represent the positions where nucleotides have been removed.

**Table 1-4. Primers used for single residue replacement.**

Mutant	Sense/Antisense	Sequence
H94S	Sense	5' -CCTACCCGTT <b>CAG</b> CGCCTTTGAGGAGGCCAAC-3'
	Antisense	5' -GTTGGCCTCCTCAAAGGC <b>GCT</b> GAACGGGTAGG-3'
D125N	Sense	5' -GGGCTCCGCCTTGAG <b>AA</b> CTTTACTTCCC GGAG-3'
	Antisense	5' -CTCCGGGAAGTAAAG <b>GTT</b> CTCAAGCGGAGCCC-3'
D137N	Sense	5' -CTCATAAGGGAGTTC <b>AA</b> CGGCCCGGCCTTCGG-3'
	Antisense	5' -CCGAAGGCCGGCC <b>GTT</b> GAACTCCCTTATGAG-3'
D385N	Sense	5' -GCCCTCGGAACC <b>AA</b> CATAGTCCTCCAGCTCG-3'
	Antisense	5' -CGAGCTGGAGGACTAT <b>GTT</b> GGTTCGGAGGGC-3'
D186N	Sense	5' -CTCTCAAACGGTGCC <b>AA</b> CTACATGAAGGACGAC-3'
	Antisense	5' -GTCGTCCTTCATGTAG <b>TG</b> TGGCACCGTTTGAGAG-3'
D190N	Sense	5' -GCCGACTACATGAAG <b>AA</b> CGACGAGAACCTCAG-3'
	Antisense	5' -CGTGAGGTTCTCGT <b>CTG</b> TCTTCATGTAGTCGGC-3'
E217Q	Sense	5' -GGCGAAGATAATTGACAAGGT <b>ACA</b> GAACGAGACGGGTGAG-3'
	Antisense	5' -CTCACCCGTCTCGTT <b>CTG</b> TACCTTGTCAATTATCTTCGCC-3'
E49Q	Sense	5' -GGAGCCGTGGCAGCT <b>CAG</b> AGCTCAACTGGAACC-3'
	Antisense	5' -GGTTCCAGTTGAGCT <b>CTG</b> AGCTGCCACGGCTCC-3'
E172Q	Sense	5' -GTCGGTTATTCTCCGGAG <b>CAG</b> TTGAGAAGCTGG-3'
	Antisense	5' -CCAGCTTCTCGAA <b>CTG</b> CTCCGGAGAATAACCGAC-3'
E97Q	Sense	5' -CGTTCCACGCCTTT <b>CAG</b> GAGGCCAACCTTCCG-3'
	Antisense	5' -CGGAAGGTTGGCCT <b>CTG</b> AAAGGCGTGGAAACG-3'
E98Q	Sense	5' -CCACGCCTTTGAG <b>CAG</b> GCCAACCTTCCG-3'
	Antisense	5' -CGGAAGGTTGGC <b>CTG</b> CTCAAAGGCGTGG-3'

The underlined nucleotides correspond to the codon that has been changed and bold letters represent exchanged nucleotides.

Plasmids used to integrate each mutant gene into the chromosome of *R. palustris* Δ3 were constructed using pSZMRbc described in CHAPTER 1. Expression plasmids harboring the mutant *rbCT<sub>k</sub>* genes were digested with MroI, and the fragments containing the mutant sequences were ligated with pSZMRbc digested with MroI.

### **Gene expression and initial examination of carboxylase activity.**

Gene expression was induced with 0.1 mM isopropyl- $\beta$ -D-thiogalactopyranoside at the mid-exponential growth phase with further incubation for 4 h at 37°C. After incubation of gene expression, *E. coli* BL21(DE3)CodonPlus RIL cells were collected (10 min, 5,000 x g, 4°C) and washed with 100 mM Bicine-NaOH (pH 8.3), 10 mM MgCl<sub>2</sub> (buffer A). The pellet was resuspended in the same buffer and disrupted by sonication on ice. Cell debris was removed by centrifugation (5 min, 5,000 x g, 4°C). Cell-free extracts were subjected to heat treatment (85°C, 30 min) and centrifugation (30 min, 20,000 x g, 4°C). Further purification of the wild-type *Tk*-Rubisco and mutant proteins SP3, SP4, and SP6 were performed as follows. The supernatant was applied to a Resource Q column (GE Healthcare Bio-Sciences, Piscataway, NJ) and eluted with a gradient of 0-1.0 M NaCl using ÄKTA explorer 10S (GE Healthcare Bio-Sciences). The recombinant protein was then applied to Superdex 200 HR 10/30 column (GE Healthcare Bio-Sciences) in buffer A containing 0.25 M NaCl. Purified recombinant proteins were concentrated with Centricon YM30 (Millipore, Bedford, MA), when necessary. Protein concentration was determined with a protein assay kit (Bio-Rad, Hercules, CA), using bovine serum albumin as a standard. Carboxylase activity was measured as described in CHAPTER 1. All assays were performed at least twice.

### **Western blot analysis.**

Western blot analysis was performed as described in CHAPTER 1. Samples were prepared from cell-free extracts of exponentially growing *R. palustris* cells. Cells were harvested by centrifugation and washed with buffer A. The pellet was resuspended

in the same buffer and disrupted by sonication. Cell debris was removed by centrifugation (5 min, 5,000 x g, 4°C) followed by ultracentrifugation (20 min, 110,000 x g, 4°C).

### **Kinetic examination.**

All buffers were autoclaved (121°C, 20 min), cooled and bubbled under a N<sub>2</sub> atmosphere free of CO<sub>2</sub> and O<sub>2</sub>. Prior to use, enzymes were treated with CO<sub>2</sub>- and O<sub>2</sub>-free buffer (10 mM Bicine-NaOH pH 8.3) on a PD-10 gel-filtration column (GE Healthcare Bio-Sciences). Enzymes were concentrated, and pre-incubated for 4 h on ice in 10 mM NaHCO<sub>3</sub>, 10 mM MgCl<sub>2</sub>, and 10 mM Bicine-NaOH (pH 8.3) for enzyme activation. The reaction was initiated by combining 230 µl of reaction buffer with 20 µl of activated enzyme, after each was pre-incubated at 25°C for 5 min. The final reaction mixture contained 10 µg activated enzyme, 20 µM RuBP (Fluka, Buchs, Switzerland), 10 mM MgCl<sub>2</sub>, 10 mM Bicine-NaOH (pH 8.3) and 0.8, 1.8, 2.8, 3.8, 4.8, 6.8, 8.8, or 10.8 mM NaHCO<sub>3</sub>. Reactions carried out at 25°C were stopped after 30 s and 60 s with 250 µl of 40 mM HCl.

K<sub>O<sub>2</sub></sub> and τ values were determined at fixed NaHCO<sub>3</sub> concentrations. O<sub>2</sub> saturating buffer (saturating [O<sub>2</sub>] = 1.23 mM, employed for 100% O<sub>2</sub>-flushed reactions (22)) was prepared by O<sub>2</sub>-bubbling of CO<sub>2</sub>- and O<sub>2</sub>- free buffer for 4 h, and added to the reaction mixture. The reaction was initiated with the addition of 230 µl reaction buffer to 20 µl of activated enzyme after each was pre-incubated at 25°C for 5 min. The final reaction mixture contained 10 µg (for wild-type *Tk*-Rubisco, SP4, and SP6) or 15 µg (for SP3) activated enzyme, 10 µM RuBP, 10 mM MgCl<sub>2</sub>, and 10 mM Bicine-NaOH (pH 8.3), a fixed concentration of NaHCO<sub>3</sub>, and 0.886 mM O<sub>2</sub> or 0 mM O<sub>2</sub>. NaHCO<sub>3</sub>

concentration was 8.8 mM (for wild-type *Tk*-Rubisco), 5.8 mM (SP4 and SP6), or 4.8 mM (SP3). Reactions at 25°C were stopped after 30 s, 60 s, and 90 s with 250 µl of 40 mM HCl. The  $K_{O_2}$  was calculated using the relationship  $1/(R-1) = K_{O_2}/[O_2] + K_{O_2}[CO_2] / K_{CO_2}[O_2]$  (12), where R is the ratio of carboxylase activities at  $O_2$  concentrations of 0 and 0.886 mM.

Reaction mixtures were analyzed as described elsewhere (25) with modifications noted below. In order to remove  $Mg^{2+}$ , reaction mixtures were mixed with Dowex 50 resin ( $H^+$ -form) (Sigma-Aldrich, St. Louis, MO) washed with 1 M NaOH, followed by 1 M HCl, and then MilliQ water. Rubisco and resin were removed with an Ultrafree-MC filter unit (Millipore) by centrifugation (60 min, 5000 x g, 4°C) and the filtrate was injected to a DX 500 anion exchange chromatographic system with an AS11 column (Dionex, Sunnyvale, CA). The developing solvent was 18 mM NaOH.

For the determination of  $K_{RuBP}$ , the reaction was initiated with the addition of 40 µl of activated enzyme to 460 µl reaction mixture after each solution was pre-incubated at 25°C for 5 min. The 500 µl reaction mixture contained 2 µg activated enzyme, 5, 10, 15, 20, or 50 µM RuBP, 10 mM  $MgCl_2$ , 2.8 mM  $NaHCO_3$ , and 1.8 mM Bicine-NaOH (pH 8.3). Reactions at 25°C were stopped after 30 s and 60 s with Dowex 50 resin ( $H^+$ -form) treated as described above. Rubisco and resin were removed with an Ultrafree-MC filter and analyzed with the DX 500 anion exchange chromatographic system.

## RESULTS

### Strategies to elevate *Tk*-Rubisco activity at ambient temperatures.

*Mutations designed to increase the flexibility of the Tk-Rubisco protein.* In general,

proteins from hyperthermophiles are extremely thermostable and can maintain their functional structure at high temperature ranges. This is mainly brought about by strengthened intramolecular interactions (e.g. electrostatic effects, hydrophobic interactions and hydrogen bonds) compared to proteins from mesophiles (28, 29). It is presumed that the flexibility of the proteins at these high temperature ranges becomes optimal for catalytic turnover. However, this in turn results in excess rigidity of these proteins at lower temperatures, and in many cases thermostable enzymes display lower activity levels at ambient temperatures compared to their mesophilic counterparts (27). Increasing the flexibility of thermostable enzymes can be expected to be one method to enhance the activity, particularly turnover rates, of these enzymes at low temperatures. One straightforward approach to add flexibility to proteins is by removing the intra-molecular ionic interactions.

The author first attempted to increase the flexibility of the *Tk*-Rubisco protein. Hydrogen bonding contacts between a particular pair of atoms in the *Tk*-Rubisco molecule were calculated using the program CONTACT in the CCP4 program package. This program predicts residue pairs that are capable to form ionic or hydrogen bond interactions. Among the predicted residue pairs, 20 ion-pairs with a distance below 3.3 Å were initially selected (Table 2). The author next took into account the degree of atom fluctuation (b-factor). Eleven ion-pairs whose b-factors were below 80, and considered relatively rigid, were chosen for further analysis. Among the 11 selected ion-pairs, 7 pairs were intra-subunit interactions (Table 2A), whereas 4 pairs were present at the interface of the two subunits that form an active dimer (Table 2B).

Eleven mutant proteins were constructed by replacing one of the residues taking part in each ion-pair. Mutations were designed to abolish individual ionic bonds

and replace them with hydrogen bonds. Aspartate residues were changed to asparagine residues and glutamate was replaced with glutamine. In one case, the histidine positioned at 94, which was predicted to interact with aspartate at position 69 (D69), was changed to serine. D69 was not mutated because this residue is involved in dimer-dimer interaction with other residues. It has previously been shown that disruption of the dimer-dimer interaction leads to a decrease in both activity and thermostability of *Tk*-Rubisco (14).

*Mutations in the loop6 and  $\alpha$ -helix6 regions.* Loop6 covers the  $\beta/\alpha$  barrel of Rubisco

**A**

	Target				Counterpart			
	No.	a.a.	side chain	B-factor	No.	a.a.	side chain	B-factor
	22	LYS	NZ	49.8	130	GLU	OE1	43.78
	30	ARG	NH2	74.3	82	ASP	OD1	91.03
	35	GLU	OE2	197.1	119	LYS	NZ	198.21
	69	ASP	OD1	61.7	↔ 94	HIS	NE2	54.13
↔	125	ASP	OD1	49.2	303	LYS	NZ	65.68
	130	GLU	OE2	43.8	134	ARG	NH2	54.45
↔	137	ASP	OD2	85.5	265	ARG	NH1	85.66
	147	ARG	NH2	66.5	↔ 385	ASP	OD1	59.37
	155	ARG	NH1	67.7	↔ 186	ASP	OD2	79.22
	155	ARG	NH2	67.7	↔ 186	ASP	OD1	79.22
↔	190	ASP	OD2	57.6	205	ARG	NH1	40.97
	192	GLU	OE1	80.9	281	HIS	NE2	90.84
↔	217	GLU	OE2	78.4	250	LYS	NZ	67.61
	222	GLU	OE1	97.3	409	ARG	NH2	75.76
	335	ARG	NH1	79.7	339	GLU	OE1	80.93
	341	HIS	NE2	81.8	363	GLU	OE2	93.63
	343	LYS	NZ	113.7	363	GLU	OE2	93.63

**B**

	Target				Counterpart			
	No.	a.a.	side chain	B-factor	No.	a.a.	side chain	B-factor
↔	49	GLU	OE2	85.78	165	LYS	NZ	46.06
	66	ARG	NH2	66.31	↔ 172	GLU	OE1	53.83
	66	ARG	NH2	66.31	↔ 172	GLU	OE2	53.83
↔	97	GLU	OE1	50.78	240	ARG	NH1	34.97
↔	97	GLU	OE1	50.78	240	ARG	NH2	34.97
↔	97	GLU	OE2	50.78	240	ARG	NH2	34.97
↔	98	GLU	OE1	62.19	201	ARG	NH1	58.21
↔	98	GLU	OE2	62.19	201	ARG	NH2	58.21

**Table 2. Predicted ionic interactions in *Tk*-Rubisco.** Ionic interactions in an active dimer of *Tk*-Rubisco (PDB file; 1GEH) were selected from residue pairs that were predicted to have a strong possibility of forming hydrogen bonds with one another (distance < 3.3 Å). Ionic interactions between residues within the monomeric *Tk*-Rubisco protein are shown in (A), and those consisting of residues from two different subunits of the active dimer are shown in (B). Residues that were replaced are indicated with arrowheads.

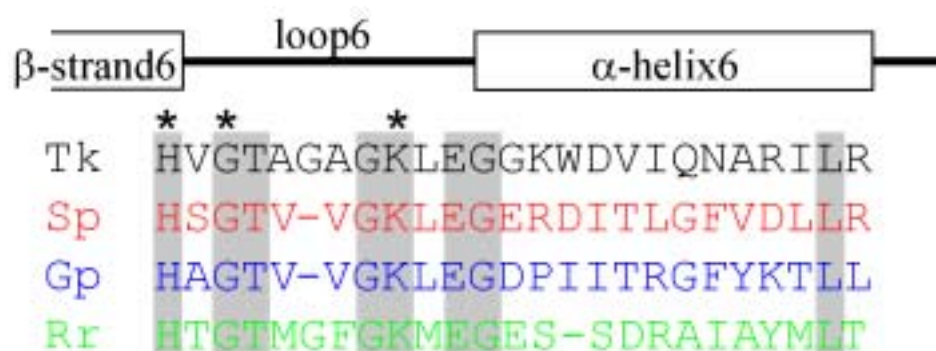
and acts as a lid during Rubisco catalysis. Loop6 is commonly found in Type I–III Rubiscos, and harbors the active site residue lysine. Structural studies have suggested that the flexible loop6 in the closed conformation serves in stabilizing the reaction intermediates during catalysis (11, 16). As differences in sequence were observed in this region among the enzymes from higher plants, algae, and cyanobacteria, loop6 and the adjacent  $\alpha$ -helix6 region have been major targets for site-directed mutagenesis. These studies have confirmed that loop6/ $\alpha$ -helix6 are involved in defining the specificity factor and turnover rate of Type I and II Rubiscos (18). An alignment of the sequences of this region in enzymes from spinach (Type I), the purple non-sulfur bacterium *Rhodospirillum rubrum* (Type II), the red alga *Galdieria partita* (Type I), and *Tk*-Rubisco (Type III) is shown in Fig. 2A. As the corresponding region in *Tk*-Rubisco displays a further variation among the Rubiscos, the author focused on the loop6/ $\alpha$ -helix6 of *Tk*-Rubisco for introducing specific mutations and examining their effects on Rubisco activity at mesophilic temperatures. In addition, the mutations may lead to increases in the flexibility of the protein at or in the vicinity of the catalytic center, resulting in increased turnover of the enzyme at lower temperatures.

Ten initial mutant proteins were constructed by replacing sequences of *Tk*-Rubisco with sequences from Type I/II Rubiscos (Fig. 2A). The mutants SP1 to SP7 are based on sequence comparison with the Type I spinach Rubisco and results of previously reported mutagenesis studies. Spinach is a terrestrial organism and its Rubisco exhibits a high CO<sub>2</sub>/O<sub>2</sub> specificity factor (8, 19). A large portion of the residues in loop6 are highly conserved among the Type I-III Rubiscos. SP1 and SP2 harbor mutations in the non-conserved residues of loop6. Within  $\alpha$ -helix6, SP3 contains a single amino acid substitution from valine to threonine, based on the finding that a

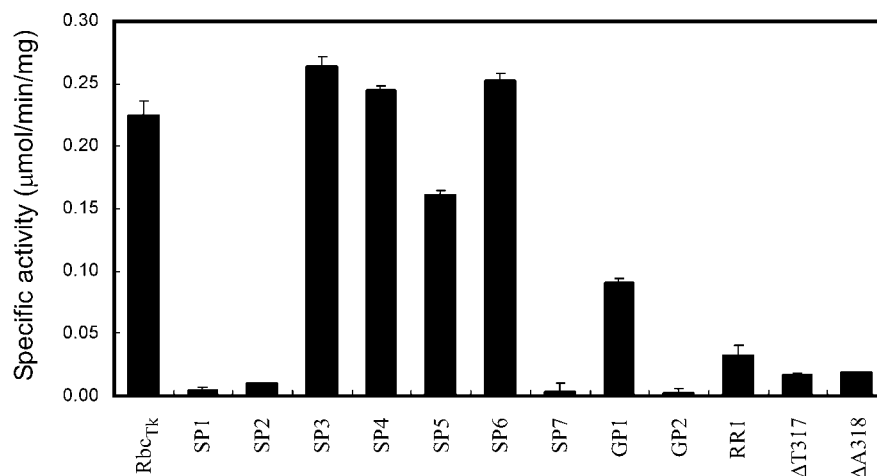


T342V mutant clearly decreased the specificity factor and the specific activity of a Type I Rubisco from cyanobacteria (19). SP4 has substitutions in 5 consecutive amino acid residues, taking into account that a DKAS338-341ERDI mutation in a cyanobacterial Type I Rubisco led to an increase in specificity factor (5, 9), in addition to the results of the T342V mutation described above. As *Tk*-Rubisco was presumed to provide a stable scaffold, the author introduced mutations to a greater extent in SP5 to SP7. SP5 has 6 amino acids substitution in  $\alpha$ -helix6, while SP6 has 11 substitutions in  $\alpha$ -helix6. In SP7, the entire loop6/ $\alpha$ -helix6 region was replaced with the corresponding region of spinach Rubisco. GP1 and GP2 mutants were designed taking into consideration the sequence of the Type I Rubisco from *G. partita*. *G. partita* is a thermophilic red alga, and the enzyme displays the highest specificity reported among Rubiscos (24). The  $\alpha$ -helix6 region of *Tk*-Rubisco was replaced with that of the *G. partita* Rubisco in GP1, and the entire loop6/ $\alpha$ -helix6 region was exchanged in GP2. RR1 is based on the sequence from a Type II Rubisco from *R. rubrum*. As the *R. rubrum* enzyme exhibits a low specificity factor compared with Type I Rubisco (8, 9), RR1 was constructed mainly to examine the significance in the length of loop6.

**A**



	314	338
SP1	HVGTV-VGKLEGGKWDVIQNARILR	
SP2	HSGTV-VGKLEGGKWDVIQNARILR	
SP3	HVGTAGAGKLEGGKWDTIQNARILR	
SP4	HVGTAGAGKLEGERDITIQNARILR	
SP5	HVGTAGAGKLEGGKWDVLGFVDLLR	
SP6	HVGTAGAGKLEGERDITLGFVDLLR	
SP7	HSGTV-VGKLEGERDITLGFVDLLR	
GP1	HVGTAGAGKLEGDPIITRGFYKTLL	
GP2	HAGTV-VGKLEGDPIITRGFYKTLL	
RR1	HTGTMGF GKLEGGKWDVIQNARILR	
$\Delta$ T317	HVG-AGAGKLEGGKWDVIQNARILR	
$\Delta$ A318	HVGT-GAGKLEGGKWDVIQNARILR	

**B**

**Fig. 2. Mutations in the loop6 and  $\alpha$ -helix6 region of *Tk*-Rubisco.** (A) Mutant design of *Tk*-Rubisco. Alignment of the loop6 and  $\alpha$ -helix6 regions of Rubisco proteins from *Thermococcus kodakaraensis* KOD1 (Tk, Type III, BAD86479), spinach (Sp, Type I, red, P00875), *Galdieria partita* (Gp, Type I, blue, BAA75796), and *Rhodospirillum rubrum* (Rr, Type II, green, P04718). Active site residues are indicated with asterisks. Residues identical in all four enzymes are shaded. Gaps in the alignment are indicated with hyphens. Secondary structural elements are shown above the alignment. Sequences of mutant *Tk*-Rubisco proteins produced in this study are shown below the alignment. Exchanged residues are indicated with the colors of the sequence the mutations were based on. The positions where single residues were deleted in  $\Delta$ T317 and  $\Delta$ A318 are underlined. (B) Carboxylase activities of partially purified wild-type and mutant *Tk*-Rubisco proteins. Activity measurements were performed at 25°C. Measurements were performed at least in duplicate.

### Carboxylase activities of recombinant mutant *Tk*-Rubisco proteins.

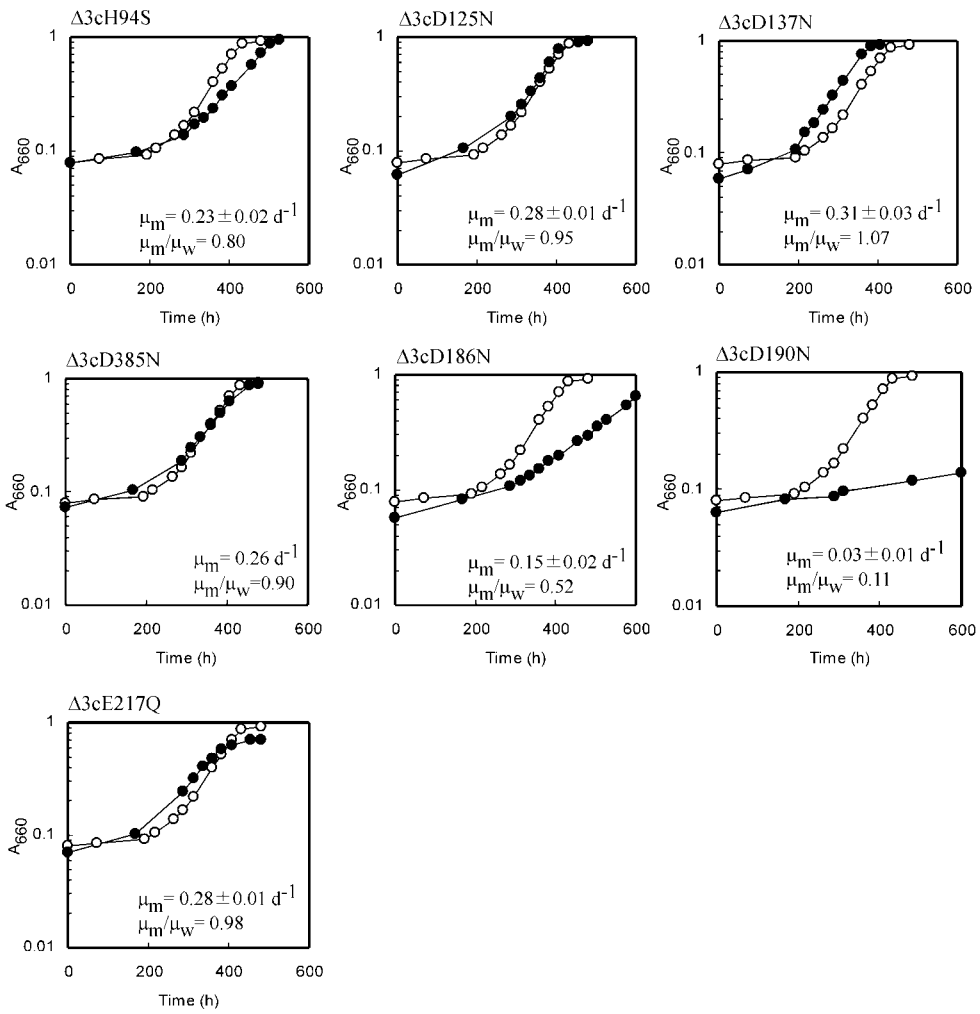
As many of the designed mutations in the loop6 and  $\alpha$ -helix6 regions involved multiple residues, it was anticipated that a number of these mutant proteins would be completely inactive. The author therefore carried out an initial examination on the activity levels of these ten mutant proteins. Plasmids were constructed for gene

expression in *E. coli*. Cells were disrupted by sonication, and the supernatants were treated with heat at 85°C for 15 min to remove proteins from the mesophilic host cells. After centrifugation, soluble proteins in the supernatants were examined by SDS-PAGE, and it was confirmed that all mutant proteins were present in a soluble form, and that the proteins were apparently homogeneous. With these samples, the author examined the Rubisco activity of the ten mutant proteins. At 25°C, activity was clearly detected in the proteins SP3, SP4, SP5, SP6, GP1, and RR1 (Fig. 2B). In particular, SP3, SP4, and SP6 exhibited activity levels comparable to the activity observed in *Tk*-Rubisco. On the other hand, SP1, SP2, SP7, and GP2 displayed dramatic decreases in carboxylase activity, indicating that the length of loop6 is important for the activity of *Tk*-Rubisco. To examine whether this was the case, the author constructed two additional mutant proteins with single amino acid deletions in T317 ( $\Delta$ T317) and A318 ( $\Delta$ A318). Dramatic decreases in activities were observed in both mutant proteins (Fig. 2B), further supporting the importance of the length of loop6 in *Tk*-Rubisco activity.

### **Growth characteristics of *R. palustris* $\Delta$ 3 strains harboring mutant *Tk*-Rubisco proteins.**

The results described in CHAPTER 1 have revealed that the specific growth rates of *R. palustris* harboring *Tk*-Rubisco correlate well with the levels of the protein present in the cell. This implies that the specific growth rates of strains harboring mutant Rubisco proteins should reflect the levels of Rubisco activity in the cells and can therefore be used to evaluate the performance of these proteins *in vivo*. Excluding the mutant proteins that displayed dramatic decreases in activity, the author introduced the mutant *Tk*-Rubisco genes into *R. palustris*  $\Delta$ 3, and examined their growth properties.

*Mutations designed to increase the flexibility of the Tk-Rubisco protein.* The eleven mutant proteins with mutations disrupting ionic interactions were examined whether they could support the growth of the Rubisco-deficient mutant strain *R. palustris*  $\Delta 3$ . The genes were individually introduced into *R. palustris*  $\Delta 3$  cells using the plasmid pSMZRbc, designed for single-crossover insertion into the *R. palustris*  $\Delta 3$  chromosome. Transformants were selected for their resistance towards zeocin, and genotypes were confirmed by PCR analyses (data not shown). The eleven strains were designated as strains  $\Delta 3cH94S$ ,  $\Delta 3cD125N$ ,  $\Delta 3cD137N$ ,  $\Delta 3cD385N$ ,  $\Delta 3cD186N$ ,  $\Delta 3cD190N$ ,  $\Delta 3cE217Q$ ,  $\Delta 3cE49Q$ ,  $\Delta 3cE172Q$ ,  $\Delta 3cE97Q$ , and  $\Delta 3cE98Q$ , corresponding to the mutant proteins which they harbor.  $\Delta 3cRbc_{Tk}$ , which is the *R. palustris* strain harboring wild-type *Tk*-Rubisco, and the eleven mutant strains were cultivated aerobically in LB medium for 2 d, and the cells were washed and grown under photoheterotrophic conditions. The growth rate of  $\Delta 3cRbc_{Tk}$  under photoheterotrophic conditions was  $0.29\text{ d}^{-1}$ . The growth rates of the strains with mutant proteins were  $0.23\pm 0.02\text{ d}^{-1}$  ( $\Delta 3cH94S$ ),  $0.28\pm 0.01\text{ d}^{-1}$  ( $\Delta 3cD125N$ ),  $0.31\pm 0.03\text{ d}^{-1}$  ( $\Delta 3cD137N$ ),  $0.26\text{ d}^{-1}$  ( $\Delta 3cD385N$ ),  $0.15\pm 0.02\text{ d}^{-1}$  ( $\Delta 3cD186N$ ),  $0.03\pm 0.01\text{ d}^{-1}$  ( $\Delta 3cD190N$ ),  $0.28\pm 0.01\text{ d}^{-1}$  ( $\Delta 3cE217Q$ ),  $0.02\pm 0.02\text{ d}^{-1}$  ( $\Delta 3cE49Q$ ),  $0.02\pm 0.02\text{ d}^{-1}$  ( $\Delta 3cE172Q$ ),  $0.20\pm 0.01\text{ d}^{-1}$  ( $\Delta 3cE97Q$ ), and  $0.32\pm 0.02\text{ d}^{-1}$  ( $\Delta 3cE98Q$ ). All recombinant strains grew at similar or lower specific growth rates than that of  $\Delta 3cRbc_{Tk}$  (Fig. 3).

**A**

## B

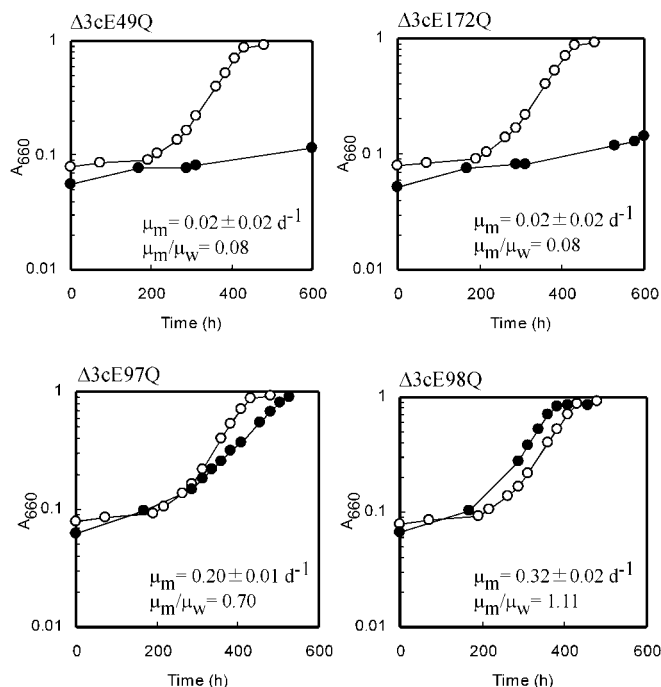


**Fig. 3. Growth of *R. palustris*  $\Delta 3$  recombinant strains harboring wild-type *Tk*-Rubisco and its mutant proteins.** The 11 mutant strains harbor the 11 mutant proteins designed to increase the flexibility of *Tk*-Rubisco. Representative growth curves of  $\Delta 3cRbc_{TK}$  (open circles) and strains harboring mutant proteins (closed circles) under photoheterotrophic conditions are shown. Heterotrophically grown cells were washed and inoculated into photoheterotrophic medium. The average specific growth rate of  $\Delta 3cRbc_{TK}$  ( $\mu_w$ ) was  $0.29 d^{-1}$ . The average specific growth rate of each strain harboring a mutant *Tk*-Rubisco ( $\mu_m$ ) (1 to 2 measurements) was compared with that of  $\mu_w$ , and is indicated in each panel. Recombinant strains that harbor mutant proteins disrupted of intra-subunit interactions and inter-subunit interactions are shown in A, B, respectively.

*Mutations in the loop6 and  $\alpha$ -helix6 regions.* The six mutant proteins described above with relevant levels of activity (SP3, SP4, SP5, SP6, GP1, and RR1) were individually introduced into *R. palustris*  $\Delta 3$  using the plasmid pSMZRbc. *R. palustris*  $\Delta 3$  strains with

the mutated *rbc<sub>Tk</sub>* genes were designated as strains  $\Delta 3cSP3$ ,  $\Delta 3cSP4$ ,  $\Delta 3cSP5$ ,  $\Delta 3cSP6$ ,  $\Delta 3cGP1$ , and  $\Delta 3cRR1$ .  $\Delta 3cRbc_{Tk}$  and the six strains with mutant proteins were cultivated aerobically in LB medium for 2 d, and the cells were washed and grown under photoheterotrophic conditions. The author found that the six strains with mutant *Tk*-Rubisco proteins could grow under photoheterotrophic conditions. The strains exhibited a broader variation of specific growth rates compared to the other set of mutant proteins disrupting single ionic interactions. Three to seven independent cultures were performed for each strain.  $\Delta 3cSP6$  cells exhibited the highest specific growth rate ( $0.39 \pm 0.02 \text{ d}^{-1}$ ), followed by  $\Delta 3cRbc_{Tk}$  ( $0.30 \pm 0.02 \text{ d}^{-1}$ ),  $\Delta 3cSP5$  ( $0.21 \pm 0.04 \text{ d}^{-1}$ ),  $\Delta 3cSP4$  ( $0.20 \pm 0.01 \text{ d}^{-1}$ ),  $\Delta 3cGP1$  ( $0.16 \pm 0.02 \text{ d}^{-1}$ ),  $\Delta 3cSP3$  ( $0.054 \pm 0.005 \text{ d}^{-1}$ ), and  $\Delta 3cRR1$  ( $0.027 \pm 0.01 \text{ d}^{-1}$ ) (Fig. 4A). The final levels of cell yield after full growth in these batch cultures were equivalent (not shown).  $\Delta 3cSP6$  displayed a 31% increase in specific growth rate compared to that of  $\Delta 3cRbc_{Tk}$ . The other recombinant strains grew at similar or lower specific growth rates than that of  $\Delta 3cRbc_{Tk}$ . To confirm the expression levels of *Tk*-Rubisco protein in each recombinant strain, Western blot analysis was carried out on the cell-free extracts of exponentially growing cells. The bands corresponding to the *Tk*-Rubisco proteins were equivalent in intensity (Fig. 4B), suggesting that the differences in growth rates were a result of differences in the performance of the individual proteins.



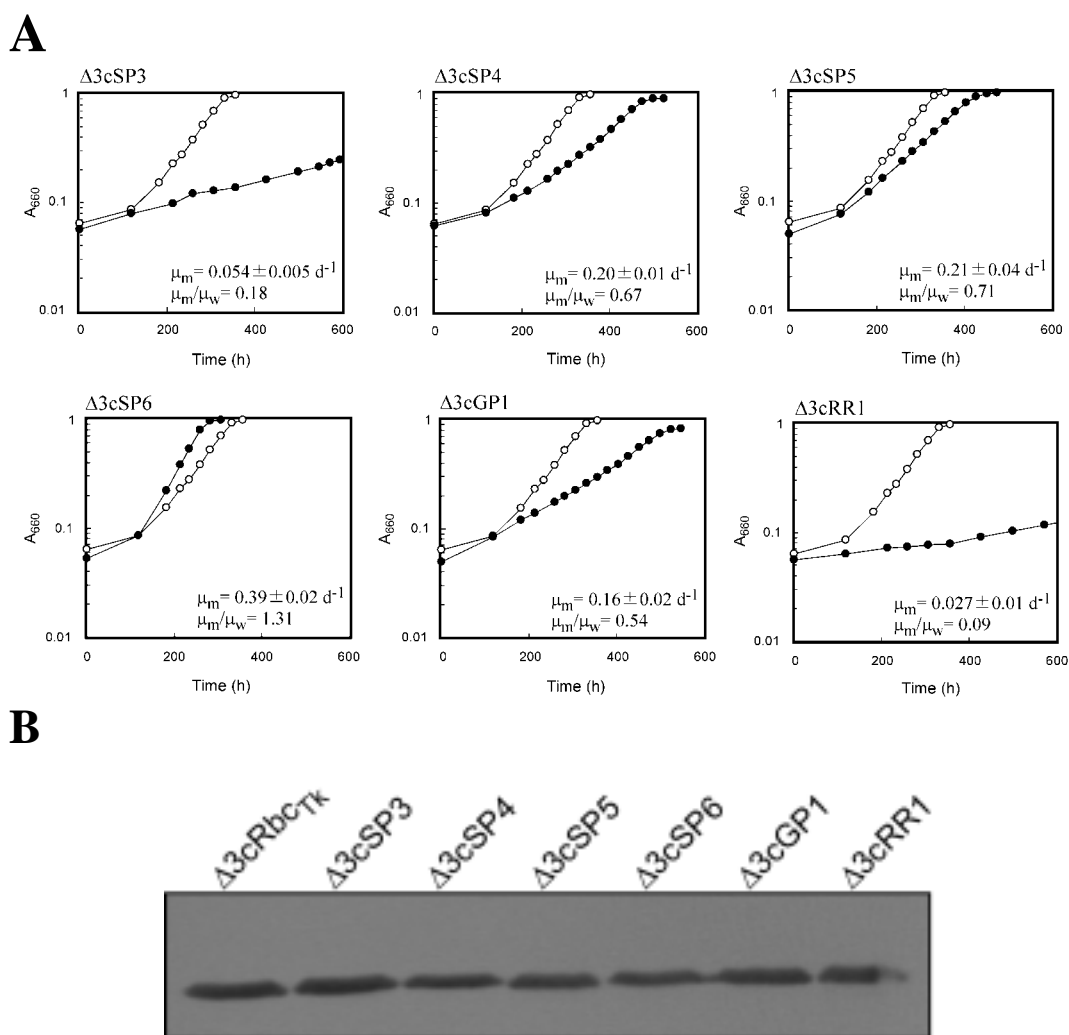


**Fig. 4. Growth of *R. palustris*  $\Delta 3$  recombinant strains harboring wild-type *Tk*-Rubisco and its mutant proteins with mutations in the loop6 and  $\alpha$ -helix6 regions.** Growth of strains harboring mutant Rubiscos that displayed relevant levels of activity in Fig. 2B are shown. (A) Representative growth curves of  $\Delta 3cRbc_{TK}$  (open circles) and strains harboring mutant proteins (closed circles) under photoheterotrophic conditions. Heterotrophically grown cells were washed and inoculated into photoheterotrophic medium. The average specific growth rate of 7 independent growth experiments of  $\Delta 3cRbc_{TK}$  ( $\mu_w$ ) was  $0.30 \pm 0.02 d^{-1}$ . The average specific growth rate of each strain harboring a mutant *Tk*-Rubisco ( $\mu_m$ ) (3 to 5 measurements) was compared with that of  $\mu_w$ , and is indicated in each panel. (B) Western blot analysis of the cell-free extracts obtained from each strain, using polyclonal antibodies against *Tk*-Rubisco. Cells were collected in the exponential growth phase, and 10  $\mu g$  were applied onto SDS-PAGE.

### **Kinetic analysis of the purified recombinant enzymes.**

The author examined and compared the kinetic parameters of *Tk*-Rubisco and mutant SP6, which led to a 31% increase in specific growth rate. The author also examined two other proteins with similar levels of activity to wild-type *Tk*-Rubisco (Fig. 2B); SP4, which led to lower growth rates than *Tk*-Rubisco, and SP3, whose performance *in vivo* was dramatically lower than the wild-type protein. *E. coli* cell extracts containing the recombinant proteins (*Tk*-Rubisco, mutants SP3, SP4, SP6) were subjected to heat treatment, anion exchange and gel-filtration chromatography and purified to apparent homogeneity. Kinetic analyses were performed at 25°C.

The maximum velocity of the carboxylase reaction ( $V_{CO_2}$ ) for wild-type *Tk*-Rubisco was  $0.30 \mu\text{mol min}^{-1} \text{mg}^{-1}$ , much lower than previously examined Rubiscos from mesophilic organisms (Table 3). The  $K_{CO_2}$  value of *Tk*-Rubisco was  $52.3 \mu\text{M}$ , a value lower than those observed in the Type I Rubiscos from cyanobacteria, but higher than those of plant Rubiscos. The substrate specificity factor  $\tau$  of *Tk*-Rubisco was 11.2 at 25°C, which is a considerably low value compared with spinach, *Synechococcus*, and other Type I Rubiscos. On the other hand, *Tk*-Rubisco exhibited an extremely low  $K_{RuBP}$  value of  $<0.5 \mu\text{M}$ , lowest among those previously reported. Accurate  $K_{RuBP}$  values could not be obtained using an anion exchange chromatographic system with an AS11 column.

The author clearly observed an increase in turnover number in the SP6 protein (32% increase in  $V_{CO_2}$ ), which resulted in a 17% increase in  $k_{cat(CO_2)}/K_{CO_2}$ . In the case of SP4, the kinetic parameters for the carboxylase activity were similar to that of *Tk*-Rubisco. In the case of SP3, the protein displayed a decrease in  $V_{CO_2}$ , along with a relatively large increase in  $K_{CO_2}$ , resulting in a 35% decrease in  $k_{cat(CO_2)}/K_{CO_2}$  (Table 3).

**Table 3. Kinetic properties of purified *Tk*-Rubisco and its mutant proteins.**

Kinetic constant	<i>Tk</i> -Rubisco <sup>at 25°C</sup>				References <sup>at 25°C</sup>		
	wild-type ( $\mu= 0.30 \text{ d}^{-1}$ ) <sup>a</sup>	SP3 ( $\mu= 0.054 \text{ d}^{-1}$ ) <sup>a</sup>	SP4 ( $\mu= 0.20 \text{ d}^{-1}$ ) <sup>a</sup>	SP6 ( $\mu= 0.39 \text{ d}^{-1}$ ) <sup>a</sup>	Spinach <sup>(24)</sup>	<i>R. rubrum</i> <sup>(20)</sup>	<i>Synechococcus</i> <sup>(19)</sup>
$V_{\text{CO}_2}$ ( $\mu\text{mol}/\text{min}/\text{mg}$ )	0.30±0.01	0.28±0.01	0.30±0.02	0.39±0.02	2.3	6.2±0.4	3.24±0.07
$k_{\text{cat}(\text{CO}_2)}$ ( $\text{s}^{-1}\cdot\text{site}^{-1}$ )	0.25	0.23	0.25	0.33	2.6	5.2	3.71
$K_{\text{CO}_2}$ ( $\mu\text{M}$ )	52±6	74±8	50±8	59±6	14.3	150±30	167±2
$k_{\text{cat}(\text{CO}_2)} / K_{\text{CO}_2}$	0.0047	0.0031	0.0050	0.0055	0.182	0.035	0.022
$V_{\text{O}_2}$ ( $\mu\text{mol}/\text{min}/\text{mg}$ )	0.46	0.06	0.17	0.29		1.57	0.25
$k_{\text{cat}(\text{O}_2)}$ ( $\text{s}^{-1}\cdot\text{site}^{-1}$ )	0.38	0.05	0.14	0.24		1.32	0.29
$K_{\text{O}_2}$ ( $\mu\text{M}$ )	900±90	280±20	300±10	460±40		380±50	529±14
$k_{\text{cat}(\text{O}_2)} / K_{\text{O}_2}$	0.00042	0.00017	0.00047	0.00051		0.0035	0.00053
$\tau$ ( $V_{\text{CO}_2}K_{\text{O}_2}/V_{\text{O}_2}K_{\text{CO}_2}$ )	11±1	18±1	11±0	11±2	93.8±0.8	10±0.5	41.0±4.4
$K_{\text{RuBP}}$ ( $\mu\text{M}$ )	< 0.5	< 0.5	< 0.5	< 0.5			19.2±3.6

<sup>a</sup>  $\mu$  represents specific growth rates of recombinant strains which harbor the proteins noted above.

## DISCUSSION

In order to examine the possibilities of improving the function of *Tk*-Rubisco at ambient temperatures, the author has performed an initial site-directed mutagenesis study on the enzyme. A first set of mutant proteins was constructed in order to increase the flexibility of *Tk*-Rubisco at lower temperatures. A second set was designed focusing on loop6 and  $\alpha$ -helix6, replacing residues or sequence stretches with those found in mesophilic or moderately thermophilic Type I and Type II enzymes. By examining the performance of these proteins *in vivo*, it became clear that the latter set of mutations had a much greater effect on the performance of *Tk*-Rubisco. The simultaneous disruption of a larger number of ionic interactions may be necessary in order to observe their effects on *Tk*-Rubisco activity at ambient temperatures. In the mutant proteins focusing on the loop6 and  $\alpha$ -helix6 regions, although a number of mutant proteins had over 10 residues exchanged, the author found that all proteins were produced in a soluble form in *E. coli*. This confirmed the assumption that the extremely thermostable scaffold of *Tk*-Rubisco is able to tolerate large extents of mutagenesis, and will provide an advantage in further studies taking a random mutagenesis approach.

The kinetic analysis on wild-type *Tk*-Rubisco indicated that the enzyme displays a very low turnover number at 25°C, which can be expected as the enzyme derives from a hyperthermophile. The affinity towards CO<sub>2</sub> was higher than that of the Type I enzyme from *Synechococcus*, but lower than the values of the spinach enzyme. A notable feature was the extremely low K<sub>m</sub> value towards RuBP. This trait is most likely due to the necessity of the enzyme to rapidly bind to RuBP in *T. kodakaraensis* at high temperatures, as RuBP is a thermolabile compound.

The loop6 and  $\alpha$ -helix6 regions have been demonstrated to play an important

role in the turnover and specificity of Type I and Type II Rubiscos (18). Results in this chapter have clarified that these regions are also important for the activity of the Type III *Tk*-Rubisco. The length of loop6 is vital; a deletion of a single amino acid residue results in almost complete loss of activity in mutants SP1, SP2, SP7, GP2,  $\Delta$ T317, and  $\Delta$ A318 regardless of the sequences in the  $\alpha$ -helix6 region. The author also found that residue replacements in loop6 (mutant RR1) also dramatically affect specific activity levels. As for  $\alpha$ -helix6, a replacement with the corresponding region from *G. partita* led to over 50% reduction in activity levels, while replacement with the region from spinach had a positive effect. The results indicate that the  $\alpha$ -helix6 region also plays a key role in *Tk*-Rubisco catalysis.

Three-dimensional structures are available for the Rubisco proteins from spinach (Type I) (23), *G. partita* (Type I) (17), *R. rubrum* (Type II) (13), and *T. kodakaraensis* (Type III) (10). Although the quaternary structures of the Type I–III Rubiscos are distinct, the monomeric folds of the proteins are well conserved. We compared the monomer structures by superimposing the structure of *Tk*-Rubisco with those of the three other enzymes. We noticed that the  $\alpha$ -helix6 region of *Tk*-Rubisco displayed a different configuration against the catalytic pocket compared to the other Rubiscos (Fig. 5A). While the positions of the  $\alpha$ -helix6 regions of the Rubiscos from spinach, *G. partita* and *R. rubrum* were well conserved (Fig. 5B, C), the  $\alpha$ -helix6 of *Tk*-Rubisco was positioned closer to the catalytic pocket. Replacing the original  $\alpha$ -helix6 of *Tk*-Rubisco with that of spinach Rubisco may have led to a conformation of this region that is more similar to the mesophilic Rubiscos, thereby increasing the catalytic turnover at 25°C.

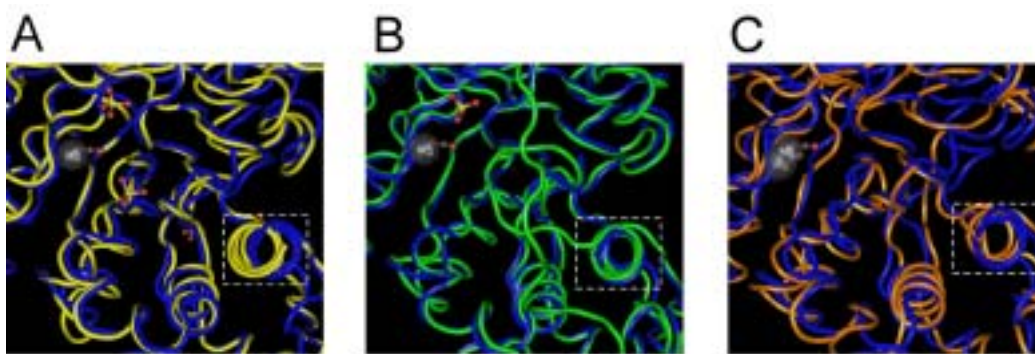


**Fig. 5. Structural comparison among the monomer structures of various Rubiscos.** The monomer structure of spinach Rubisco (Protein Data Bank accession number 1AUS, blue ribbon) was superimposed with (A) *Tk*-Rubisco (1GEH, yellow ribbon), (B) *G. partita* Rubisco (1IWA, green ribbon) or (C) *R. rubrum* Rubisco (2RUS, orange ribbon). Superimpositions were performed with Vast Structure Neighbors (NCBI), and visualized using Cn3D software (available at NCBI). The  $\alpha$ -helix6 regions are boxed.

The growth experiments under photoheterotrophic conditions were performed in the presence of 5 mM  $\text{NaHCO}_3$  concentrations and with little head-space in the sealed vials. The turnover rate of the carboxylase activity ( $V_{\text{CO}_2}$ ) was thus expected to have a large effect on the specific growth rates. The  $k_{\text{cat}(\text{CO}_2)}/K_{\text{CO}_2}$  values may also be relevant, depending on the capacity of  $\text{NaHCO}_3$  uptake in *R. palustris* and the intracellular levels of carbonic anhydrase activity. Growth examinations of the initial six recombinant strains (Fig. 4A) revealed that  $\Delta 3\text{cSP6}$  grew at a higher rate than  $\Delta 3\text{cRbc}_{\text{Tk}}$  (31% increase). This correlates well with the fact that the SP6 protein exhibited higher  $V_{\text{CO}_2}$  and  $k_{\text{cat}(\text{CO}_2)}/K_{\text{CO}_2}$  values than wild-type *Tk*-Rubisco (Table 3). The increases in these values most likely override the slight decrease in  $\tau$  value. As for  $\Delta 3\text{cSP3}$ , the strain exhibited much slower growth than that of  $\Delta 3\text{cRbc}_{\text{Tk}}$  (82% decrease). Accordingly, the  $V_{\text{CO}_2}$  and  $k_{\text{cat}(\text{CO}_2)}/K_{\text{CO}_2}$  values displayed 9% and 34% decreases,

respectively. The increase in  $\tau$  value, mainly due to the decrease in oxygenase activity (and not an increase in carboxylase activity), was not reflected under these growth conditions. In the case of SP4, it was difficult to determine what properties of the protein were responsible for the 33% decrease in specific growth rate, as the kinetic properties *in vitro* were apparently equivalent to those of the wild-type *Tk*-Rubisco.

## SUMMARY

In this chapter, the author has examined the enzymatic properties of *Tk*-Rubisco at 25°C and has constructed mutant proteins in order to enhance its performance in mesophilic host cells. Two sets of mutant proteins were designed and constructed. The first set aimed to increase the flexibility of *Tk*-Rubisco at ambient temperatures by individually disrupting various ionic interactions predicted to be present in the protein. A second set focused on sequence differences in the loop6 and  $\alpha$ -helix6 regions among *Tk*-Rubisco and the enzymes from spinach, *Galdieria partita*, and *Rhodospirillum rubrum*. The latter set of mutations had greater effects on enzyme activity, as judged by comparing specific growth rates of *R. palustris* harboring each mutant protein.

Loop6 of *Tk*-Rubisco is one residue longer than those found in the spinach and *G. partita* enzymes, and replacing the *Tk*-Rubisco loop6 with these regions led to dramatic decreases in activity. Six mutant enzymes retaining significant levels of Rubisco activity were selected, and their genes were introduced into *R. palustris*  $\Delta 3$ . Cells harboring mutant protein SP6 displayed a 31% increase in specific growth rate under photoheterotrophic conditions compared to cells harboring wild-type *Tk*-Rubisco. SP6 corresponds to a complete substitution of the original  $\alpha$ -helix6 of *Tk*-Rubisco with

that of the spinach enzyme. Compared to the wild-type *Tk*-Rubisco, the purified SP6 mutant protein exhibited a 32% increase in turnover number ( $k_{\text{cat}}$ ) of the carboxylase activity and a 17% increase in  $k_{\text{cat}}/K_m$  value.

## REFERENCES

1. **Andrews, T. J., and G. H. Lorimer.** 1987. Rubisco: Structure, mechanisms, and prospects for improvement., p. 131-218. *In* M. D. Hatch and N. K. Boardman (ed.), The Biochemistry of Plants. Academic Press, San Diego.
2. **Ezaki, S., N. Maeda, T. Kishimoto, H. Atomi, and T. Imanaka.** 1999. Presence of a structurally novel type ribulose-bisphosphate carboxylase/oxygenase in the hyperthermophilic archaeon, *Pyrococcus kodakaraensis* KOD1. *J. Biol. Chem.* **274**:5078-5082.
3. **Gatenby, A. A.** 1988. Synthesis and assembly of bacterial and higher plant Rubisco subunits in *Escherichia coli*. *Photosynth. Res.* **17**:145-157.
4. **Gatenby, A. A., S. M. van der Vies, and D. Bradley.** 1985. Assembly in *E. coli* of a functional multi-subunit ribulose bisphosphate carboxylase from a blue-green alga. *Nature* **314**:617-620.
5. **Gutteridge, S., D. F. Rhoades, and C. Herrmann.** 1993. Site-specific mutations in a loop region of the C-terminal domain of the large subunit of ribulose bisphosphate carboxylase/oxygenase that influence substrate partitioning. *J. Biol. Chem.* **268**:7818-7824.
6. **Gutteridge, S., I. Sigal, B. Thomas, R. Arentzen, A. Cordova, and G. Lorimer.** 1984. A site-specific mutation within the active site of ribulose-1,5-bisphosphate carboxylase of *Rhodospirillum rubrum*. *EMBO J.*



- 3:2737-2743.
7. **Harpel, M. R., E. H. Serpersu, and F. C. Hartman.** 1995. Utilization of partial reactions, side reactions, and chemical rescue to analyse site-directed mutants of ribulose 1,5-bisphosphate (RuBP) carboxylase/oxygenase (Rubisco), p. 357-364. *In* J. W. Crabb (ed.), *Techniques in Protein Chemistry*. Academic Press, San Diego.
  8. **Jordan, D. B., and W. L. Ogren.** 1981. Species variation in the specificity of ribulose biphosphate carboxylase-oxygenase. *Nature* **291**:513-515.
  9. **Kane, H. J., J. Viil, B. Entsch, K. Paul, M. K. Morell, and T. J. Andrews.** 1994. An improved method for measuring the CO<sub>2</sub>/O<sub>2</sub> specificity of ribulosebisphosphate carboxylase-oxygenase. *Aust. J. Plant Physiol.* **21**:449-461.
  10. **Kitano, K., N. Maeda, T. Fukui, H. Atomi, T. Imanaka, and K. Miki.** 2001. Crystal structure of a novel-type archaeal Rubisco with pentagonal symmetry. *Structure* **9**:473-481.
  11. **Knight, S., I. Andersson, and C. I. Brändén.** 1990. Crystallographic analysis of ribulose 1,5-bisphosphate carboxylase from spinach at 2.4 Å resolution. Subunit interactions and active site. *J. Mol. Biol.* **215**:113-160.
  12. **Laing, W. A., W. L. Ogren, and R. H. Hageman.** 1975. Bicarbonate stabilization of ribulose 1,5-diphosphate carboxylase. *Biochemistry* **14**:2269-2275.
  13. **Lundqvist, T., and G. Schneider.** 1991. Crystal structure of the ternary complex of ribulose-1,5-bisphosphate carboxylase, Mg(II), and activator CO<sub>2</sub> at 2.3-Å resolution. *Biochemistry* **30**:904-908.

14. **Maeda, N., T. Kanai, H. Atomi, and T. Imanaka.** 2002. The unique pentagonal structure of an archaeal Rubisco is essential for its high thermostability. *J. Biol. Chem.* **277**:31656-31662.
15. **Maeda, N., K. Kitano, T. Fukui, S. Ezaki, H. Atomi, K. Miki, and T. Imanaka.** 1999. Ribulose biphosphate carboxylase/oxygenase from the hyperthermophilic archaeon *Pyrococcus kodakaraensis* KOD1 is composed solely of large subunits and forms a pentagonal structure. *J. Mol. Biol.* **293**:57-66.
16. **Newman, J., and S. Gutteridge.** 1993. The X-ray structure of *Synechococcus* ribulose-biphosphate carboxylase/oxygenase-activated quaternary complex at 2.2-Å resolution. *J. Biol. Chem.* **268**:25876-25886.
17. **Okano, Y., E. Mizohata, Y. Xie, H. Matsumura, H. Sugawara, T. Inoue, A. Yokota, and Y. Kai.** 2002. X-ray structure of *Galdieria* Rubisco complexed with one sulfate ion per active site. *FEBS Lett.* **527**:33-36.
18. **Parry, M. A. J., P. J. Andralojc, R. A. Mitchell, P. J. Madgwick, and A. J. Keys.** 2003. Manipulation of Rubisco: the amount, activity, function and regulation. *J. Exp. Bot.* **54**:1321-1333.
19. **Read, B. A., and F. R. Tabita.** 1994. High substrate specificity factor ribulose-biphosphate carboxylase/oxygenase from eukaryotic marine algae and properties of recombinant cyanobacterial Rubisco containing "algal" residue modifications. *Arch. Biochem. Biophys.* **312**:210-218.
20. **Smith, H. B., F. W. Larimer, and F. C. Hartman.** 1990. An engineered change in substrate specificity of ribulosebiphosphate carboxylase/oxygenase. *J. Biol. Chem.* **265**:1243-1245.

21. **Somerville, C. R., and S. C. Somerville.** 1984. Cloning and expression of the *Rhodospirillum rubrum* ribulosebiphosphate carboxylase gene in *Escherichia coli*. *Mol. Gen. Genet.* **193**:214-219.
22. **Spreitzer, R. J., D. B. Jordan, and W. L. Ogren.** 1982. Biochemical and genetic analysis of an RuBP carboxylase/oxygenase-deficient mutant and revertants of *Chlamydomonas reinhardtii*. *FEBS Lett.* **148**:117-121.
23. **Taylor, T. C., and I. Andersson.** 1997. Structure of a product complex of spinach ribulose-1,5-bisphosphate carboxylase/oxygenase. *Biochemistry* **36**:4041-4046.
24. **Uemura, K., Anwaruzzaman, S. Miyachi, and A. Yokota.** 1997. Ribulose-1,5-bisphosphate carboxylase/oxygenase from thermophilic red algae with a strong specificity for CO<sub>2</sub> fixation. *Biochem. Biophys. Res. Commun.* **233**:568-571.
25. **Uemura, K., Y. Suzuki, T. Shikanai, A. Wadano, R. G. Jensen, W. Chmara, and A. Yokota.** 1996. A rapid and sensitive method for determination of relative specificity of RuBisCO from various species by anion-exchange chromatography. *Plant Cell Physiol.* **37**:325-331.
26. **van der Vies, S. M., D. Bradley, and A. A. Gatenby.** 1986. Assembly of cyanobacterial and higher plant ribulose bisphosphate carboxylase subunits into functional homologous and heterologous enzyme molecules in *Escherichia coli*. *EMBO J.* **5**:2439-2444.
27. **Varley, P. G., and R. H. Pain.** 1991. Relation between stability, dynamics and enzyme activity in 3-phosphoglycerate kinases from yeast and *Thermus thermophilus*. *J. Mol. Biol.* **220**:531-538.

28. **Vihinen, M.** 1987. Relationship of protein flexibility to thermostability. *Protein Eng.* **1**:477-480.
29. **Závodszky, P., J. Kardos, A. Svingor, and G. A. Petsko.** 1998. Adjustment of conformational flexibility is a key event in the thermal adaptation of proteins. *Proc. Natl. Acad. Sci. USA* **95**:7406-7411.

## CHAPTER 3

### Optimizing the $\alpha$ -helix6 region of *Tk*-Rubisco to enhance catalytic performance of the enzyme at ambient temperatures

#### INTRODUCTION

In CHAPTER 2, the author designed and constructed two sets of mutant proteins of the Type III Rubisco from *Thermococcus kodakaraensis* (*Tk*-Rubisco), aiming to enhance the catalytic performance of the enzyme in mesophilic host cells. The first set was designed to confer greater flexibility to the protein at ambient temperatures. Various ionic interactions, expected to add rigidity to the protein, were disrupted by site-directed mutagenesis. A second set was based on sequence differences in the loop6 and  $\alpha$ -helix6 regions among *Tk*-Rubisco and the enzymes from spinach, *Galdieria partita*, and *Rhodospirillum rubrum*. Structural studies on Type I and Type II enzymes have revealed that loop6 covers the  $\beta/\alpha$  barrel of Rubisco and acts as a lid during Rubisco catalysis. Loop6 harbors the active site residue lysine and has been proposed to stabilize reaction intermediates during catalysis (1, 2). The author replaced various residues or regions of the loop6 region and the adjacent  $\alpha$ -helix6 region of *Tk*-Rubisco with corresponding residues found in the enzymes from spinach, *G. partita*, and *R. rubrum*.

The mutant genes were individually introduced into *Rhodopseudomonas palustris*  $\Delta 3$ , a strain whose three endogenous Rubisco genes had been deleted in studies described in CHAPTER 1. By comparing specific growth rates of *R. palustris* harboring each mutant protein, the author found that the latter set of mutations focusing on the loop6 and  $\alpha$ -helix6 regions had greater effects on the performance of *Tk*-Rubisco

*in vivo*. In particular, cells harboring mutant protein SP6, whose  $\alpha$ -helix6 region was replaced with that of the spinach enzyme, displayed a 31% increase in specific growth rate under photoheterotrophic conditions compared to cells harboring wild-type *Tk*-Rubisco. The SP6 mutant protein was thus purified and subjected to biochemical and kinetic analysis. As expected, the SP6 protein exhibited a 30% increase in turnover number ( $k_{cat}$ ) of the carboxylase activity and a 17% increase in  $k_{cat}/K_m$  value at 25°C compared to the wild-type *Tk*-Rubisco. The results indicated that the structure of the loop6 and  $\alpha$ -helix6 regions have a direct effect on the catalytic performance of *Tk*-Rubisco, and raise the possibilities that additional changes in the  $\alpha$ -helix6 region could lead to further improvements in *Tk*-Rubisco catalysis at ambient temperatures.

In this chapter, the author has carried out an extensive site-directed mutagenesis study on the  $\alpha$ -helix6 region of *Tk*-Rubisco. Mutants were designed based on the results of the mutant proteins constructed and examined in CHAPTER 2, with particular focus on the mutant protein SP6, which exhibited improved properties compared to the wild-type protein at ambient temperatures.

## **MATERIALS AND METHODS**

### **Site-directed mutagenesis.**

Site-directed mutagenesis was carried out using a QuikChange XL site-directed kit (Stratagene, La Jolla, CA). Primers and plasmids used as templates for the introduction of residue exchanges are described in Table 1.

**Table 1. Primers used for site-directed mutagenesis.**

Mutant	Template plasmid	Sequence
SP4-T330V	pET21a(+)/SP4	5' -GAGGGCGAGCGCGACATAG <u>CTC</u> ATTTCAGAACGCCAGG-3' 5' -CCTGGCGTTCTGAATG <u>ACT</u> TATGTGCGCTCGCCCTC-3'
SP4-Q332G	pET21a(+)/SP4	5' -GAGCGCGACATAACCATT <u>GGC</u> AACGCCAGGATTCTCAG-3' 5' -CTGAGAATCCTGGCGTT <u>GCC</u> AATGGTTATGTGCGCTC-3'
SP4-N333F	pET21a(+)/SP4	5' -CGCGACATAACCATTTCAG <u>TTC</u> GCCAGGATTCTCAGGGAG-3' 5' -CTCCCTGAGAATCCTGGC <u>GAA</u> CTGAATGGTTATGTGCGC-3'
SP4-R335D	pET21a(+)/SP4	5' -GACATAACCATTTCAGAACGCC <u>GAC</u> ATTCTCAGGGAGAGCCAC-3' 5' -GTGGCTCTCCCTGAGAAT <u>GTC</u> GGCGTTCTGAATGGTTATGTC-3'
SP4-QNR/GFD	pET21a(+)/SP4-Q332G	5' -GCGACATAACCATTGGC <u>TTC</u> GCCAGGATTCTCAGGGAG-3' 5' -CTCCCTGAGAATCCTGGCG <u>AAG</u> CCAATGGTTATGTGCGC-3'
	pET21a(+)/SP4-Q332G/ N333F	5' -CCATTGGCTTCGCC <u>GAC</u> ATTCTCAGGGAGAGCCAC-3' 5' -GTGGCTCTCCCTGAGAAT <u>GTC</u> GGCGAAGCCAATGG-3'
SP5-G326E	pET21a(+)/SP5	5' -GGCAAGCTTGAGGGC <u>GAG</u> AAGTGGGACGTCCTC-3' 5' -GAGGACGTCCCACTT <u>CTC</u> GCCCTCAAGCTTGCC-3'
SP5-K327R	pET21a(+)/SP5	5' -GCAAGCTTGAGGGCGGC <u>CGC</u> TGGGACGTCCTCGG-3' 5' -CCGAGGACGTCCCA <u>GCG</u> GCCGCCCTCAAGCTTGC-3'
SP5-W328D	pET21a(+)/SP5	5' -GCTTGAGGGCGGCAAG <u>GAC</u> GACGTCCTCGGCTTC-3' 5' -GAAGCCGAGGACGTC <u>GTC</u> CCTTGCCGCCCTCAAGC-3'
SP5-D329I	pET21a(+)/SP5	5' -GAGGGCGGCAAGTGG <u>ATC</u> GTCTCCTCGGCTTCG-3' 5' -CGAAGCCGAGGAC <u>GAT</u> CCACTTGCCGCCCTC-3'
SP5-V330T	pET21a(+)/SP5	5' -GAGGGCGGCAAGTGGGAC <u>ACC</u> TGCGCTTCGTTGAC-3' 5' -GTCAACGAAGCCGAG <u>GGT</u> GTCCCACTTGCCGCCCTC-3'
N333F	pET21a(+)/ <i>rbcTk</i>	5' -GTGGGACGTCATTCAGT <u>TTC</u> GCCAGGATTCTCAGG-3' 5' -CCTGAGAATCCTGGC <u>GAA</u> CTGAATGACGTCCCAC-3'
V330T/N333F	pET21a(+)/V330T	5' -GTGGGACACCATTTCAGT <u>TTC</u> GCCAGGATTCTCAGG-3' 5' -CCTGAGAATCCTGGC <u>GAA</u> CTGAATGGTGTCCCAC-3'

The three consecutive hyphens represent the positions where nucleotides have been removed. The underlined nucleotides correspond to the codon that has been changed.

### Gene expression and protein purification.

In this chapter, the wild-type *Tk*-Rubisco and the mutant proteins SP4-N333F and SP5-V330T were expressed and purified. *E. coli* strains and plasmids used for gene expression are the same as those used in the previous chapter. Growth media and conditions for gene expression, as well as the protein purification procedure, are described in CHAPTER 2.

### **Kinetic examination.**

The conditions for activity measurements in the kinetic examination of mutant proteins SP4-N333F and SP5-V330T were the same as those applied for wild-type *Tk*-Rubisco, and the mutant proteins SP3, SP4 and SP6 (CHAPTER 2).

### **Effects of temperatures on enzyme stabilities.**

Thermostabilities of *Tk*-Rubisco, SP4, SP6, and SP4-N333F were analyzed by measuring the residual carboxylase activities of the proteins after incubation at 90°C or 100°C in buffer A (100 mM Bicine-NaOH (pH 8.3), 10 mM MgCl<sub>2</sub>). Denatured proteins were removed by centrifugation (20 min, 15,000 x g, 4°C) and the supernatant was used for activity measurements. Residual activities were measured with the enzymatic assay methods described in CHAPTER 1.

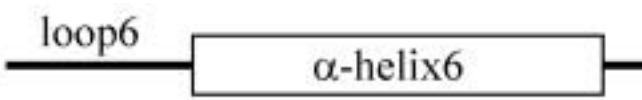
## **RESULTS**

### **Mutation design in the $\alpha$ -helix6 region of *Tk*-Rubisco.**

As described in CHAPTER 2, both *in vitro* (kinetics) and *in vivo* (growth rates) analyses indicated that the SP6 mutant protein displayed improved catalytic properties at ambient temperature. The SP6 protein corresponds to a complete replacement of the  $\alpha$ -helix6 region of *Tk*-Rubisco with that of the spinach Rubisco. In order to determine which residue(s) in the  $\alpha$ -helix6 region were mainly responsible for the increase in activity, further mutations were designed. Intriguingly, the improved performance of SP6 was not a simple additive sum of effects brought about by individual residue replacements. SP4 and SP5, whose mutations when combined correspond to SP6, neither exhibited improved enzyme performance. The author thus



focused on the residues responsible for the differences in performance observed between SP4 and SP6, and between SP5 and SP6. The sequences of mutant proteins designed and examined in this chapter are shown in Fig. 1.

		
	Tk	GGKWDVIQNARILR
	Sp	GERDITLGFVDLLR
	SP4	GERDITIQNARILR
	SP5	GGKWDVLGFVDLLR
	SP6	GERDITLGFVDLLR
<b>A</b>	SP4-QNR/GFD	GERDITIGFADILR
	SP4-Q332G	GERDITIGNARILR
	SP4-N333F	GERDITIQFARILR
	SP4-R335D	GERDITIQNADILR
<b>B</b>	SP5-G326E	GEKWDVLGFVDLLR
	SP5-K327R	GGRWDVLGFVDLLR
	SP5-W328D	GGKDDVLGFVDLLR
	SP5-D329I	GGKWI <sup>I</sup> VLGFVDLLR
	SP5-V330T	GGKWD <sup>T</sup> LGFVDLLR
<b>C</b>	V330T(SP3)	GGKWD <sup>T</sup> IQNARILR
	N333F	GGKWDVIQ <sup>F</sup> ARILR
	V330T/N333F	GGKWD <sup>T</sup> IQ <sup>F</sup> ARILR

**Fig. 1. Site-directed mutagenesis on the  $\alpha$ -helix6 region of *Tk*-Rubisco.** Alignment of the  $\alpha$ -helix6 regions of Rubiscos from *T. kodakaraensis* KOD1 (Tk, Type III, BAD86479), spinach (Sp, Type I, red, P00875), and mutant *Tk*-Rubisco proteins produced in CHAPTER 2 is shown with their secondary structures. (A-C) Mutant design of *Tk*-Rubisco. Alignment of mutant proteins based on the sequence differences between SP4/SP6 (A), SP5/SP6 (B), and mutants focused on V330T and N333F (C). Exchanged residues are indicated in red.

## **Determination of the residues governing the difference in performance between SP4 and SP6.**

Six residues are different between SP4 and SP6 (positions 331–336). Among these, the author presumed that the differences in residues at positions 332 (SP4:Gln/SP6:Gly), 333 (SP4:Asn/SP6:Phe) and 335 (SP4:Arg/SP6:Asp) would have greater effects than the differences at positions 331 (Ile/Leu), 334 (Ala/Val) and 336 (Ile/Leu). The latter three residues are replacements between similar aliphatic hydrophobic residues. The author therefore constructed a mutant protein (SP4-QNR/GFD) where residues of SP4 at positions 332/333/335 were replaced by the corresponding residues of SP6. The SP4-QNR/GFD gene was introduced into *R. palustris*  $\Delta 3$  cells ( $\Delta 3$ cSP4-QNR/GFD) and photoheterotrophic growth rates were examined (Fig. 2A). The specific growth rate of  $\Delta 3$ cSP4-QNR/GFD ( $0.43 \text{ d}^{-1}$ ) displayed a significant increase compared to that of SP4 ( $0.20 \text{ d}^{-1}$ ), and was even higher than the specific growth rate of SP6 ( $0.39 \text{ d}^{-1}$ ). This strongly suggests that the residue(s) responsible for the differences in activity between SP4 and SP6 are included in these three residues. The author thus examined the effects of changing each individual residue (SP4-Q332G, SP4-N333F, SP4-R335D). *R. palustris*  $\Delta 3$  cells harboring the SP4-R335D gene exhibited a specific growth rate ( $0.15 \text{ d}^{-1}$ ) even lower than that of the SP4 strain ( $0.20 \text{ d}^{-1}$ ), indicating that D335 of SP6 does not contribute to the increase in SP6 activity compared to SP4, and rather has a negative effect. Growth rates of cells producing SP4-Q332G were higher than those of  $\Delta 3$ cSP4 cells, indicating that the Q332G mutation does have a positive effect, but growth rates were still lower than  $\Delta 3$ cSP6 and  $\Delta 3$ cRbc<sub>TK</sub>. The specific growth rate of cells harboring the SP4-N333F gene ( $\Delta 3$ cSP4-N333F) displayed a dramatic increase ( $0.39 \text{ d}^{-1}$ ) compared to that of  $\Delta 3$ cSP4,

and was equivalent to that of  $\Delta 3cSP6$  ( $0.39\text{ d}^{-1}$ ), suggesting that F333 is the residue most responsible for the differences in enzyme performance between SP4 and SP6 (Fig. 2A).

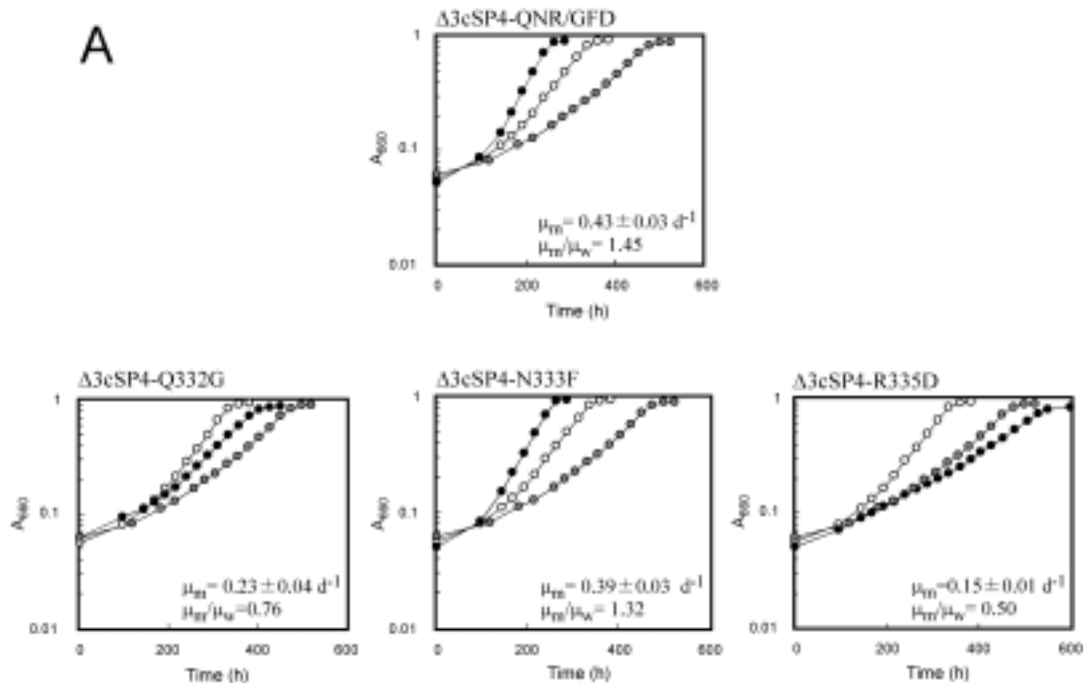
### **Determination of the residues governing the difference in performance between SP5 and SP6.**

The mutant proteins SP5 and SP6 (positions 326–330) differ in 5 residues (Fig. 1). The author therefore replaced each of the five residues individually with the residue found in SP6, resulting in the mutant proteins SP5-G326E, SP5-K327R, SP5-W328D, SP5-D329I, and SP5-V330T. The mutant genes were introduced into *R. palustris*  $\Delta 3$  cells, and the author examined the specific growth rates of each recombinant strain. *R. palustris*  $\Delta 3$  cells harboring SP5-G326E, SP5-K327R, SP5-W328D, and SP5-D329I ( $\Delta 3cSP5$ -G326E,  $\Delta 3cSP5$ -K327R,  $\Delta 3cSP5$ -W328D, and  $\Delta 3c$  SP5-D329I, respectively) displayed specific growth rates that were lower than that of  $\Delta 3cRbc_{Tk}$  ( $0.31\text{ d}^{-1}$ ). They were in fact lower than the specific growth rate of  $\Delta 3cSP5$  ( $0.23\text{ d}^{-1}$ ) cells. In contrast, cells harboring the SP5-V330T gene ( $\Delta 3cSP5$ -V330T) exhibited a specific growth rate ( $0.48\text{ d}^{-1}$ ) higher than that of  $\Delta 3cRbc_{Tk}$ , indicating that T330 is the residue most responsible for the differences in enzyme performance between SP5 and SP6 (Fig. 2B).

### **Growth characteristics of *R. palustris* $\Delta 3$ strains harboring V330T (SP3), N333F, or V330/N333F mutant proteins.**

SP4-N333F and SP5-V330T mutant proteins greatly enhanced the growth rate of *R. palustris*  $\Delta 3$  strain, indicating that N333F and V330T mutations were important factors for the improvement of the wild-type protein in *R. palustris*. As SP6 mutations

correspond to the sum of mutations introduced in SP4 and SP5, the author presumed that the improved performance of SP6 was due to a synergistic effect of the F333 and T330 mutations. In order to examine this hypothesis, in addition to the strain  $\Delta 3cV330T$  (SP3) (examined in CHAPTER 2), the author further constructed two recombinant strains  $\Delta 3cN333F$  and  $\Delta 3cV330T/N333F$ . When photoheterotrophic growth of these strains were examined, the observed specific growth rates were contrary to the author's expectations.  $\Delta 3cN333F$  displayed a higher specific growth rate ( $0.37 \text{ d}^{-1}$ ) than  $\Delta 3cRbc_{Tk}$  ( $0.29 \text{ d}^{-1}$ ), indicating that the mutation N333F alone improves the functional performance of *Tk*-Rubisco. The other strain,  $\Delta 3cV330T/N333F$ , displayed a much lower specific growth rate ( $0.12 \text{ d}^{-1}$ ) compared with  $\Delta 3cRbc_{Tk}$ , indicating that the enhanced performance of SP6 was not brought about solely by the presence of F333 and T330.



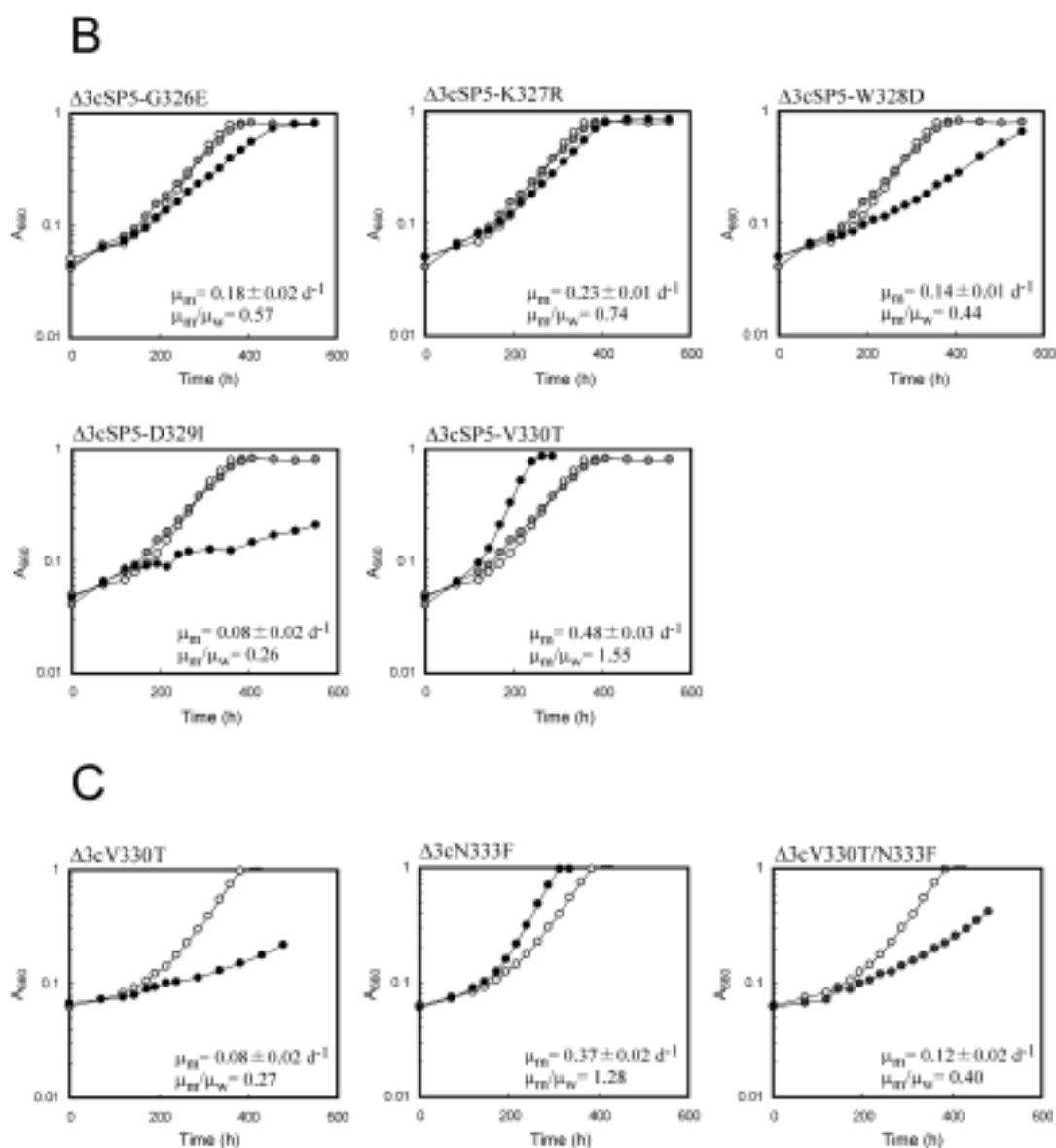


**Fig. 2. Growth of *R. palustris*  $\Delta 3$  recombinant strains harboring wild-type *Tk*-Rubisco and its mutant proteins with mutations in the  $\alpha$ -helix6 regions.** Representative growth curves of  $\Delta 3cRbc_{TK}$  (open circles) and strains harboring mutant proteins (closed circles) under photoheterotrophic conditions. Heterotrophically grown cells were washed and inoculated into photoheterotrophic medium. The recombinant strains in A-C harbor the mutant *Tk*-Rubisco proteins corresponding to Fig. 1A-C. The average specific growth rate of each strain harboring a mutant *Tk*-Rubisco ( $\mu_m$ ) (3 to 5 measurements) was compared with that of  $\mu_w$ , and is indicated in each panel. The average specific growth rate of  $\Delta 3cRbc_{TK}$  ( $\mu_w$ ) was  $0.30 \pm 0.02 \text{ d}^{-1}$  ( $n=7$ ) (A),  $0.31 \pm 0.02 \text{ d}^{-1}$  ( $n=4$ ) (B), and  $0.29 \pm 0.02 \text{ d}^{-1}$  ( $n=3$ ) (C). Representative growth curves of  $\Delta 3cSP4$  (A) and  $\Delta 3cSP5$  (B) are also indicated with gray circles as a comparison. The average specific growth rate of  $\Delta 3cSP4$  was  $0.20 \pm 0.01 \text{ d}^{-1}$  ( $n=5$ ), and that of  $\Delta 3cSP5$  was  $0.23 \pm 0.02 \text{ d}^{-1}$  ( $n=4$ ).

### Kinetic analysis of the purified recombinant enzymes.

The SP4-N333F and SP5-V330T proteins were purified and subjected to kinetic analyses. As in the case of SP6, the most significant change in properties between the SP4-N333F protein and the wild-type *Tk*-Rubisco was in the turnover numbers of their carboxylase activities, with a 46% increase in  $V_{CO_2}$  observed in SP4-N333F. The  $K_{CO_2}$  value of SP4-N333F increased to 68  $\mu$ M compared with that of the wild-type protein (60  $\mu$ M), resulting in a 29% decrease in  $k_{cat(CO_2)}/K_{CO_2}$  (Table 2). The SP5-V330T protein also displayed a clear 73% increase in  $V_{CO_2}$  compared with wild-type protein. Additionally, the SP5-V330T protein increased its  $K_{CO_2}$  value to 67  $\mu$ M compared with wild-type protein (60  $\mu$ M), resulting in an overall 57% increase in  $k_{cat(CO_2)}/K_{CO_2}$  (Table 2).

**Table 2. Kinetic properties of purified *Tk*-Rubisco and its mutant proteins.**

Kinetic constant	wild-type	SP4-N333F	SP5-V330T
	( $\mu = 0.30 \text{ d}^{-1}$ ) <sup>a</sup>	( $\mu = 0.39 \text{ d}^{-1}$ ) <sup>a</sup>	( $\mu = 0.48 \text{ d}^{-1}$ ) <sup>a</sup>
$V_{CO_2}$ ( $\mu\text{mol}/\text{min}/\text{mg}$ )	0.37 $\pm$ 0.02	0.54 $\pm$ 0.04	0.64 $\pm$ 0.03
$k_{cat(CO_2)}$ ( $\text{s}^{-1} \cdot \text{site}^{-1}$ )	0.31	0.45	0.53
$K_{CO_2}$ ( $\mu\text{M}$ )	60 $\pm$ 7	68 $\pm$ 10	67 $\pm$ 6
$k_{cat(CO_2)} / K_{CO_2}$	0.0051	0.0066	0.0080

<sup>a</sup>  $\mu$  represents specific growth rates of recombinant strains which harbor the indicated proteins noted above.

### **Effects of the mutations on protein stability.**

The author has shown that by replacing residues of the thermostable *Tk*-Rubisco protein with residues found in mesophilic Rubiscos, it was possible to enhance the performance of *Tk*-Rubisco at ambient temperatures. In general, thermostable proteins are presumed to obtain their thermostability by increasing their conformational rigidity compared to enzymes from mesophiles (7, 8). This in turn, in many cases, results in lower activity levels of the thermostable enzymes compared to their mesophilic counterparts at ambient temperatures (6). Increasing the flexibility of these enzymes can be expected to be one method to enhance the activity, particularly turnover rates, of these enzymes at low temperatures. On the other hand, adding flexibility to an enzyme can also be considered to have a negative effect on the thermostability of the enzyme. To examine whether this was the case in the *Tk*-Rubisco mutant proteins examined in this chapter and CHAPTER 2, the author measured and compared the thermostabilities of the wild-type *Tk*-Rubisco, and the mutant proteins SP4, SP6, SP4-N333F and SP5-V330T. At both 90°C and 100°C, there was a tendency that proteins with higher numbers of residues from the mesophilic spinach Rubisco were less stable (Table 3). Moreover, the author found that SP6, SP4-N333F and SP5-V330T, whose  $k_{cat}$  values were considerably higher than those of *Tk*-Rubisco and SP4, exhibited large decreases in thermostability. This raises the possibilities that in SP6, SP4-N333F and SP5-V330T, the increase in turnover rates may be brought about by the increased flexibility of the  $\alpha$ -helix6 region, at the expense of decreasing the overall thermostability of the enzyme.

**Table 3. Thermostability of *Tk*-Rubisco and its mutant proteins.**

Temperature	Half-lives of protein activities (min)				
	wild-type	SP4	SP6	SP4-N333F	SP5-V330T
90°C	220±10	190±19	120±8	160±13	150±3
100°C	48±2	33±3	2.5±0.1	17±1	2.9±0.2

## DISCUSSION

The loop6 and  $\alpha$ -helix6 regions have been demonstrated to play an important role in the turnover and specificity of Type I and Type II Rubiscos (3). In CHAPTER 2, the author has shown that this is also the case in the Type III *Tk*-Rubisco. Exchanging the loop6 of *Tk*-Rubisco with those of the Rubiscos from spinach, *G. partita* or *R. rubrum* led to dramatic decreases in the activity of *Tk*-Rubisco (SP1~2, GP2 and RR1). The activity levels of SP3~6 and GP1 indicate that the  $\alpha$ -helix6 region also plays an important role in *Tk*-Rubisco activity. As the SP6 mutation in  $\alpha$ -helix6 led to improvements in the functional capacity of *Tk*-Rubisco at ambient temperatures, the author focused on this region to determine the residues involved in the improved performance of SP6, as well as to explore the possibilities of further improvement of the enzyme.

Among the three residues exchanged between SP4 and SP6 in the C-terminal half of  $\alpha$ -helix6, the author found that the presence of phenylalanine at position 333 contributed most to the improved performance in SP6. The effects of a mutation in the corresponding position (F345V) in a Type I Rubisco from *Synechococcus* have been



examined both *in vitro* and *in vivo*. Although the kinetic parameters displayed only an improvement in the affinity towards RuBP, Rubisco-deficient *Rhodobacter capsulatus* cells harboring the F345V *Synechococcus* enzyme displayed significantly higher rates of photoautotrophic growth compared with cells with the wild-type enzyme (5). Among the five residues distinct between SP5 and SP6 in the N-terminal half of  $\alpha$ -helix6, the author found that the threonine positioned at 330 contributed most to the improved performance of SP6. The T342V mutation of a cyanobacterial Type I Rubisco corresponding to this position clearly decreased the specificity factor and the specific activity (4). The results of this study confirm that residues present at positions corresponding to 330 and 333 in *Tk*-Rubisco play an important role in defining the enzymatic performance of various Rubisco proteins.

SP6, SP4-N333F and SP5-V330T, three mutant proteins that supported higher growth rates in *R. palustris*  $\Delta 3$ , displayed increases in their turnover numbers compared to the wild-type *Tk*-Rubisco. In addition to the effect of specific residue replacements, the increase in turnover number may also be due to an increase in flexibility in these regions, as a clear decrease in the thermostability of these proteins was observed. Further mutations aimed to decrease the rigidity of *Tk*-Rubisco near its active site, such as disrupting residue interactions found in *Tk*-Rubisco but not in mesophilic Rubiscos, may lead to further increases in the catalytic activity of *Tk*-Rubisco at mesophilic temperatures.

## **SUMMARY**

This chapter describes a detailed site-directed mutagenesis analysis on the  $\alpha$ -helix6 region of *Tk*-Rubisco. This region was focused upon based on the results of

CHAPTER 2 that the mutant protein SP6, which harbors the entire  $\alpha$ -helix6 region of spinach Rubisco, displayed improved catalytic properties at ambient temperatures compared to the wild-type protein. Single residue replacements were introduced in the SP4 and SP5 proteins, which harbor the N- and C-terminal portions of the spinach  $\alpha$ -helix6 region, respectively. Individual genes were introduced into *R. palustris*  $\Delta 3$ , and specific growth rates were compared under photoheterotrophic conditions. In the N-terminal half of  $\alpha$ -helix6, a Val to Thr replacement at position 330 was found to be the most effective, whereas in the C-terminal half of this region, an Asn to Phe exchange at position 333 was most favorable. Among the mutant proteins examined in this and the previous chapter, SP5-V330T displayed the most efficient  $k_{\text{cat}(\text{CO}_2)}/K_{\text{CO}_2}$  value, and supported the highest growth rates under photoheterotrophic conditions when introduced into *R. palustris*  $\Delta 3$ . It should be noted that the effects of T330 was relevant only when the SP5 portion of the  $\alpha$ -helix6 region was occupied with residues from spinach Rubisco. The activity of the V330T (SP3) and V330T/N333F mutant proteins did not reach the levels exhibited by SP5-V330T, indicating the presence of a complex structural relationship among residues in the  $\alpha$ -helix6 region.

## REFERENCES

1. **Knight, S., I. Andersson, and C. I. Brändén.** 1990. Crystallographic analysis of ribulose 1,5-bisphosphate carboxylase from spinach at 2.4 Å resolution. Subunit interactions and active site. *J. Mol. Biol.* **215**:113-160.
2. **Newman, J., and S. Gutteridge.** 1993. The X-ray structure of *Synechococcus* ribulose-bisphosphate carboxylase/oxygenase-activated quaternary complex at 2.2-Å resolution. *J. Biol. Chem.* **268**:25876-25886.

3. **Parry, M. A. J., P. J. Andralojc, R. A. Mitchell, P. J. Madgwick, and A. J. Keys.** 2003. Manipulation of Rubisco: the amount, activity, function and regulation. *J. Exp. Bot.* **54**:1321-1333.
4. **Read, B. A., and F. R. Tabita.** 1994. High substrate specificity factor ribulose-bisphosphate carboxylase/oxygenase from eukaryotic marine algae and properties of recombinant cyanobacterial Rubisco containing "algal" residue modifications. *Arch. Biochem. Biophys.* **312**:210-218.
5. **Smith, S. A., and F. R. Tabita.** 2003. Positive and negative selection of mutant forms of prokaryotic (cyanobacterial) ribulose-1,5-bisphosphate carboxylase/oxygenase. *J. Mol. Biol.* **331**:557-569.
6. **Varley, P. G., and R. H. Pain.** 1991. Relation between stability, dynamics and enzyme activity in 3-phosphoglycerate kinases from yeast and *Thermus thermophilus*. *J. Mol. Biol.* **220**:531-538.
7. **Vihinen, M.** 1987. Relationship of protein flexibility to thermostability. *Protein Eng.* **1**:477-480.
8. **Závodszky, P., J. Kardos, A. Svingor, and G. A. Petsko.** 1998. Adjustment of conformational flexibility is a key event in the thermal adaptation of proteins. *Proc. Natl. Acad. Sci. USA* **95**:7406-7411.

## GENERAL CONCLUSIONS

In this study, the author has examined the enzymatic performance of a Type III Rubisco from the hyperthermophilic archaeon, *Thermococcus kodakaraensis*, at ambient temperatures. The research was performed in order to explore the possibilities of utilizing the enzyme (*Tk*-Rubisco) as a CO<sub>2</sub>-fixing Rubisco in the Calvin-Benson-Bassham pathway (CBB pathway) of mesophilic organisms. This would provide a new alternative in Rubisco engineering, which has been carried out since long ago with the Type I and Type II enzymes with little success. Even the slightest improvement in the catalytic performance of Rubiscos is expected to have a great impact in the fields of agriculture and may also contribute in solving the recent accumulation of carbon dioxide in our atmosphere.

As *Tk*-Rubisco is derived from a hyperthermophilic organism, the author first had to determine the enzymatic properties of the protein at ambient temperature ranges. The author took a straightforward approach, and introduced the gene into a mesophilic photosynthetic organism, *Rhodospseudomonas palustris*, whose three endogenous Rubisco genes had been disrupted beforehand. Although specific growth rates were lower than the wild-type *R. palustris*, the recombinant strain with only a single copy of the *Tk*-Rubisco gene was capable of photoautotrophic and photoheterotrophic growth. This clearly indicated that *Tk*-Rubisco could act as the CO<sub>2</sub>-fixing Rubisco in the CBB pathway of mesophiles. Additional analyses revealed that the levels of Rubisco activity observed in the cell-free extracts of *R. palustris* displayed a good correlation with the specific growth rates of the respective host cells, indicating that growth rate can be used as a parameter in further studies to evaluate the catalytic performance of *Tk*-Rubisco

and its mutant proteins at ambient temperature.

Encouraged by the fact that the carboxylase activity of *Tk*-Rubisco was sufficient to support the phototrophic growth of *R. palustris* at mesophilic temperatures, the author proceeded to enhance the performance of the enzyme through protein engineering. Although single residue replacements aimed to decrease the rigidity of the thermostable *Tk*-Rubisco did not lead to significant positive effects, mutations replacing the entire  $\alpha$ -helix6 region of *Tk*-Rubisco with that of the spinach enzyme were clearly effective. One mutant protein, SP6, exhibited a 30% increase in  $k_{\text{cat}}$  value of the carboxylase activity and a 17% increase in the  $k_{\text{cat}}/K_{\text{m}}$  value. *R. palustris* cells harboring SP6 displayed a 31% increase in specific growth rate compared to the strain expressing the wild-type *Tk*-Rubisco. A further, detailed mutagenesis study was performed to elucidate the residues responsible for the enhanced activity in SP6. Twelve mutant proteins, all with residue replacements in the  $\alpha$ -helix6 region, were constructed and examined. The author found that residues at positions 330 and 333 were the most important in defining the performance of the enzyme at ambient temperatures. Among the mutant proteins, SP5-V330T exhibited the best performance with a 35% increase in catalytic turnover, and a 23% increase in the carboxylase  $k_{\text{cat}}/K_{\text{m}}$  value. *R. palustris* cells harboring SP5-V330T displayed a 60% increase in specific growth rate compared to the strain expressing wild-type *Tk*-Rubisco. This specific growth rate corresponds to 80% of that observed in the wild-type *R. palustris* utilizing its three endogenous Rubiscos. As this study has displayed that *Tk*-Rubisco can tolerate high degrees of mutations and/or secondary structure replacements, applying similar strategies (taken in this study) to other regions of the enzyme will most likely lead to the generation of a Type III-based Rubisco with properties superior to those found in phototrophic bacteria.

## LIST OF PUBLICATIONS

1. Phototrophic growth of a Rubisco-deficient mesophilic purple nonsulfur bacterium harboring a Type III Rubisco from a hyperthermophilic archaeon.  
**Shosuke Yoshida**, Masayuki Inui, Hideaki Yukawa, Tadayoshi Kanao, Ken-ichi Tomizawa, H. Atomi, and Tadayuki Imanaka.  
*Journal of Biotechnology*. 2006. 124(3), 532-544.
2. Engineering of a Type III Rubisco from a hyperthermophilic archaeon in order to enhance catalytic performance in mesophilic host cells.  
**Shosuke Yoshida**, Haruyuki Atomi, and Tadayuki Imanaka.  
*Applied and Environmental Microbiology*. 2007. 73(19), 6254-6261.
3. Optimizing the  $\alpha$ -helix6 region of *Tk*-Rubisco to enhance catalytic performance of the enzyme at ambient temperatures.  
**Shosuke Yoshida**, Haruyuki Atomi, and Tadayuki Imanaka.  
*In preparation*.